NASA Technical Paper 3631

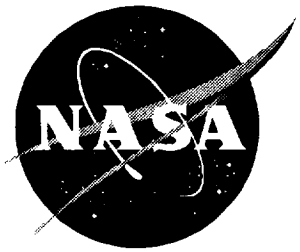

Multistage Schemes With Multigrid for Euler and Navier-Stokes Equations

Components and Analysis

R. C. Swanson
Langley Research Center • Hampton, Virginia

Eli Turkel
Tel-Aviv University • Tel-Aviv, Israel

National Aeronautics and Space Administration
Langley Research Center • Hampton, Virginia 23681-2199

August 1997

Available electronically at the following URL address: http://techreports.larc.nasa.gov/ltrs/ltrs.html

Printed copies available from the following:

NASA Center for AeroSpace Information
800 Elkridge Landing Road
Linthicum Heights, MD 21090-2934
(301) 621-0390

National Technical Information Service (NTIS)
5285 Port Royal Road
Springfield, VA 22161-2171
(703) 487-4650

Contents

List of Figures

Abstract

A class of explicit multistage time-stepping schemes with centered spatial differencing and multigrid is considered for the compressible Euler and Navier-Stokes equations. These schemes are the basis for a family of computer programs (flow codes with multigrid (FLOMG) series) currently used to solve a wide range of fluid dynamics problems, including internal and external flows. In this paper, the components of these multistage time-stepping schemes are defined, discussed, and in many cases analyzed to provide additional insight into their behavior. Special emphasis is given to numerical dissipation, stability of Runge-Kutta schemes, and the convergence-acceleration techniques of multigrid and implicit residual smoothing. Both the Baldwin and Lomax algebraic equilibrium model and the Johnson and King one-half equation nonequilibrium model are used to establish turbulence closure. Implementation of these models is described.

1. Introduction

Computational fluid dynamics (CFD) is a multidisciplinary field involving fluid mechanics, numerical analysis, and computer science. The evolution of CFD over the last three decades has fostered a broad range of methods for computing the aerodynamics of flight vehicles. At cruise flight conditions, a variety of approximate techniques are applied by the aircraft industry when designing flight vehicles.

With inviscid and irrotational flow assumptions, versatile and reliable panel methods and nonlinear potential equation solvers are used for aircraft design. To determine viscous effects, either an integral or finite-difference approach is employed to solve the boundary-layer equations. When the interaction between the viscous and inviscid flow regions is important, the computational procedures for these regions are coupled in either the direct mode (i.e., surface pressure is specified) or the inverse mode (i.e., surface shear stress in the case of a solid wall is specified). Although these computational techniques are efficient and usually provide reasonable estimates of viscous effects, they can be difficult to implement for three-dimensional (3-D) flows when strong viscous-inviscid interactions occur (such as aircraft wing and body juncture flow).

In the past few years, substantial improvements were made on the mathematical models of aerodynamic prediction techniques used for aircraft design. The Euler equations allow rotational effects (i.e., vortical structures) and nonisentropic shock waves and thus provide a better inviscid model for flows over aerodynamic configurations. The Navier-Stokes equations model weak and strong interactions between viscous and inviscid flow regions without special consideration. Both the Euler and the time-averaged Navier-Stokes equations are currently being introduced into the aircraft design process.

Progress in aircraft design can be attributed to several factors. A primary factor is the considerable improvement in the accuracy and efficiency of numerical algorithms used to solve the Euler and Navier-Stokes equations. Another factor is the significant advancements in computer memory capacity and processing times. Although new technologies in computers and computer science will continue to help decrease processing times, the need still exists for strong effort to increase the robustness, accuracy, and efficiency of the flow solvers to allow their use in analysis of complex fluid dynamics phenomena and aircraft design.

An extensive range of numerical algorithms was developed during the last decade to solve the Euler and Navier-Stokes equations. These numerical algorithms can be classified by the type of time-stepping scheme and the type of spatial-discretization scheme used. Both

explicit and implicit time-stepping schemes have been constructed. Explicit schemes require less computational storage and a lower number of operations for time integration, but have a stricter limit on the allowable time step. If temporal and spatial differencing are decoupled, both schemes are amenable to a variety of convergence-acceleration techniques for steady-state problems. The explicit multistage Runge-Kutta scheme of Jameson, Schmidt, and Turkel (ref. 1) and the implicit approximate factorization (AF) scheme of Beam and Warming (ref. 2) are two schemes that employ temporal and spatial decoupling. The multistage schemes, in conjunction with local time stepping and other convergence enhancements (ref. 3), and the AF scheme, with local time stepping and diagonalization of the implicit operator (ref. 4), are efficient schemes for the Euler equations.

Central and one-sided differencing have been considered for the spatial derivatives in the flow equations. When selecting one type of differencing over another, it is important to understand the dominating design criterion for central and upwind schemes. When constructing a central difference scheme, the principal underlying guideline is to minimize the arithmetic operation count while simultaneously maintaining the highest possible accuracy. The multistage schemes and Lax-Wendroff schemes (refs. 5–11) are currently the most widely used explicit algorithms with central spatial differencing. The AF scheme is the most frequently used implicit scheme with centered differencing.

A primary objective of an upwind scheme is to capture flow discontinuities such as shock waves using the minimum number of mesh cells. To accomplish this, many upwind schemes utilize the signs of the slopes of characteristics to determine the direction of propagation of information, and thus, the type of differencing for approximating spatial derivatives. Two procedures for constructing upwind schemes for hyperbolic systems of conservation laws are the flux vector splitting scheme of Van Leer (ref. 12) and the flux difference splitting scheme of Roe (ref. 13). Upwind schemes have become popular because of their shock-capturing capability. Generally, upwind schemes represent shock waves with two interior cells rather than the three or four interior cells usually needed by central difference schemes. However, upwind schemes can require as much as twice the computational effort.

Multistage time-stepping schemes with central differencing for spatial discretization on both structured and unstructured meshes are now being used to solve the Euler equations for flows over complex configurations, including airplanes (refs. 14 and 15). Members of this class of algorithm have also been extended to allow the solution of the compressible Navier-Stokes equations in both two and three dimensions (refs. 16 and 17). Including convergence-acceleration methods, such as local time stepping and constant coefficient implicit residual smoothing (which extends the explicit time step limit), has made these solvers reasonably effective. Significant performance improvements are achieved principally by using the multistage scheme as a driver of a multigrid method. The multigrid method involves a sequence of successively coarser meshes and enhances the convergence rate and the robustness of the single-grid scheme. In reference 18, a three-stage Runge-Kutta scheme with multigrid was successfully applied to the two-dimensional (2-D) Navier-Stokes equations. Then, both Swanson and Turkel (ref. 19) and Martinelli and Jameson (ref. 20) demonstrated that the type of convergence behavior described in reference 18 could be substantially improved. The multigrid procedure was used to solve flow over a wing (ref. 21). Significant performance improvements detailed in reference 21 were obtained (refs. 22 and 23) by closely following and extending the ideas developed in the 2-D solvers (refs. 19, 20, and 24).

This paper describes an efficient and versatile class of central difference, finite-volume multigrid schemes for the 2-D compressible Euler and Navier-Stokes equations. The elements of these schemes are the basis for a family of computer codes (flow codes with multigrid (FLOMG) series) developed by the authors that are now being used in both industry and universities. These computer codes have been applied to numerous fluid dynamics problems over the last

several years, and have been employed as an analysis code in airfoil design procedures (ref. 25). The primary purpose of this paper is to discuss, and in many instances, analyze, the components of the schemes in these codes.

Sections 2 and 3 of this report give the flow equations and describe the finite-volume formulation for spatial discretization. Three alternatives for numerical approximation of viscous stress and heat flux terms are discussed, and the influence of grid stretching on numerical accuracy is determined.

Section 4 of this report discusses artificial dissipation. After outlining the historical development of a form for dissipation, the scalar dissipation model frequently used with the present schemes is given in section 4.2. The selection of boundary-point difference operators is an important consideration for the dissipation model. Suitable operators are given, and how local mode analysis can often provide an evaluation for a proposed boundary-point difference operator is shown. Analysis based on considering the dissipative character of the discrete system of equations is also performed. Section 4.5 examines the intimate connection between the formulation of an upwind scheme and a central difference scheme, and a foundation for a matrix dissipation model is established. Section 4.6 describes the matrix dissipation model used with the present schemes.

Section 5 discusses the discrete boundary conditions. Section 6 defines the class of explicit multistage time-stepping schemes considered and summarizes their properties. Next, the stability of Runge-Kutta schemes for systems of equations is examined. Subsequently, a time-step estimate for pseudotime integration of the flow equations is given. Since the temporal and spatial discretizations are decoupled, these explicit schemes are amenable to convergence-acceleration techniques. Section 7 addresses techniques used in this report, including local time stepping, implicit residual smoothing, and multigrid. The initial part of section 7 indicates how the discrete system of flow equations is preconditioned with local time stepping. Section 7.2 first discusses constant coefficients for implicit residual smoothing, and also presents basic properties of residual smoothing. Next, a form for variable coefficients for implicit residual smoothing based on stability analysis of a 2-D linear wave equation is introduced. From this form, two different formulas for variable smoothing coefficients evolve, and these formulas are compared. These variable smoothing coefficients still generally require a time-step estimate that depends on a diffusion limit. The last part of section 7.2 shows how to use variable smoothing coefficients to construct new coefficients that can allow removal of the diffusion restriction. Section 7.3 describes the basic elements of multigrid methods and delineates the salient features of the present multigrid algorithm.

Section 8 discusses turbulence modeling. Both an algebraic equilibrium model and a half-equation nonequilibrium model are considered. Details for implementation of the turbulence models are given. Section 9 states concluding remarks.

2. Mathematical Formulation

In this section the integral form of the full Navier-Stokes equations is defined. Boundary conditions for the infinite domain problem are then given to complete the general mathematical formulation. Section 3 discusses the discrete analogue of the full Navier-Stokes equations, section 4 introduces the reduced form of these equations that is frequently solved in aerodynamic applications, and section 5 gives boundary conditions for the truncated (finite) domain problem.

2.1. Equations

Let ρ denote the density, u and v represent velocity components in the x and y Cartesian directions, respectively; p is pressure, T is temperature, E is specific total internal energy, and

H is specific total enthalpy. If body forces and heat sources are neglected, the 2-D, unsteady Navier-Stokes equations can be written in conservative form in a Cartesian coordinate system as

$$\frac{\partial}{\partial t}\iint_{\mathcal{V}} \mathbf{W}\, d\mathcal{V} + \int_S \mathcal{F}\cdot\mathbf{n}\; dS = 0 \tag{2.1.1}$$

where t is time, $\mathcal{V}$ is the region being considered,

$$\mathbf{W} = \begin{bmatrix} \rho \\ \rho u \\ \rho v \\ \rho E \end{bmatrix}$$

$$\mathcal{F} = \begin{bmatrix} \rho\mathbf{q} \\ \rho u\mathbf{q} + p\mathbf{e}_x + \bar{\tau}\cdot\mathbf{e}_x \\ \rho v\,\mathbf{q} + p\mathbf{e}_y + \bar{\tau}\cdot\mathbf{e}_y \\ \rho H\mathbf{q} + \bar{\tau}\cdot\mathbf{q} - \mathbf{Q} \end{bmatrix}$$

and

$$\mathbf{q} = u\mathbf{e}_x + v\mathbf{e}_y$$

$$\bar{\tau} = \sigma_x\mathbf{e}_x\mathbf{e}_x + \tau_{xy}\mathbf{e}_x\mathbf{e}_y + \tau_{yx}\mathbf{e}_y\mathbf{e}_x + \sigma_y\mathbf{e}_y\mathbf{e}_y$$

$$\sigma_x = -\lambda\left(\frac{\partial u}{\partial x} + \frac{\partial v}{\partial y}\right) - 2\mu\frac{\partial u}{\partial x}$$

$$\tau_{xy} = \tau_{yx} = -\lambda\left(\frac{\partial u}{\partial y} + \frac{\partial v}{\partial x}\right)$$

$$\sigma_y = -\lambda\left(\frac{\partial u}{\partial x} + \frac{\partial v}{\partial y}\right) - 2\mu\frac{\partial v}{\partial y}$$

$$\mathbf{Q} = k\nabla T = k\left(\frac{\partial T}{\partial x}\mathbf{e}_x + \frac{\partial T}{\partial y}\mathbf{e}_y\right)$$

$$E = e + \frac{1}{2}(u^2 + v^2)$$

$$H = E + \frac{p}{\rho}$$

Here, $\mathbf{e}_x$ and $\mathbf{e}_y$ are unit vectors of the Cartesian coordinate system (x,y), and $\mathbf{n}$ is an outward-pointing unit vector normal to the curve S enclosing the region $\mathcal{V}$. Air is the working fluid used in this paper. The air is assumed to be thermally and calorically perfect. The equation of state is

$$p = \rho RT \tag{2.1.2}$$

where $R = \bar{c}_p - \bar{c}_v$, and the specific heats $\bar{c}_p$ and $\bar{c}_v$ are constant. The quantities μ and λ are the first and second coefficients of viscosity, respectively, and λ is taken to be $-\frac{2}{3}\mu$ (Stokes hypothesis). Either a simple power law or Sutherland's law can be used to determine the molecular viscosity coefficient μ. The coefficient of thermal conductivity k is evaluated using the constant Prandtl number assumption. The effect of turbulence is accounted for by using the eddy-viscosity hypothesis. (See section 8 on turbulence modeling.)

2.2. Physical Boundary Conditions

In the continuum case, either an external or an internal flow problem defined for an infinite domain is considered. Thus, appropriate conditions at wall boundaries, which are assumed to be solid, must be defined. Later, in the discrete case, finite domains are defined. Suitable inflow and outflow boundary conditions must then be defined.

For inviscid flows, the tangency (or nonpenetration) condition

$$\mathbf{q} \cdot \mathbf{n} = 0 \tag{2.2.1}$$

must be satisfied, where $\mathbf{q}$ is the velocity vector and $\mathbf{n}$ is the unit vector normal to the surface. Now, consider the vector momentum equation

$$\rho \frac{D\mathbf{q}}{Dt} = -\nabla p \tag{2.2.2}$$

where $D\mathbf{q}/Dt$ denotes the substantial derivative of $\mathbf{q}$, and ∇ is the gradient operator. Clearly, the substantial derivative of $\mathbf{q} \cdot \mathbf{n}$ must vanish along the surface boundary. Therefore

$$\rho \left(\frac{\partial}{\partial t} + \mathbf{q} \cdot \nabla \right) (\mathbf{q} \cdot \mathbf{n}) = 0 \tag{2.2.3}$$

If the inner product of the unit normal and equation (2.2.2) is subtracted from equation (2.2.3), then

$$\rho \mathbf{q} \cdot (\mathbf{q} \cdot \nabla) \mathbf{n} = \mathbf{n} \cdot \nabla p \tag{2.2.4}$$

Now, consider the transformation $(x, y) \rightarrow (\xi, \eta)$, take $\eta(x, y) =$ constant to coincide with the surface boundary, and note that the contravariant velocity component $V = -(y_\xi / J^{-1})\, u + (x_\xi / J^{-1})\, v$ (where the subscripts mean differentiation and J is the transformation Jacobian) is zero because of equation (2.2.1). Then, from equation (2.2.4)

$$p_\eta = \frac{1}{\left(x_\xi^2 + y_\xi^2 \right)} \left[\left(x_\xi x_\eta + y_\xi y_\eta \right) p_\xi + \left(y_\eta u - x_\eta v \right) \left(\rho v x_{\xi\xi} - \rho u y_{\xi\xi} \right) \right] \tag{2.2.5}$$

For viscous flows, the nonpenetration condition (eq. (2.2.1)) and the no-slip condition

$$\mathbf{q} \cdot \mathbf{t} = 0 \tag{2.2.6}$$

(where $\mathbf{t}$ is the unit vector tangent to the surface) must be satisfied. In addition, a boundary condition is required to determine the surface temperature. For this boundary condition either the wall temperature is set to a specified value or the adiabatic condition

$$\mathbf{Q} \cdot \mathbf{n} = 0 \tag{2.2.7}$$

is imposed, where $\mathbf{Q}$ is the heat flux vector given in equation (2.1.1).

3. Spatial Discretization

A finite-volume approach is applied to discretize the equations of motion. The computational domain is divided into quadrilateral cells that are fixed in time. For each cell, the governing equations can be nondimensionalized and written in integral form as follows:

$$\frac{\partial}{\partial t} \iint_\Omega \mathbf{W}\, dx\, dy + \int_{\partial\Omega} (\mathbf{F}\, dy - \mathbf{G}\, dx) = \frac{\sqrt{\gamma} M}{Re} \int_{\partial\Omega} (\mathbf{F}_v\, dy - \mathbf{G}_v\, dx) \tag{3.1}$$

where Ω is a generic cell (or cell area) with $\partial\Omega$ the cell boundary. In the scaling factor for the viscous terms on the right side of equation (3.1), the quantities γ, M, and Re are the specific heat ratio, Mach number, and Reynolds number, respectively, with M and Re defined by nominal conditions. These factors arise because of the choice of nondimensionalization of the equations. The flux vectors are defined by

$$\mathbf{F} = \begin{bmatrix} \rho u \\ \rho u^2 + p \\ \rho uv \\ \rho uH \end{bmatrix}$$

$$\mathbf{G} = \begin{bmatrix} \rho v \\ \rho uv \\ \rho v^2 + p \\ \rho vH \end{bmatrix}$$

$$\mathbf{F}_v = \begin{bmatrix} 0 \\ \sigma_x \\ \tau_{xy} \\ u\sigma_x + v\tau_{xy} - k\dfrac{\partial T}{\partial x} \end{bmatrix}$$

$$\mathbf{G}_v = \begin{bmatrix} 0 \\ \tau_{yx} \\ \sigma_y \\ u\tau_{yx} + v\sigma_y - k\dfrac{\partial T}{\partial y} \end{bmatrix}$$

The independent variables x, y, and t are nondimensionalized as

$$x = \frac{\tilde{x}}{\tilde{l}_{\text{ref}}}$$

$$y = \frac{\tilde{y}}{\tilde{l}_{\text{ref}}}$$

$$t = \tilde{t}\,\frac{\tilde{u}_{\text{ref}}}{\tilde{l}_{\text{ref}}}$$

where $\tilde{u}_{\text{ref}} = \sqrt{\tilde{p}_{\text{ref}}/\tilde{\rho}_{\text{ref}}}$, and the tilde in this section represents a dimensional variable. Examples of a reference length are the chord for an airfoil and the throat height for a nozzle flow. The thermodynamic variables p, ρ, and T and the transport coefficients μ and k are nondimensionalized by their corresponding quantity evaluated at some reference condition. The velocity components are scaled by $\tilde{u}_{\text{ref}}$, and the total quantities E and H are scaled by $\tilde{u}^2_{\text{ref}}$. For external flows, the nominal conditions are based on free-stream values, and for internal flows, the nominal conditions are based on stagnation values.

Partition the computational region with quadrilaterals and apply equation (3.1) to each quadrilateral. This process is equivalent to performing a mass, momentum, and energy balance on each cell. A system of ordinary differential equations is obtained by decoupling the temporal

and spatial terms. In particular, consider an arbitrary quadrilateral (fig. 1, $ABCD$), and approximate the line integrals of equation (3.1) with the midpoint rule. Let the indices (i,j) identify a cell. Then, by taking $\mathbf{W}_{i,j}$ as the cell-averaged solution vector, equation (3.1) can be written in semidiscrete form as

$$\frac{d}{dt}(\Omega_{i,j}\mathbf{W}_{i,j}) + \mathcal{L}\mathbf{W}_{i,j} = 0 \tag{3.2}$$

where $\Omega_{i,j}$ is the area of the cell, and $\mathcal{L}$ is a spatial discretization operator defined by $\mathcal{L} = \mathcal{L}_C + \mathcal{L}_D + \mathcal{L}_{AD}$, with the subscripts C, D, and AD referring to convection, diffusion, and artificial dissipation, respectively. The convective fluxes at the cell faces are obtained by an averaging process. The convective flux balance is computed by summing over the cell faces as

$$\mathcal{L}_C\mathbf{W}_{i,j} = \sum_{l=1}^{4}(\mathcal{F}_C)_l \cdot \mathbf{S}_l \tag{3.3}$$

with the flux tensor associated with convection given by $(\mathcal{F}_C)_l = \mathbf{F}_l\mathbf{e}_x + \mathbf{G}_l\mathbf{e}_y$, and for each cell face l, the directed length $\mathbf{S}_l$ is expressed as

$$\mathbf{S}_l = (\Delta y)_l\,\mathbf{e}_x - (\Delta x)_l\,\mathbf{e}_y \tag{3.4}$$

where the proper signs of $(\Delta x)_l$ and $(\Delta y)_l$ produce an outward normal to the cell face. The augmented, convective flux tensor is evaluated as

$$(\mathcal{F}_C)_l = \frac{1}{2}(\mathbf{W}^-\mathbf{q}^- + \mathbf{W}^+\mathbf{q}^+)_l + P_l \tag{3.5}$$

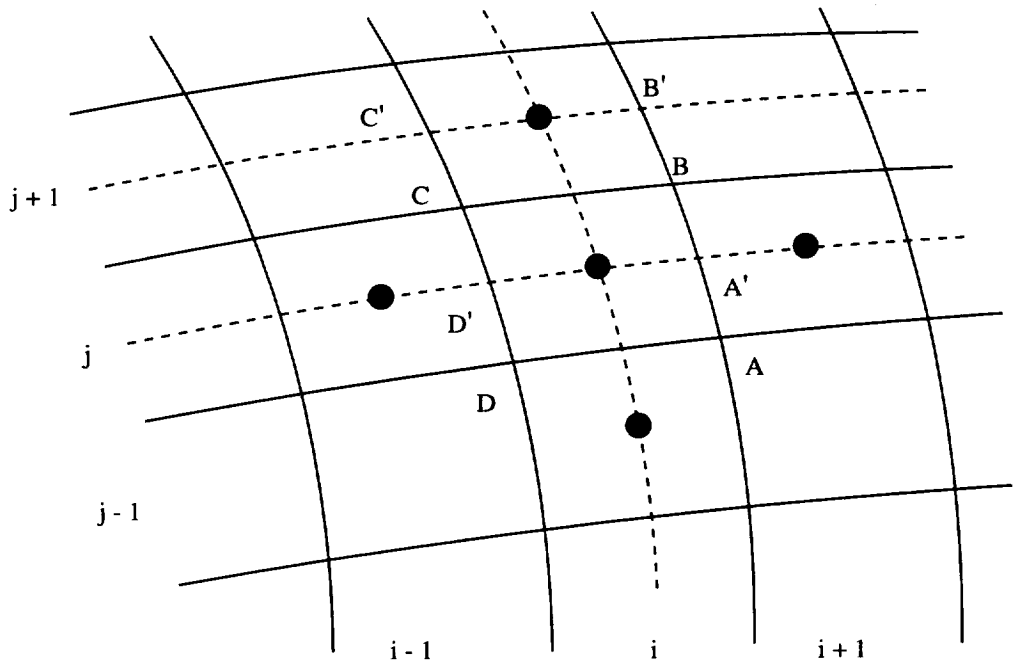

Figure 1. Finite-volume discretization.

where

$$P_l = \begin{bmatrix} 0 & (p_{\text{avg}})_l \mathbf{e}_x & (p_{\text{avg}})_l \mathbf{e}_y & ((p\mathbf{q})_{\text{avg}})_l \end{bmatrix}^T$$

$$(p_{\text{avg}})_l = \frac{1}{2}(p^- + p^+)_l$$

$$((p\mathbf{q})_{\text{avg}})_l = \frac{1}{2}(p^-\mathbf{q}^- + p^+\mathbf{q}^+)_l$$

and the superscripts minus $(-)$ and plus $(+)$ indicate quantities taken from the two cell centers adjacent to the edge l. The symbol $\mathbf{q}$ denotes the velocity vector. In this section, the subscript avg always refers to the simple average defined in equation (3.5) for a given edge l.

The contribution of the diffusive fluxes in equation (3.2) is evaluated as

$$\mathcal{L}_D \mathbf{W}_{i,j} = \sum_{l=1}^{4} (\mathcal{F}_D)_l \cdot \mathbf{S}_l \tag{3.6}$$

where $\mathbf{S}_l$ is given by equation (3.4), and $(\mathcal{F}_D)_l = (\mathbf{F}_v)_l \mathbf{e}_x + (\mathbf{G}_v)_l \mathbf{e}_y$. First-order spatial derivatives are in the flux vectors $\mathbf{F}_v$ and $\mathbf{G}_v$. In the present finite-volume method, these derivatives are determined using Green's theorem. For example, consider the cell face BC in figure 1. The contributions u_x and u_y to the viscous flux across BC are approximated by their mean values as follows:

$$\begin{aligned}(u_x)_{i,j+1/2} = (u_x)_{BC} &= \frac{1}{\Omega'} \iint_{\Omega'} u_x \, dx \, dy \\ &= \frac{1}{\Omega'} \int_{\partial\Omega'} u \, dy \end{aligned} \tag{3.7}$$

$$\begin{aligned}(u_y)_{i,j+1/2} = (u_y)_{BC} &= \frac{1}{\Omega'} \iint_{\Omega'} u_y \, dx \, dy \\ &= -\frac{1}{\Omega'} \int_{\partial\Omega'} u \, dx \end{aligned} \tag{3.8}$$

where Ω' is the area of an appropriate auxiliary cell.

Three alternatives for computing the diffusion-type terms have been considered. The first two approximations for a diffusive flux are obtained with finite-volume methods, and the third approximation is determined with a frequently used method based on a local transformation of coordinates. A comparison is now made between these three choices.

For the comparison, consider the molecular transport processes associated with cell face BC for the x-momentum equation only. Let $\Phi_{BC} = [(\mathcal{F}_D)_{BC} \cdot \mathbf{S}_{BC}]_2 = (\sigma_x \, \Delta y - \tau_{yx} \, \Delta x)_{BC}$. In one finite-volume method the integration path $A'B'C'D'$ (fig. 1) used in references 16 and 26 is considered. Applying the midpoint rule for the required line integrals results in

$$\begin{aligned}\Phi_{BC} = &\frac{\mu_{\text{avg}}}{\Omega'} \left[\phi_1 u_{i,j+1} + \phi_2 u_{i,j} + \phi_3 u_B + \phi_4 u_C\right] \\ &+ \frac{\mu_{\text{avg}}}{\Omega'} \left[\phi_5 v_{i,j+1} + \phi_6 v_{i,j} + \phi_7 v_B + \phi_8 v_C\right] \end{aligned} \tag{3.9}$$

where

$$\phi_1 = \frac{4}{3}\Delta y_{BC'}\,\Delta y_{B'C''} + \Delta x_{BC'}\,\Delta x_{B'C''}$$

$$\phi_2 = \frac{4}{3}\Delta y_{BC'}\,\Delta y_{D'A''} + \Delta x_{BC'}\,\Delta x_{D'A''}$$

$$\phi_3 = \frac{4}{3}\Delta y_{BC'}\,\Delta y_{A'B''} + \Delta x_{BC'}\,\Delta x_{A'B''}$$

$$\phi_4 = \frac{4}{3}\Delta y_{BC'}\,\Delta y_{C''D''} + \Delta x_{BC'}\,\Delta x_{C''D''}$$

$$\phi_5 = \frac{2}{3}\Delta y_{BC'}\,\Delta x_{B'C''} - \Delta x_{BC'}\,\Delta y_{B'C''}$$

$$\phi_6 = \frac{2}{3}\Delta y_{BC'}\,\Delta x_{D'A''} - \Delta x_{BC'}\,\Delta y_{D'A''}$$

$$\phi_7 = \frac{2}{3}\Delta y_{BC'}\,\Delta x_{A'B''} - \Delta x_{BC'}\,\Delta y_{A'B''}$$

$$\phi_8 = \frac{2}{3}\Delta y_{BC'}\,\Delta x_{C''D''} - \Delta x_{BC'}\,\Delta y_{C''D''}$$

$$u_B = \frac{1}{4}\left(u_{i,j} + u_{i+1,j} + u_{i,j+1} + u_{i+1,j+1}\right)$$

$$u_{C'} = \frac{1}{4}\left(u_{i,j} + u_{i-1,j} + u_{i,j+1} + u_{i-1,j+1}\right)$$

with v_B and $v_{C'}$ defined similarly, and

$$\Delta x_{BC'} = x_{C'} - x_B$$

$$\Delta y_{BC'} = y_{C'} - y_B$$

$$\mu_{\text{avg}} = \frac{1}{2}\left(\mu_{i,j} + \mu_{i,j+1}\right)$$

$$\Omega' = \frac{1}{2}\left(\Omega_{i,j} + \Omega_{i,j+1}\right)$$

Martinelli (ref. 27) introduced a different integration path for calculating the viscous terms (delineated as $BFCE$ in fig. 2). Integrating around the boundary $BFCE$ with the trapezoidal rule results in

$$\begin{aligned}\Phi_{BC'} = {} & \frac{\mu_{\text{avg}}}{2\Omega''}\left[\left(\frac{4}{3}\Delta y_{BC'}^2 + \Delta x_{BC'}^2\right)(u_{i,j+1} - u_{i,j}) - \left(\frac{1}{3}\Delta x_{BC'}\,\Delta y_{BC'}\right)(v_{i,j+1} - v_{i,j})\right] \\ & + \frac{\mu_{\text{avg}}}{2\Omega''}\left[\left(\frac{4}{3}\Delta y_{EF}\,\Delta y_{BC'} + \Delta x_{EF}\,\Delta x_{BC'}\right)(u_B - u_{C'})\right] \\ & + \frac{\mu_{\text{avg}}}{2\Omega''}\left[\left(\frac{2}{3}\Delta x_{EF}\,\Delta y_{BC'} - \Delta y_{EF}\,\Delta x_{BC'}\right)(v_B - v_{C'})\right] \qquad (3.10)\end{aligned}$$

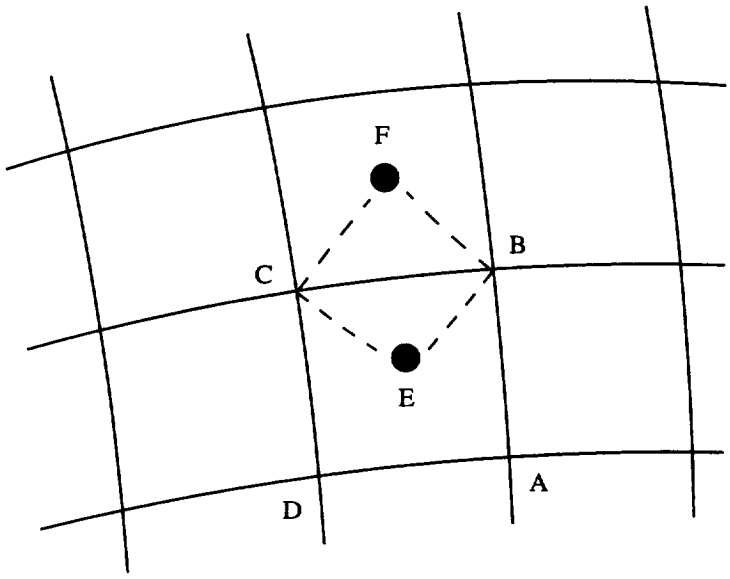

Figure 2. Alternative integration path for physical diffusive fluxes.

where

$$\Delta x_{EF} = x_{i,j+1} - x_{i,j}$$

$$\Delta y_{EF} = y_{i,j+1} - y_{i,j}$$

and Ω'' is the area of the region enclosed by $BFCE$. The area Ω'' is given by

$$\Omega'' = \frac{1}{2}\left(\Delta x_{CB}\,\Delta y_{EF} - \Delta x_{EF}\,\Delta y_{CB}\right)$$

All other quantities in equation (3.10) are defined the same as in equation (3.9). The form of Φ_{BC} given by equation (3.10) is much more compact, requiring fewer arithmetic operations than the form of Φ_{BC} given by equation (3.9).

A third approach for computing the diffusion-type terms is based on a local transformation from Cartesian coordinates (x, y) to arbitrary curvilinear coordinates (ξ, η). Derivatives with respect to x and y are expanded according to the chain rule for partial differentiation. The resulting relation for Φ_{BC} is as follows:

$$\Phi_{BC} = \frac{\mu_{\text{avg}}}{\Omega'}\left[\left(\frac{4}{3}\Delta y_{CB} y_\xi + \Delta x_{CB} x_\xi\right) u_\eta + \left(\frac{2}{3}\Delta y_{CB} x_\xi - \Delta x_{BC} y_\xi\right) v_\eta\right]_{BC}$$
$$+ \frac{\mu_{\text{avg}}}{\Omega'}\left[\left(\frac{4}{3}\Delta y_{BC} y_\eta + \Delta x_{BC} x_\eta\right) u_\xi + \left(\frac{2}{3}\Delta y_{BC} x_\eta - \Delta x_{BC} y_\eta\right) v_\xi\right]_{BC} \qquad (3.11)$$

where

$$x_\xi = \Delta x_{CB}$$
$$y_\xi = \Delta y_{CB}$$
$$x_\eta = \Delta x_{EF}$$
$$y_\eta = \Delta y_{EF}$$

With a uniformly spaced computational domain ($\Delta\xi = \Delta\eta = 1$), Φ_{BC} in equation (3.11) is the same as Φ_{BC} in equation (3.10), except for the area factor. For a Cartesian mesh, the expressions for Φ_{BC} in equations (3.9), (3.10), and (3.11) are equivalent. If the streamwise-like differences associated with the viscous flux quantities are neglected, which is the thin-layer Navier-Stokes assumption, only the terms inside the first set of brackets are retained.

Note that with the thin-layer formulation, there are viscous contributions to the fluxes at faces BC and DA only. The following vector approximates the integrand of the right side of equation (3.1) at cell faces BC and DA:

$$\Phi_l = \begin{bmatrix} 0 \\ \tau_1 \\ \tau_2 \\ u_{\text{avg}}\tau_1 + v_{\text{avg}}\tau_2 + \tilde{Q} \end{bmatrix}_l$$

where

$$\tau_1 = \frac{\mu_{\text{avg}}}{\Omega_{\text{avg}}}\left(\phi_1 u_\eta - \phi_2 v_\eta\right)$$

$$\tau_2 = \frac{\mu_{\text{avg}}}{\Omega_{\text{avg}}}\left(\phi_3 v_\eta - \phi_2 u_\eta\right)$$

$$\tilde{Q} = \frac{\mu_{\text{avg}}}{Pr\,\Omega_{\text{avg}}}\left(\frac{\gamma}{\gamma - 1}\right)\phi_4 T_\eta$$

$$\phi_1 = \frac{4}{3}y_\xi^2 + x_\xi^2$$

$$\phi_2 = \frac{1}{3}x_\xi y_\xi$$

$$\phi_3 = \frac{4}{3}x_\xi^2 + y_\xi^2$$

$$\phi_4 = x_\xi^2 + y_\xi^2$$

Unless otherwise indicated in the text, the thin-layer form of the equations is solved.

Significant differences in the numerical solutions have not been observed when applying the three methods for approximating the diffusive terms. Notable differences in the numerical solutions were not expected when solving the Navier-Stokes (thin-layer or full) equations on sufficiently smooth meshes (i.e., meshes without kinks or sudden jumps in mesh intervals). In this paper the integration path of Martinelli (ref. 27) is used in the finite-volume method for computing the viscous fluxes. With this choice of integration path (ref. 27), the mean values of the viscous stresses for a given cell edge are obtained at the midpoint of the edge, even when there is a kink in the grid. This is not true for the path used in equation (3.9). Also, with the integration path of equation (3.10), there are fewer arithmetic operations required than with the path of equation (3.9).

Theoretical estimates of the order of accuracy of the cell-averaged scheme are now introduced based on one-dimensional (1-D) analysis using Taylor-series expansions. Consider the coordinate grid around the location denoted by the index i (fig. 3). Let ϕ be a test function. The numerical values of the first and second derivatives of this function are then given by

$$(\phi_x)_{\text{num}} = \frac{1}{2}\phi_x\frac{\Delta x_+ + \Delta x_-}{\Delta x} + \frac{1}{4}\phi_{xx}\frac{\Delta x_+^2 - \Delta x_-^2}{\Delta x} + O(\Delta x^2) \tag{3.12}$$

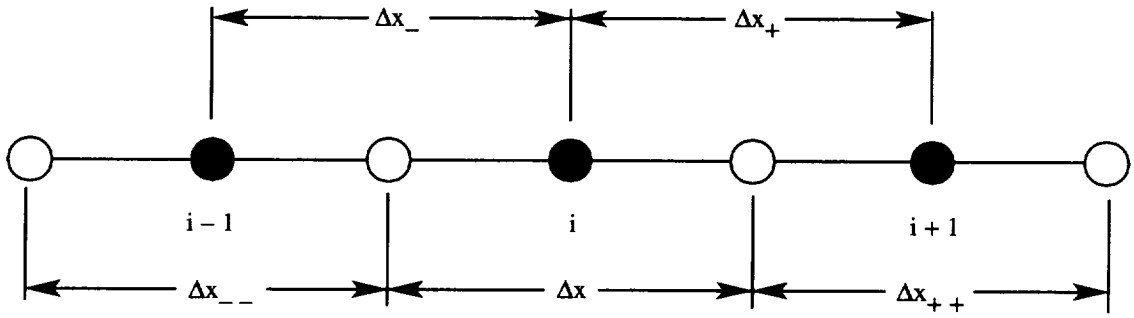

Figure 3. One-dimensional discretization for three-point cell-centered scheme.

and

$$(\phi_{xx})_{\text{num}} = \frac{1}{2}\phi_{xx}\frac{\Delta x_+ \Delta x_-}{\Delta x} + \frac{1}{6}\phi_{xxx}\frac{\Delta x_+^2 - \Delta x_-^2}{\Delta x}$$

$$+ \frac{1}{24}\phi_{xxxx}\frac{\Delta x_+^3 + \Delta x_-^3}{\Delta x} + O(\Delta x^3) \tag{3.13}$$

respectively, where the derivatives in the expansions are evaluated at i. The approximations of equations (3.12) and (3.13) are zeroth-order accurate on arbitrarily stretched meshes. However, assuming a constant stretching factor of the grid (i.e., $\beta = \Delta x_{++}/\Delta x = \text{constant}$), the following relations are obtained:

$$\left.\begin{aligned} \Delta x_{--} &= \Delta x\,\frac{1}{\beta} \\ \Delta x_{-} &= \frac{1}{2}\Delta x\left(1 + \frac{1}{\beta}\right) \\ \Delta x_{++} &= \Delta x\,\beta \\ \Delta x_{+} &= \frac{1}{2}\Delta x\,(1+\beta) \end{aligned}\right\} \tag{3.14}$$

For viscous flows, grids with constant stretching factor β are often used. If these grids are refined by doubling the number of points, then

$$\beta_f = \sqrt{\beta_c} < 1 + \frac{\beta_c - 1}{2}$$

where $\beta \geq 1$ and the subscripts f and c refer to fine and coarse grids, respectively. To estimate the error reduction when refining the stretched mesh, the approximation

$$\beta \approx 1 + C_\beta\,\Delta x \tag{3.15}$$

is used. Then, if the quantities in equations (3.14) and (3.15) are substituted into equations (3.12) and (3.13), respectively, the result is

$$(\phi_x)_{\text{num}} = \phi_x + \frac{1}{4}\phi_x\,(C_\beta\,\Delta x)^2 + \frac{1}{2}C_\beta\phi_{xx}\,\Delta x^2 + O(\Delta x^2) \tag{3.16}$$

and

$$(\phi_{xx})_{\text{num}} = \phi_{xx} + \frac{1}{4}\phi_{xx}\,(C_\beta\,\Delta x)^2 + \frac{1}{3}C_\beta\phi_{xxx}\,\Delta x^2 + \frac{1}{12}\phi_{xxxx}\,\Delta x^2 + O(\Delta x^3) \qquad (3.17)$$

respectively, for $\Delta x << 1$. Thus, second-order accuracy is achieved for the inviscid and viscous terms in the flow equations on smoothly stretched meshes. Additional discussion of accuracy is found in reference 28.

4. Artificial Dissipation

The basic finite-volume scheme described in section 3 contains no dissipative terms in the case of inviscid flows. To prevent oscillations near shock waves or stagnation points, artificial dissipation terms are added to the governing discrete equations. The introduction of appropriate dissipation in the vicinity of shock waves satisfies an entropy condition. In gas dynamics, an entropy condition can be the second law of thermodynamics, which states that the physical entropy cannot decrease. The entropy condition guarantees the uniqueness of weak solutions (i.e., solutions containing shock waves) and thus ensures a physically correct solution. (See ref. 29 for further discussion.)

Another type of dissipation term is added to the discrete flow equations. This term is included to provide background dissipation, which is important for converging the numerical scheme that will be used to compute flow solutions. These dissipation terms also prevent odd-even point decoupling (i.e., creation of sawtooth, or plus-minus waves, with wavelength of two times the mesh spacing). For viscous flows, dissipative properties are present because of diffusive terms. However, because of the nonlinearity of the equations of motion, the physical dissipation may not be sufficient to guarantee stability, especially for the highly stretched meshes generally used to resolve the steep gradients in shear layers. Thus, artificial dissipation is also included in viscous regions to maintain the stability and robustness of the numerical procedure.

In this section some historical information regarding the form of the artificial (or numerical) dissipation model used with many central difference schemes is discussed. This discussion describes how the model evolved, and provides a rudimentary understanding of the model. Next, the basic dissipation formulation and various modifications that have been investigated are discussed. Boundary-point difference stencils are required for the dissipation model. Several stencils are considered and analyzed. Next, the intimate connection between the formulation for an upwind scheme and a central difference scheme is examined, establishing a foundation for a matrix dissipation model. Section 4.6 presents the matrix dissipation model currently used. This model relies upon characteristic decomposition of a flux vector.

4.1. Development of Dissipation Form

To simplify the historical notes in this section, consider the 1-D system of hyperbolic equations $(\partial\mathbf{W}/\partial t) + (\partial\mathbf{F}/\partial x) = 0$, where $\mathbf{W}$ and $\mathbf{F}$ are three-component state and flux vectors, respectively. Let the 1-D domain be partitioned by intervals defined by $\Delta x = x_{i+1/2} - x_{i-1/2}$, where the indices refer to interface points for adjacent intervals. Suppose the Lax-Wendroff scheme is applied as follows:

$$\mathbf{W}^{n+1} = \mathbf{W}^n - \tau(\mathbf{F}_{i+1/2} - \mathbf{F}_{i-1/2}) \qquad (4.1.1)$$

where the superscript n indicates time level, $\tau = \Delta t/\Delta x$, and the interface flux is

$$\mathbf{F}_{i+1/2} = \mathbf{F}^{LW}_{i+1/2} = \frac{1}{2}(\mathbf{F}_i + \mathbf{F}_{i+1}) - \frac{1}{2}\tau A^2_{i+1/2}(\mathbf{W}_{i+1} - \mathbf{W}_i) \qquad (4.1.2)$$

with A representing the flux Jacobian matrix (an element $A_{jk} = \partial F_j / \partial W_k$). All quantities are evaluated at time level n unless noted otherwise.

In the initial work of computing flows with shock waves by using the Lax-Wendroff scheme, the solutions contained oscillations in the vicinity of the shock wave. Then, Von Neumann and Richtmyer (ref. 30) introduced an additional dissipation term to remove shock wave oscillations. Including this term, equation (4.1.2) is rewritten as

$$\mathbf{F}_{i+1/2} = \mathbf{F}^{LW}_{i+1/2} - d^{(2)}_{i+1/2}(\mathbf{W}_{i+1} - \mathbf{W}_i)$$

or in the continuum

$$\mathbf{F} = \mathbf{F}^* - \Delta x \, d^{(2)} \frac{\partial \mathbf{W}}{\partial x} = \mathbf{F}^* - \mathbf{D}^{(2)}$$

where $\mathbf{F}^*$ is the physical flux function. The term $d^{(2)}$ is often called an artificial (or numerical) viscosity and plays the role of a control function. Hirsch (ref. 29) showed that the form of $\mathbf{D}^{(2)}$ considered by Von Neumann and Richtmyer (ref. 30) can be written for a system as

$$\mathbf{D}^{(2)} = \varepsilon^{(2)} \Delta x^2 \Psi \left| \frac{\partial \mathbf{W}}{\partial x} \right| \frac{\partial \mathbf{W}}{\partial x} \tag{4.1.3}$$

where the coefficients $\Psi \geq 0$ and can depend on the mesh index i, and each element of $\mathbf{D}^{(2)}$ depends on the corresponding element of $\mathbf{W}$. Now, suppose the flux difference is computed by $(\mathbf{F}_{i+1/2} - \mathbf{F}_{i-1/2})$ in equation (4.1.1) using equation (4.1.3). Then, in the case of the continuum, the total dissipation is given by

$$\mathbf{D}^{(2)}_{\text{tot}} = \varepsilon^{(2)} \Delta x^3 \frac{\partial}{\partial x} \left(\Psi \left| \frac{\partial \mathbf{W}}{\partial x} \right| \frac{\partial \mathbf{W}}{\partial x} \right) \tag{4.1.4}$$

This dissipation term can be characterized as third order. However, Δx^{-1} appears in equation (4.1.1), so effectively, equation (4.1.4) defines a second-order term.

In 1975, MacCormack and Baldwin (ref. 31) appended a dissipation term for shock capturing to the 1969 scheme of MacCormack (a two-step Lax-Wendroff type scheme (ref. 32)). This dissipation term was introduced to remove oscillations at shock waves caused by the spatial differencing of the MacCormack scheme. This dissipation term is proportional to a second difference of the pressure and is given by

$$\mathbf{D}^{(2)} = \varepsilon^{(2)} \Delta x^3 \frac{|u| + c}{4p} \left| \frac{\partial^2 p}{\partial x^2} \right| \frac{\partial \mathbf{W}}{\partial x} \tag{4.1.5}$$

In smooth regions of a flow field, the product of Δx^{-1} and the dissipative flux balance $\mathbf{D}^{(2)}_{\text{tot}}$ is third order, while the product of Δx^{-1} and $\mathbf{D}^{(2)}_{\text{tot}}$ is first order in the neighborhood of a shock wave.

As indicated, numerical dissipation is not only important in capturing discontinuities, it is also generally required to maintain stability and provide necessary background dissipation for convergence. In 1976, Beam and Warming (ref. 2) added to the explicit side of their implicit approximate factorization (AF) scheme with what they called a fourth-order dissipation term to damp high-frequency error components. With the Lax-Wendroff scheme, this fourth-order dissipation term would appear as

$$\mathbf{D}^{(4)}_{\text{tot}} = -\varepsilon^{(4)} \Delta x^4 \frac{\partial^4 \mathbf{W}}{\partial x^4} \tag{4.1.6}$$

It seems more appropriate to define the order of the dissipation relative to the spatial discretization of the physical terms in the flow equations. So when considering $\Delta x^{-1}\mathbf{D}_{tot}^{(4)}$, the dissipation term is third order. At any rate, a fourth-difference dissipation is included, and along with the second-difference term of equation (4.1.5), provides the basic ingredients for constructing a complete, adaptive dissipation model. The second-difference term of equation (4.1.5) allows shock capturing without oscillations, while the linear fourth-difference term of equation (4.1.6) provides the important background dissipation. The critical element missing is a switching function that would turn on the appropriate dissipation form in a region and turn off the dissipation form that is not the desirable type (i.e., near shocks $\mathbf{D}^{(2)}$ of eq. (4.1.5) should dominate, with $\mathbf{D}^{(4)}$ of eq. (4.1.6) negligible, while in smooth regions, $\mathbf{D}^{(4)}$ of eq. (4.1.6) should dominate, with $\mathbf{D}^{(2)}$ of eq. (4.1.5) negligible). In section 4.2, the dissipation model that adds a switching function to the two basic types of dissipation terms just discussed is described.

4.2. Dissipation Model

To permit a complete description of the dissipation model, the two-dimensional Euler equations are now considered. The dissipation is based on the model introduced by Jameson, Schmidt, and Turkel (ref. 1) that defined a suitable switching function (at least for transonic and low supersonic flow) to allow blending of the second and fourth differences. According to the nonlinear model (ref. 1), the quantity $\mathcal{L}_{AD}\mathbf{W}_{i,j}$ in equation (3.2) is expressed as

$$\mathcal{L}_{AD}\mathbf{W}_{i,j} = -(D_\xi^2 - D_\xi^4 + D_\eta^2 - D_\eta^4)\mathbf{W}_{i,j} \tag{4.2.1}$$

where (ξ, η) are arbitrary, curvilinear coordinates, and

$$D_\xi^2\mathbf{W}_{i,j} = \nabla_\xi \left[(\lambda_{i+1/2,j}\,\varepsilon^{(2)}_{i+1/2,j})\,\Delta_\xi\right]\mathbf{W}_{i,j} \tag{4.2.2}$$

$$D_\xi^4\mathbf{W}_{i,j} = \nabla_\xi \left[(\lambda_{i+1/2,j}\,\varepsilon^{(4)}_{i+1/2,j})\,\Delta_\xi\,\nabla_\xi\,\Delta_\xi\right]\mathbf{W}_{i,j} \tag{4.2.3}$$

where i and j are indices (for a cell center) associated with the ξ and η directions, respectively, and Δ_ξ and ∇_ξ are forward and backward difference operators in the ξ direction, respectively. The definitions are similar in the η direction. The variable scaling factor λ is defined as

$$\lambda_{i+1/2,j} = \frac{1}{2}\left[(\lambda_\xi)_{i,j} + (\lambda_\xi)_{i+1,j} + (\lambda_\eta)_{i,j} + (\lambda_\eta)_{i+1,j}\right] \tag{4.2.4}$$

where λ_ξ and λ_η are the largest eigenvalues in absolute value (i.e., spectral radii) of the flux Jacobian matrices associated with the Euler equations. These spectral radii are given by

$$\left.\begin{aligned}\lambda_\xi &= |uy_\eta - vx_\eta| + c\sqrt{y_\eta^2 + x_\eta^2} \\ \lambda_\eta &= |vx_\xi - uy_\xi| + c\sqrt{x_\xi^2 + y_\xi^2}\end{aligned}\right\} \tag{4.2.5}$$

where u and v are Cartesian velocity components, and c is the speed of sound. The coefficients $\varepsilon^{(2)}$ and $\varepsilon^{(4)}$ use the pressure as a sensor for shocks and stagnation points, respectively, and are defined as

$$\left.\begin{aligned} \varepsilon^{(2)}_{i+1/2,j} &= \kappa^{(2)} \max(\nu_{i-1,j}, \nu_{i,j}, \nu_{i+1,j}, \nu_{i+2,j}) \\ \nu_{i,j} &= \left| \frac{p_{i-1,j} - 2p_{i,j} + p_{i+1,j}}{p_{i-1,j} + 2p_{i,j} + p_{i+1,j}} \right| \\ \varepsilon^{(4)}_{i+1/2,j} &= \max\left[0, (\kappa^{(4)} - \varepsilon^{(2)}_{i+1/2,j})\right] \end{aligned}\right\} \tag{4.2.6}$$

where typical values for the constants $\kappa^{(2)}$ and $\kappa^{(4)}$ are in the ranges 1/4 to 1/2 and 1/64 to 1/32, respectively. This paper shall refer to equations (4.2.1) and (4.2.6) as the Jameson, Schmidt, Turkel (JST) scheme (or dissipation model), and shall designate ν as the JST switch. It should be mentioned that in reference 1, the coefficient $\varepsilon^{(2)}_{i+1/2,j} = \kappa^{(2)} \max(\nu_{i,j}, \nu_{i+1,j})$. The switching function ν can be interpreted as a limiter, in the sense that it activates the second-difference contribution at extrema and switches off the fourth-difference term. Moreover, at shock waves, the dissipation is first order, and a first-order upwind scheme is produced for a scalar equation. In smooth regions of the flow field the dissipation is third order.

Thus, two different dissipation mechanisms are at work, and the switch determines which one is active in any given region. For smooth flows, ν is small, and the dissipation terms consist of a linear fourth difference that damps the high frequencies the central difference scheme does not damp. This dissipation is useful mainly for achieving a steady state and is less important for time-dependent problems. In the neighborhood of large gradients in pressure, ν becomes large and switches on the second-difference viscosity while simultaneously reducing the fourth-difference dissipation. This viscosity is needed mainly to introduce an entropy condition so that the correct shock relationships are satisfied and to prevent oscillations near discontinuities. For subsonic steady-state flow, this viscosity can be turned off by choosing $\epsilon^{(2)} = 0$.

The isotropic scaling factor of equation (4.2.4) is generally satisfactory for inviscid flow problems when typical inviscid flow meshes (i.e., cell aspect ratio $O(1)$) are used. The isotropic scaling factor can create too much numerical dissipation in cases of meshes with high-aspect-ratio cells. The adverse effect of high-aspect-ratio cells is an important consideration for high Reynolds number viscous flows, where a mesh providing appropriate spatial resolution can have cell aspect ratios $O(10^3)$. In an effort to improve this cell aspect ratio situation and obtain sharper shock resolution on a given grid, Swanson and Turkel (ref. 19) replaced the isotropic scaling factor of equation (4.2.4) with the anisotropic scaling factor

$$\lambda_{i+1/2,j} = \frac{1}{2}\left[(\lambda_\xi)_{i,j} + (\lambda_\xi)_{i+1,j}\right] \tag{4.2.7}$$

A similar scaling is used in the η direction.

The anisotropic scaling idea was motivated by the scaling of dissipation occurring in dimensionally split, upwind schemes (i.e., the flux vector split scheme (ref. 12) and the approximate Riemann solver (ref. 13)). Anisotropic scaling is often referred to as individual eigenvalue scaling. While the accuracy is improved with equation (4.2.7), particularly with respect to shock resolution, individual eigenvalue scaling in the streamwise (ξ) direction can be too severe for a standard multigrid algorithm. Moreover, the effectiveness of the multigrid driving scheme in damping high frequencies in the ξ direction can be significantly diminished, resulting in a much slower convergence rate.

An alternative to the individual eigenvalue scaling was proposed by Martinelli (ref. 27), and considered by Swanson and Turkel (ref. 19). This modified scaling factor, which is a function of mesh-cell-aspect ratio, is defined as

$$\lambda_{i+1/2,j} = \frac{1}{2}[(\bar{\lambda}_\xi)_{i,j} + (\bar{\lambda}_\xi)_{i+1,j}] \tag{4.2.8}$$

where

$$\left.\begin{aligned} (\bar{\lambda}_\xi)_{i,j} &= \phi_{i,j}(r)\,(\lambda_\xi)_{i,j} \\ \phi_{i,j}(r) &= 1 + r^{\zeta}_{i,j} \end{aligned}\right\} \tag{4.2.9}$$

Here, r is the ratio λ_η/λ_ξ, and the exponent ζ is generally taken to be between 1/2 and 2/3. In the normal direction (η), $(\bar{\lambda}_\eta)_{i,j} = \phi_{i,j}(r^{-1})(\lambda_\eta)_{i,j}$ is defined. Thus, the scaling factor of equation (4.2.8) is bounded from below by equation (4.2.7), and bounded from above by equation (4.2.4). As demonstrated in references 19 and 20, the scaling factor of equation (4.2.8) produces a significant improvement in accuracy for high-aspect-ratio meshes, and permits good convergence rates with a multigrid method. The scheme in this paper uses this modified scaling factor.

The impact of the dissipation form on the energy of a system of flow equations is now examined. For simplicity, consider the 1-D, time-dependent Euler equations, with numerical dissipation terms given by

$$J^{-1}\frac{\partial \mathbf{W}}{\partial t} + \frac{\partial \mathbf{F}}{\partial \xi} = D_\xi^2 \mathbf{W} - D_\xi^4 \mathbf{W} \tag{4.2.10}$$

where

$$D_\xi^2 \mathbf{W} = \frac{\partial}{\partial \xi}\left(\bar{\varepsilon}^{(2)}\frac{\partial \mathbf{W}}{\partial \xi}\right)$$

$$D_\xi^4 \mathbf{W} = \frac{\partial}{\partial \xi}\left(\bar{\varepsilon}^{(4)}\frac{\partial^3 \mathbf{W}}{\partial \xi^3}\right)$$

and $\bar{\varepsilon}^{(2)} = \lambda\varepsilon^{(2)}$, $\bar{\varepsilon}^{(4)} = \lambda\varepsilon^{(4)}$, and J^{-1} is the inverse transformation Jacobian. Form the inner products of $\mathbf{W}^T$, with T denoting transpose, and both sides of equation (4.2.10), and then integrate over a domain Ω. After integration by parts and neglecting boundary terms, the equation

$$\frac{1}{2}\frac{\partial}{\partial t}\|\mathbf{W}\|^2 = \text{flux term} + J\left[I^{(2)} - I^{(4)}\right] \tag{4.2.11}$$

is obtained, where

$$\|\mathbf{W}\|^2 = \int_\Omega \mathbf{W}^2\, d\xi$$

$$I^{(2)} = -\int_\Omega \bar{\varepsilon}^{(2)}\left(\frac{\partial \mathbf{W}}{\partial \xi}\right)^2 d\xi$$

$$I^{(4)} = -\int_\Omega \bar{\varepsilon}^{(4)}\left(\frac{\partial^2 \mathbf{W}}{\partial \xi^2}\right)^2 d\xi + \int_\Omega \frac{\partial \bar{\varepsilon}^{(4)}}{\partial \xi}\left(\frac{\partial \mathbf{W}^T}{\partial \xi}\right)\cdot\left(\frac{\partial^2 \mathbf{W}}{\partial \xi^2}\right) d\xi$$

The second-difference dissipation term $I^{(2)}$ only decreases the L^2 norm of the solution vector (i.e., it decreases the energy of the system), and thus, is strictly dissipative. The fourth-difference dissipation term $I^{(4)}$ contains a dispersive part and a dissipative contribution.

An alternative form for the third-order dissipation term (the last term in eq. (4.2.10)) is

$$D_\xi^4 \mathbf{W} = \frac{\partial^2}{\partial \xi^2}\left(\bar{\varepsilon}^{(4)} \frac{\partial^2 \mathbf{W}}{\partial \xi^2}\right)$$

which can be written in the discrete case as

$$D_\xi^4 \mathbf{W}_i = \nabla_\xi \Delta_\xi \left[(\lambda_i \varepsilon_i^{(4)}) \nabla_\xi \Delta_\xi\right] \mathbf{W}_i \tag{4.2.12}$$

This modified form produces only dissipative contributions. If $\mathbf{Q}_i = \lambda_i \varepsilon_i^{(4)} \nabla_\xi \Delta_\xi \mathbf{W}_i$, then $\nabla_\xi \Delta_\xi \mathbf{Q}_i = \delta \mathbf{Q}_{i+1/2} - \delta \mathbf{Q}_{i-1/2}$, where δ is the standard, centered-difference operator. Therefore, the form of equation (4.2.12) is conservative, provided λ and $\varepsilon^{(4)}$ are evaluated at the cell centers rather than at the cell faces. In reference 19, numerical tests were performed with the dissipation terms of equations (4.2.3) and (4.2.12). For steady state, there seems to be no consistent benefit for either convergence or accuracy when using the form of equation (4.2.12). Based on these results, the form of equation (4.2.3) is still used. However, for unsteady flows, equation (4.2.12) may offer an advantage because of the absence of dispersive effects that can cause phase errors.

Until now, a scalar viscosity in which the viscosity is based on differences of the same quantity advanced in time has been considered. (See eq. (4.2.10).) The disadvantage is that the total enthalpy is no longer constant in the steady state, even when total enthalpy should be identically constant for the inviscid equations. The total enthalpy is constant for the steady-state Euler equations because the energy equation is a constant multiple of the continuity equation when H is constant. Hence, reference 1 suggests that the dissipation for the energy equation be based on differences of the total enthalpy rather than the total energy. Thus, a typical situation in one dimension is to replace equation (4.2.10) for the energy equation by

$$J^{-1}\frac{\partial \rho E}{\partial t} + \frac{\partial (\rho H u)}{\partial \xi} = D_\xi^2(\rho H) - D_\xi^4(\rho H) \tag{4.2.13}$$

where $\rho H = \rho E + p$. Reference 33 shows that equation (4.2.13) indeed yields a constant total enthalpy, but that the entropy tends to be less accurate than if the dissipation term for the energy equation is based on differences of ρE rather than ρH. Thus, both choices have advantages and disadvantages. The total enthalpy formulation is used in this paper.

4.3. Boundary Treatment of Dissipative Terms

In a cell-centered, finite-volume method, the first and last cells in each coordinate direction are auxiliary cells where the flow equations are usually not solved. The solution in these cells is found by a combination of the given physical boundary conditions and numerical boundary conditions. Thus, there is no difficulty evaluating the second-difference dissipation term at the first or last interior cell in a given coordinate direction. In the case of the fourth-difference dissipation term, the treatment must be modified at the boundaries of the physical domain because only one layer of auxiliary cells is considered. Moreover, the standard five-point difference stencil must be replaced at the first two interior mesh cells relative to a wall boundary; thus, one-sided or one-sided biased stencils are used at these cells. The dissipative character of these stencils is important because it influences both stability and accuracy. For example, if the dissipation is too large at a solid boundary, an artificial boundary layer is created in an inviscid flow, and the effective Reynolds number for a viscous flow is altered.

4.3.1. Boundary-point operators. In this section, the two types of discrete boundary-point operators (difference stencils) used with the present scheme for solid surfaces are defined.

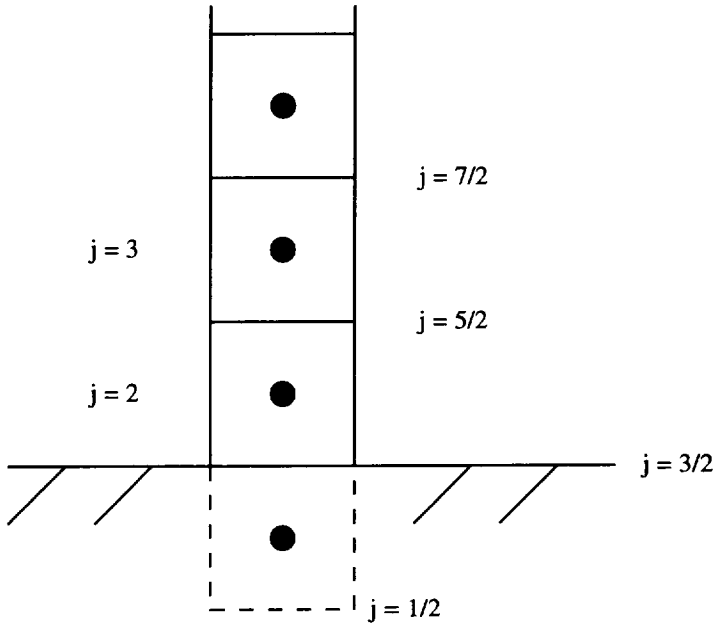

Figure 4. Boundary-point dissipation.

Next, these operators are evaluated by applying a local mode analysis. In addition, this section shows how this local mode analysis can provide an evaluation of candidate boundary-point operators once a basis for comparison is established. A more complete analysis for the boundary-point operators is based on the dissipation matrix for the system of difference equations approximating the governing flow equations. Sometimes the dissipation matrix can be characterized analytically. In general, the eigenvalues of the dissipation matrix must be determined. The approach for analyzing the dissipation stencils is discussed.

Consider the total dissipation resulting from a numerical flux balance for a mesh cell in a particular coordinate direction. Let w_j and d_j denote a component of the solution vector $\mathbf{W}$ and the corresponding total dissipation, respectively. The index j indicates the mesh cell being considered. Let $d_{j+1/2}$ and $d_{j-1/2}$ represent the dissipative fluxes at the cell interfaces $j+1/2$ and $j-1/2$, respectively (fig. 4). At a cell interface (for example, $j+1/2$), let $(\Delta w)_{j+1/2}$ denote the difference between the solution for the adjacent cells $(w_{j+1} - w_j)$. For simplicity, assume $\lambda\varepsilon^{(4)} = 1$. Then, for any cell j

$$d_j = d_{j+1/2} - d_{j-1/2} \tag{4.3.1}$$

where the dissipative fluxes are

$$d_{j+1/2} = (\Delta w)_{j+3/2} - 2(\Delta w)_{j+1/2} + (\Delta w)_{j-1/2}$$
$$d_{j-1/2} = (\Delta w)_{j+1/2} - 2(\Delta w)_{j-1/2} + (\Delta w)_{j-3/2}$$

Thus

$$d_j = (\Delta w)_{j+3/2} - 3(\Delta w)_{j+1/2} + 3(\Delta w)_{j-1/2} - (\Delta w)_{j-3/2} \tag{4.3.2}$$

or

$$d_j = w_{j+2} - 4w_{j+1} + 6w_j - 4w_{j-1} + w_{j-2}$$

Consider the first two interior cells adjacent to a solid boundary (fig. 4). The total dissipation for these cells is denoted by d_2 and d_3. At $j = 2$, a value for $(\Delta w)_{1/2}$ must be determined because

$(\Delta w)_{1/2}$ is undefined. Also, in this formulation of the boundary-point dissipation stencil, no functional dependence on w_1 is desired because w_1 is outside the domain. Hence, a value for $(\Delta w)_{3/2}$ must also be provided. If

$$\left.\begin{aligned}(\Delta w)_{1/2} &= (\Delta w)_{5/2} \\ (\Delta w)_{3/2} &= (\Delta w)_{5/2}\end{aligned}\right\} \tag{4.3.3}$$

then equation (4.3.2) gives

$$d_2 = w_4 - 2w_3 + w_2 \tag{4.3.4}$$

$$d_3 = w_5 - 4w_4 + 5w_3 - 2w_2 \tag{4.3.5}$$

These boundary stencils are fairly standard and are used for inviscid flow calculations. An alternative form, which reduces the sensitivity to solid-surface, normal mesh spacing for viscous flow calculations without compromising stability or convergence, is obtained by replacing $(\Delta w)_{1/2}$ with $(\Delta w)_{1/2} = 2(\Delta w)_{3/2} - (\Delta w)_{5/2}$ and leaving $(\Delta w)_{3/2}$ unchanged. This form is given by

$$d_2 = w_4 - 3w_3 + 3w_2 - w_1 \tag{4.3.6}$$

$$d_3 = w_5 - 4w_4 + 6w_3 - 4w_2 + w_1 \tag{4.3.7}$$

For turbulent flows, this boundary dissipation formulation (eq. (4.3.7)) is advantageous when the mesh is fine enough to adequately represent the laminar sublayer region of the boundary layer (i.e., at least two points are inside the sublayer). For coarse meshes, this treatment of the dissipation can be less accurate than the zeroth-order extrapolation of equations (4.3.3).

*4.3.2. **Local mode analysis.*** A local mode analysis is now considered to evaluate the relative damping behavior of boundary-cell difference operators. For comparison purposes, the interior fourth difference is first characterized. Taking a Fourier transform of equation (4.3.2) yields $z_j(\theta) = 4(\cos\theta - 1)^2$, where $z_j(\theta)$ is the Fourier symbol of the transformed d_j, and θ is the product of the wave number and the mesh spacing. Then, $z_j(\theta) \sim \theta^4$ for small θ, and $z_j(\pi) = 16$. The dissipation of long wavelengths is dictated by the behavior of $z_j(\theta)$ at small θ, and the dissipation of short wavelengths is governed by $z_j(\pi)$. As mentioned initially in this section, this simple analysis assumes that $\lambda\varepsilon^{(4)} = 1$. In practice, the coefficient $\kappa^{(4)}$ used in the evaluation of $\varepsilon^{(4)}$ for the fourth-difference dissipation affects the behavior of the boundary dissipation stencil. The coefficient $\kappa^{(4)}$ is chosen such that the highest frequency is highly damped according to a stability analysis using the interior-point stencil. This is important for a multigrid method and will be discussed in section 7.3. Near a boundary, the dissipation should behave in a similar manner. In this dissipation model, the same value of $\kappa^{(4)}$ used for interior points of the domain is also used near a boundary.

A general form of the difference stencils at $j = 2, 3$ can be written as

$$d_j = \alpha w_{j+2} - \beta w_{j+1} + (\beta + \gamma - \alpha) w_j - \gamma w_{j-1}$$

The associated Fourier symbol is given by

$$\begin{aligned} z_j(\theta) = {} & [\beta + \gamma - 2\alpha(1 + \cos\theta)](1 - \cos\theta) \\ & + i(\gamma - \beta + 2\alpha\cos\theta)\sin\theta \end{aligned}$$

For small θ this Fourier symbol is replaced by

$$z_j(\theta) = (\beta + \gamma - 4\alpha)\frac{\theta^2}{2} + \alpha\frac{\theta^4}{2} + i(2\alpha - \beta + \gamma)\theta - i\alpha\theta^3 \tag{4.3.8}$$

and at $\theta = \pi$ reduces to

$$z_j(\pi) = 2(\beta + \gamma) \tag{4.3.9}$$

In the case of equation (4.3.4)

$$z_2(\theta) \approx \frac{\theta^4}{2} - i\theta^3 \tag{4.3.10}$$

for small θ, with $z_2(\pi) = 4$, and for equation (4.3.5)

$$z_3(\theta) \approx \frac{\theta^2}{2} - i\theta^3 \tag{4.3.11}$$

for small θ, with $z_3(\pi) = 12$. Note that $z_2(\theta)$ and $z_3(\theta)$ are not real. Thus, there are both dissipation and dispersion near the boundary. For the stencil of equation (4.3.6)

$$z_2(\theta) \approx \frac{\theta^4}{2} - i\theta^3 \tag{4.3.12}$$

for small θ, with $z_2(\pi) = 8$, and for the stencil of equation (4.3.7)

$$z_3(\theta) \approx \theta^4 \tag{4.3.13}$$

for small θ, with $z_3(\pi) = 16$. Comparing equations (4.3.10) and (4.3.12), which correspond to the stencils of equations (4.3.4) and (4.3.6), respectively, shows that both stencils behave the same for the long wavelengths, while equation (4.3.12) is twice as dissipative for the short wavelengths. At $j = 3$, the stencil corresponding to equation (4.3.13) is fourth order on the long wavelengths, whereas the stencil associated with equation (4.3.11) is only second order. In addition, the symbol of equation (4.3.13) is more dissipative on the short wavelengths. Thus, the improved accuracy and high-frequency damping observed for the stencils of equations (4.3.6) and (4.3.7) in practice is substantiated with this simple analysis.

The method of combining the simple local mode analysis with the evaluations just considered to quickly evaluate candidate dissipation stencils can now be shown. Consider a different set of boundary-point stencils. If Δw is taken to represent either the component ρu or ρv of the solution vector $\mathbf{W}$, and the antisymmetry constraint $(\Delta w)_{1/2} = (\Delta w)_{5/2}$ is imposed for viscous flows, then equation (4.3.2) gives

$$d_2 = w_4 - 5w_3 + 7w_2 - 3w_1 \tag{4.3.14}$$

$$d_3 = w_5 - 4w_4 + 6w_3 - 4w_2 + w_1 \tag{4.3.15}$$

The Fourier symbols of equation (4.3.14), using equations (4.3.8) and (4.3.9), are

$$z_2(\theta) \approx 2\theta^2 \tag{4.3.16}$$

for small θ, with $z_2(\pi) = 16$, and the symbols for equation (4.3.15) are the same as given in equation (4.3.13). Comparing equation (4.3.16) with equation (4.3.12) shows that the highest frequency is damped better with the proposed stencil, but that the proposed stencil is only second

order on the long wavelengths, while the stencil of equation (4.3.6) is fourth order, indicating that better accuracy is obtained with equations (4.3.6) and (4.3.7). The improved accuracy has been verified with numerical experiments (i.e., skin-friction solutions for turbulent airfoil flows have been computed on 160 by 32 meshes and compared with high-density-mesh results).

4.4. Matrix Analysis

The associated dissipation matrix is examined to determine the numerical dissipativity of a discrete system of equations, such as equation (3.2). For simplicity, consider the 1-D system

$$\frac{d\mathbf{w}}{dt} = D^{(4)}\mathbf{w} \tag{4.4.1}$$

where $\mathbf{w}$ is a discrete solution vector, and $D^{(4)}$ is a dissipation matrix corresponding to fourth-difference terms. Taking the inner product $\mathbf{w}^T$ (the transpose of $\mathbf{w}$) with each side of equation (4.4.1), obtain $1/2\ d\mathbf{w}^2/dt = \mathbf{w}^T D^{(4)}\mathbf{w}$. If the quadratic form $\mathbf{w}^T D^{(4)}\mathbf{w}$ is nonpositive definite, then the matrix $D^{(4)}$ is strictly dissipative. Moreover, the energy of the system is nonincreasing. Assume there are boundaries at $j = 3/2$ and $j = jl + 1/2$, and assume $j = 2$ and $j = jl$ are the indices for the first and last interior points, respectively. Apply the boundary point stencils of equations (4.3.4) and (4.3.5) at the first two interior cell centers at both boundaries, and the standard stencil everywhere else. The resulting dissipation matrix is given by

$$D^{(4)} = \begin{bmatrix}
-1 & 2 & -1 & & & & & & \\
2 & -5 & 4 & -1 & & & & & \\
-1 & 4 & -6 & 4 & -1 & & & & \\
0 & -1 & 4 & -6 & 4 & -1 & & & \\
 & & \ddots & \ddots & \ddots & \ddots & \ddots & & \\
 & & & -1 & 4 & -6 & 4 & -1 & 0 \\
 & & & & -1 & 4 & -6 & 4 & -1 \\
 & & & & & -1 & 4 & -5 & 2 \\
 & & & & & & -1 & 2 & -1
\end{bmatrix} \tag{4.4.2}$$

and the corresponding solution vector is given by

$$\mathbf{w} = \begin{bmatrix} w_2 & w_3 & w_4 & w_5 & \dots & w_{jl-2} & w_{jl-1} & w_{jl} \end{bmatrix}^T$$

Then

$$\mathbf{w}^T D^{(4)}\mathbf{w} = -\sum_{j=3}^{jl-1} \left(w_{j+1} - 2w_j + w_{j-1}\right)^2 \leq 0 \tag{4.4.3}$$

Thus, $D^{(4)}$ is strictly dissipative. This same result is obtained by Eriksson and Rizzi (ref. 34). For a 10 by 10 matrix with the form of equation (4.4.2), Pulliam (ref. 35) obtains two zero eigenvalues. Ideally, $D^{(4)}$ should have no zero eigenvalues, since zero eigenvalues can possibly produce undamped modes that cause instabilities (ref. 35).

Pulliam (ref. 35) recommends applying a stencil with the weights of equation (4.3.5) at the first interior cell, and a standard stencil with the weights of equation (4.3.7) at the second interior cell. Then

$$D^{(4)} = \begin{bmatrix} -5 & 4 & -1 & & & & & & \\ 4 & -6 & 4 & -1 & & & & & \\ -1 & 4 & -6 & 4 & -1 & & & & \\ 0 & -1 & 4 & -6 & 4 & -1 & & & \\ & & \ddots & \ddots & \ddots & \ddots & \ddots & & \\ & & & -1 & 4 & -6 & 4 & -1 & 0 \\ & & & & -1 & 4 & -6 & 4 & -1 \\ & & & & & -1 & 4 & -6 & 4 \\ & & & & & & -1 & 4 & -5 \end{bmatrix} \tag{4.4.4}$$

and

$$\mathbf{w}^T D^{(4)} \mathbf{w} = -\sum_{j=3}^{jl-1} (w_{j+1} - 2w_j + w_{j-1})^2 - (w_3 - 2w_2)^2 - (w_{jl-1} - 2w_{jl})^2 \leq 0 \tag{4.4.5}$$

Again, the dissipation matrix is strictly dissipative. Moreover, a 10 by 10 matrix with the structure of equation (4.4.4) has zero eigenvalues (ref. 35). However, indications are that for a cell-centered, finite-volume formulation, this boundary-point treatment of the dissipation with the weights of equations (4.3.5) and (4.3.7), although appropriate at inflow and outflow boundaries, is generally too dissipative at solid boundaries. Thus the stencils of equations (4.3.4) and (4.3.5) are preferred at a wall boundary.

Now consider the stencils with the weights of equations (4.3.6) and (4.3.7). The dissipation matrix is given by

$$D^{(4)} = \begin{bmatrix} -3 & 3 & -1 & & & & & & \\ 4 & -6 & 4 & -1 & & & & & \\ -1 & 4 & -6 & 4 & -1 & & & & \\ 0 & -1 & 4 & -6 & 4 & -1 & & & \\ & & \ddots & \ddots & \ddots & \ddots & \ddots & & \\ & & & -1 & 4 & -6 & 4 & -1 & 0 \\ & & & & -1 & 4 & -6 & 4 & -1 \\ & & & & & -1 & 4 & -6 & 4 \\ & & & & & & -1 & 3 & -3 \end{bmatrix} \tag{4.4.6}$$

and

$$\mathbf{w}^T D^{(4)} \mathbf{w} = -\sum_{j=3}^{jl-1} (w_{j+1} - 2w_j + w_{j-1})^2 + w_2(w_3 - w_2) - (w_3 - w_2)^2 - (w_{jl-1} - w_{jl})^2 + w_{jl}(w_{jl} - w_{jl-1}) \leq 0 \tag{4.4.7}$$

From the quadratic form of equation (4.4.7), it does not directly follow that $D^{(4)}$ is nonpositive definite, which is generally the case with the quadratic form. If the eigenvalues of a 10 by 10 matrix with the structure of equation (4.4.6) are determined, one is zero and the others are negative. Therefore, the matrix $D^{(4)}$ is nonpositive definite. Although there is one zero eigenvalue, the present scheme performs well using the boundary-point operators associated with equations (4.3.6) and (4.3.7) at solid boundaries when solving viscous flow problems.

4.5. The Upwind Connection

Upwind schemes for solving hyperbolic systems of conservation laws (i.e., Euler equations of gas dynamics) generally rely upon characteristic theory to determine the direction of propagation of information and, thus, the direction required for one-sided differencing approximations of the spatial derivatives. With upwind schemes, shock waves can be captured without oscillations. Thus, a successful artificial dissipation model for a central difference scheme should imitate an upwind scheme in the neighborhood of shocks. The connection between upwind and central difference schemes is now reviewed.

Consider the 1-D scalar wave equation

$$\frac{\partial u}{\partial t} + a\frac{\partial u}{\partial x} = 0$$

with a constant. The first-order upwind scheme can be written as

$$u_j^{n+1} = u_j - a\frac{\Delta t}{\Delta x}\begin{cases} u_{j+1} - u_j & (a < 0) \\ u_j - u_{j-1} & (a > 0) \end{cases} \tag{4.5.1}$$

where all discrete quantities are evaluated at time level $n\,\Delta t$ unless otherwise denoted. The scheme of equation (4.5.1) can be rewritten as

$$u_j^{n+1} = u_j - a\frac{\Delta t}{2\,\Delta x}(u_{j+1} - u_{j-1}) + |a|\frac{\Delta t}{2\,\Delta x}(u_{j+1} - 2u_j + u_{j-1}) \tag{4.5.2}$$

Equation (4.5.2) now contains a central difference term and a second-difference dissipation term. Now consider the system

$$\frac{\partial \mathbf{u}}{\partial t} + A\frac{\partial \mathbf{u}}{\partial x} = 0 \tag{4.5.3}$$

where $\mathbf{u}$ is an N-component vector. The system case can be converted to a scalar system by diagonalizing the N by N matrix A with a similarity transformation $\Lambda = T^{-1}AT$, where the columns of T are the right eigenvectors of A. After diagonalizing equation (4.5.3), and applying the scheme of equation (4.5.2), the first-order upwind scheme is given by

$$\mathbf{u}_j^{n+1} = \mathbf{u}_j - a\frac{\Delta t}{2\,\Delta x}(\mathbf{u}_{j+1} - \mathbf{u}_{j-1}) + |A|\frac{\Delta t}{2\,\Delta x}(\mathbf{u}_{j+1} - 2\mathbf{u}_j + \mathbf{u}_{j-1}) \tag{4.5.4}$$

where

$$\left.\begin{aligned} |A| &= T|\Lambda|T^{-1} \\ \Lambda &= \mathrm{Diag}\,[|\lambda_1| \cdots |\lambda_N|] \end{aligned}\right\} \tag{4.5.5}$$

Note that since A has only three distinct eigenvalues, by using the Cayley-Hamilton theorem, $|A|$ can be expressed as a quadratic polynomial in A. The generalization to a system of conservation laws is as follows:

$$\frac{\partial \mathbf{u}}{\partial t} + \frac{\partial \mathbf{f}}{\partial x} = 0$$

with $\mathbf{f}$ being an N-component flux vector, and

$$\mathbf{u}_j^{n+1} = \mathbf{u}_j - \frac{\Delta t}{2\,\Delta x}(\mathbf{f}_{j+1} - \mathbf{f}_{j-1}) + \frac{\Delta t}{2\,\Delta x}\left[\left|A_{j+1/2}\right|(\mathbf{u}_{j+1} - \mathbf{u}_j) - \left|A_{j-1/2}\right|(\mathbf{u}_j - \mathbf{u}_{j-1})\right] \quad (4.5.6)$$

where the Jacobian matrix $A = \partial \mathbf{f}/\partial \mathbf{u}$, and $|A|$ is defined the same as for equation (4.5.4). The matrix $\left|A_{j+1/2}\right|$ can be computed as either an arithmetic average or a Roe average (ref. 13). For transonic, steady flows the differences are negligible and the simpler arithmetic average is used. Yee (ref. 36) found that the Roe average yields better results for hypersonic flows. The Roe average also seems to give slightly better results for time-dependent problems.

4.6. Matrix Dissipation Model

As indicated in section 4.5, high resolution of shock waves without oscillations can be achieved by closely imitating an upwind scheme in the neighborhood of a shock wave. A key feature of upwind schemes is a matrix evaluation of the numerical dissipation. With this matrix evaluation, the dissipative terms of each discrete equation (associated with a given coordinate direction) are scaled by the appropriate eigenvalues of the flux Jacobian matrix rather than by the spectral radius, as in the JST scheme. Such a matrix dissipation also allows high resolution of wall bounded shear layers (ref. 37). The modifications of the JST dissipation model required to produce the matrix dissipation model currently used are now presented.

Consider the two-dimensional, time-dependent Euler equations in the form

$$\frac{\partial (J^{-1}\mathbf{W})}{\partial t} + \frac{\partial \mathbf{F}}{\partial \xi} + \frac{\partial \mathbf{G}}{\partial \eta} = 0 \quad (4.6.1)$$

where $\mathbf{F}$ and $\mathbf{G}$ are flux vectors, $\mathbf{W}$ is the solution vector, and (ξ, η) are arbitrary curvilinear coordinates. Define A and B as the flux Jacobian matrices $\partial \mathbf{F}/\partial \mathbf{W}$ and $\partial \mathbf{G}/\partial \mathbf{W}$, respectively. By extending the scheme given in equation (4.5.6) to two dimensions, it follows that the matrices $|A|$ and $|B|$ must be the scaling factors in a matrix dissipation model. Now, consider the JST dissipation model. The necessary modification to the contributions for the ξ direction of the artificial dissipation term defined by equation (4.2.1) is to substitute matrix $|A|$ for the eigenvalue scaling factor λ in equations (4.2.2) and (4.2.3). For the η direction, ξ and matrix $|A|$ are replaced by η and matrix $|B|$, respectively. Next, define explicitly the form for the matrix $|A|$. Let $\Lambda = \text{Diag}\,[\lambda_1\ \lambda_2\ \lambda_3\ \lambda_3]$ with

$$\begin{aligned}
\lambda_1 &= q + \sqrt{a_1^2 + a_2^2}\ c \\
\lambda_2 &= q - \sqrt{a_1^2 + a_2^2}\ c \\
\lambda_3 &= q \\
a_1 &= J^{-1}\xi_x \\
a_2 &= J^{-1}\xi_y \\
q &= a_1 u + a_2 v
\end{aligned}$$

Then,

$$|A| = |\lambda_3| I + \left(\frac{|\lambda_1| + |\lambda_2|}{2} - |\lambda_3| \right) \left(\frac{\gamma - 1}{c^2} E_1 + \frac{1}{a_1^2 + a_2^2} E_2 \right) + \frac{|\lambda_1| - |\lambda_2|}{2} \left(\frac{1}{\sqrt{a_1^2 + a_2^2}\, c} \right) [E_3 + (\gamma - 1) E_4] \tag{4.6.2}$$

where

$$E_1 = \begin{bmatrix} \phi & -u & -v & 1 \\ u\phi & -u^2 & -uv & u \\ v\phi & -uv & -v^2 & v \\ H\phi & -uH & -vH & H \end{bmatrix}$$

$$E_2 = \begin{bmatrix} 0 & 0 & 0 & 0 \\ -a_1 q & a_1^2 & a_1 a_2 & 0 \\ -a_2 q & a_1 a_2 & a_2^2 & 0 \\ -q^2 & q a_1 & q a_2 & 0 \end{bmatrix}$$

$$E_3 = \begin{bmatrix} -q & a_1 & a_2 & 0 \\ -uq & u a_1 & u a_2 & 0 \\ -vq & v a_1 & v a_2 & 0 \\ -Hq & H a_1 & H a_2 & 0 \end{bmatrix}$$

$$E_4 = \begin{bmatrix} 0 & 0 & 0 & 0 \\ a_1\phi & -a_1 u & -a_1 v & a_1 \\ a_2\phi & -a_2 u & -a_2 v & a_2 \\ q\phi & -qu & -qv & q \end{bmatrix}$$

Here, H is the total enthalpy, and $\phi = (u^2 + v^2)/2$. Note that for the matrices E_j, each row is a scalar multiple of the other rows (except for zero rows). Hence, to find the product $E_j \mathbf{W}$, simply find one element of the product $E_j \mathbf{W}$, and the other rows are then scalar multiples of that element. Because of the special form of matrix $|A|$ for any λ_1, λ_2, and λ_3, an arbitrary vector $\mathbf{x}$ can be multiplied by matrix $|A|$ very quickly. That is, calculate $\left|A_{j+1/2}\right| (\mathbf{W}_{j+1} - \mathbf{W}_j)$ directly rather than calculate $\left|A_{j+1/2}\right|$ and multiply a matrix by a vector. The matrix $|B|$ is computed the same way as matrix $|A|$ by simply replacing ξ with η.

In practice, λ_1, λ_2, and λ_3 cannot be chosen as given above. Near stagnation points, λ_3 approaches zero, while λ_1 or λ_2 approach zero near sonic lines. A zero artificial viscosity creates numerical difficulties. Hence, these values are limited as

$$\left.\begin{aligned} |\tilde{\lambda}_1| &= \max[|\lambda_1|, V_n\rho(A)] \\ \rho(A) &= |q| + c\sqrt{a_1^2 + a_2^2} \\ |\tilde{\lambda}_2| &= \max[|\lambda_2|, V_n\rho(A)] \\ |\tilde{\lambda}_3| &= \max[|\lambda_3|, V_t\rho(A)] \end{aligned}\right\}$$

where the linear eigenvalue λ_3 can be limited differently than the nonlinear eigenvalues. The parameters V_n and V_t were determined numerically. Various values were evaluated by comparing their corresponding computed solutions based on the sharpness of shock waves captured (without producing oscillations) and convergence rate of numerical scheme. Based on this evaluation, a good choice for V_n and V_t is 0.2. However, in reference 37, accurate coarse-grid solutions for a low-speed, high Reynolds number (5×10^5) laminar flow over a flat plate were not obtained with $V_t = 0.2$. Accurate coarse-grid results (i.e., 5 to 10 points in boundary layer) were computed with $V_t = 0.01$ for the direction normal to the plate, and $V_t = 0.2$ for the streamwise-like direction.

Thus far, $\lambda_{i+1/2,j}$ in equations (4.2.2) and (4.2.3) has been replaced by a matrix while leaving the limiters $\epsilon^{(2)}$ and $\epsilon^{(4)}$ as scalars. Also, $\epsilon^{(2)}$ and $\epsilon^{(4)}$ can be introduced into the diagonal matrix Λ, allowing different limiters to be chosen for different characteristic variables. For example, the limiter may be based on pressure for the nonlinear waves. However, the pressure is smooth through a contact discontinuity. Hence, a switch based on temperature may be more appropriate for the linear wave. Different mesh scalings, and thus different $\phi(r)$ for the linear and nonlinear waves, could also be used.

5. Discrete Boundary Conditions

An important element when developing an accurate and efficient algorithm for solving the Euler and Navier-Stokes equations is selection of proper boundary conditions. The choice of conditions must be consistent with physical constraints of the problem of interest and the interior discrete formulation. Moreover, the physical conditions generally must be supplemented with a sufficient number of numerical relations to allow determination of all dependent variables.

In addition to defining the conditions at solid or porous wall boundaries, the infinite domain problem must be adequately simulated for external airflows. External airflow simulation is usually done by delineating boundaries at some distance from the primary region of consideration, and then prescribing suitable boundary conditions for that location. In the case of a lifting airfoil, the outer boundary position must be far enough away from the airfoil not to compromise the development of the lift. For example, 5 airfoil chords would be too close, whereas 20 chords would be satisfactory if the far-field vortex effect (ref. 38) is considered. Even for inviscid, non-lifting airflow over a circular cylinder, an outer boundary placed too close to the cylinder can cause inaccurate prediction of the airflow over the aft portion of the cylinder.

At a solid boundary, a row of auxiliary cells is created exterior to the domain of the airflow. By approximating the normal pressure gradient of equation (2.2.4) with a three-point centered difference at the surface, the auxiliary cell pressure is obtained. The density at this cell is

equated to the density at the first point off the surface. The tangency condition is enforced by determining the Cartesian velocity components from

$$\begin{bmatrix} u \\ v \end{bmatrix}_{i,1} = \begin{bmatrix} \bar{x}_\xi & -\bar{y}_\xi \\ \bar{y}_\xi & \bar{x}_\xi \end{bmatrix}_w \begin{bmatrix} q_t \\ q_n \end{bmatrix}_{i,2}$$

where ξ is the coordinate aligned with the surface boundary, q_t and q_n are the tangential and normal velocity components, respectively, the subscript w means wall, and the indices $(i,1)$ and $(i,2)$ refer to the centers of the auxiliary and the first interior cells, respectively. The overbar means the quantity is divided by $\sqrt{(x_\xi^2 + y_\xi^2)}$. Finally, the total internal energy is computed using the relation

$$\rho E = \frac{1}{\gamma - 1} p + \frac{1}{2} \rho (u^2 + v^2)$$

In the case of viscous flows, the no-slip condition is required, and is imposed by treating the Cartesian velocity components as antisymmetric functions with respect to the solid surface. Thus

$$u_{i,1} = -u_{i,2}$$
$$v_{i,1} = -v_{i,2}$$

The surface values of pressure (p) and temperature (T) are computed using the reduced normal momentum and energy equations

$$\left.\begin{aligned} \frac{\partial p}{\partial \eta} &= 0 \\ \frac{\partial T}{\partial \eta} &= 0 \end{aligned}\right\} \tag{5.1}$$

where η is the coordinate normal to the surface. As part of the boundary conditions, the option to specify the wall temperature instead of imposing the adiabatic condition of equations (5.1) is included.

To compute the unknown flow variables at the outer boundary of an external aerodynamics problem, characteristic theory, some simplifying assumptions, and the concept of a point vortex are used. In appendix A, a point on the outer boundary and the two-dimensional Euler equations are considered. Then, assuming a locally homentropic flow, the one-dimensional equations of gas dynamics are derived (for completeness) for the direction normal to the boundary. The elements of the solution vector are proportional to the local tangential velocity component and the Riemann invariants

$$R^+ = q_n + \frac{2c}{\gamma - 1}$$

and

$$R^- = q_n - \frac{2c}{\gamma - 1}$$

respectively, where the tangential and normal velocity components are defined as

$$q_t = \frac{x_\xi u + y_\xi v}{\sqrt{(x_\xi^2 + y_\xi^2)}}$$

and

$$q_n = \frac{-y_\xi u + x_\xi v}{\sqrt{(x_\xi^2 + y_\xi^2)}}$$

respectively. This set of dependent variables, the homentropic assumption, and characteristic theory are used to determine the unknown flow variables.

To compute the discrete solution at the outer boundary points (as for the wall boundary), a row of auxiliary (boundary) cells exterior to the domain is introduced. Then, at a boundary cell, the normal velocity component q_n and the speed of sound c are computed from the relations

$$q_n = \frac{1}{2}(R^+ + R^-)$$

$$c = \frac{\gamma - 1}{4}(R^+ - R^-)$$

where the characteristic variables R^+ and R^- are appropriately determined. Assume that the flow normal to the boundary is subcritical. If inflow occurs, the characteristic variables corresponding to the ingoing characteristics are specified. Since this is actually a two-dimensional system, an additional quantity must be given. It follows directly that the entropy s should be specified (the flow is assumed to be locally homentropic). In practice, for convenience define $s^* = p/\rho^\gamma$, which has the same functional dependence as entropy, and use this variable in place of entropy. So, for an inflow situation, set

$$\left.\begin{aligned} q_t &= q_{t\infty} \\ R^+ &= R^+_\infty \\ s^* &= s^*_\infty \end{aligned}\right\} \tag{5.2}$$

and extrapolate R^- from the interior. If outflow occurs at the boundary, there is only one ingoing characteristic (corresponding to R^+), and thus, set $R^+ = R^+_\infty$ and extrapolate q_t, R^-, and s^* from the interior. In the particular case of supersonic flow, all characteristics are ingoing if there is inflow, and are outgoing if there is outflow. Therefore, the dependent variables are specified with their free-stream values if inflow occurs, and extrapolation is used to determine the boundary flow variables if outflow occurs.

At a distance far enough away from a 2-D lifting body, the lifting body can be viewed as a point vortex, with strength proportional to the circulation associated with the lift. The components of the induced velocity at the far-field boundary caused by the vortex can then be computed. Moreover, the effective velocity components at the far-field boundary are computed as (ref. 38)

$$\left.\begin{aligned} u &= u_\infty \cos\alpha + F \sin\phi \\ v &= v_\infty \sin\alpha - F \cos\phi \end{aligned}\right\} \tag{5.3}$$

where

$$F = \frac{c_l\, c}{4\pi}\frac{\beta}{R}\left[1 - M^2_\infty \sin^2(\phi - \alpha)\right]^{-1}$$

$$\beta = \sqrt{1 - M^2_\infty}$$

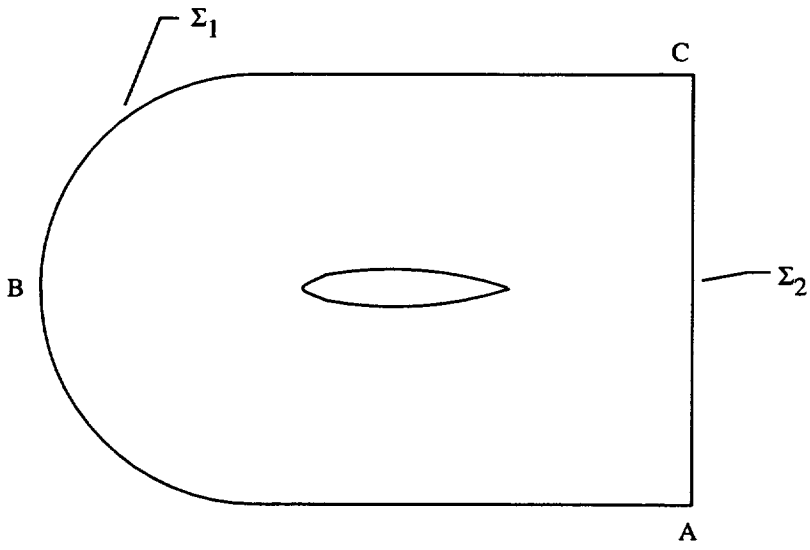

Figure 5. Physical domain for airfoil calculations.

Here, the subscript ∞ refers to free-stream values, α is the angle of attack, R and ϕ are the magnitude and angle of the position vector originating from a reference point at the body (i.e., quarter-chord point for airfoil) and extending to the far-field boundary point, respectively, c is the body length, and c_l is the lift coefficient. The polar angle ϕ is defined as positive in the counterclockwise direction relative to a reference line (i.e., coinciding with chord for airfoil) emanating from the leading edge of the body and proceeding downstream. The Cartesian velocity components u and v of equations (5.3) are used to compute the local tangential and normal velocity components, respectively, required in the boundary conditions.

Consider the case of a C-type mesh wrapped around an airfoil, and denote the outer boundary of a finite domain as $\Sigma_1 + \Sigma_2$ (fig. 5). For airfoil computations, the boundary cells at Σ_1 are treated as described in this section. The boundary cells at Σ_2 are also treated in this way when the flow is inviscid. In the viscous flow problem, a portion of the boundary Σ_2 can generally be wake flow. If the boundary conditions applied at Σ_2 for inviscid flows are used for viscous flows, instabilities can occur. One way to treat the boundary cells at Σ_2 is to specify the pressure and extrapolate the variables ρ, ρu, and ρv, which would satisfy the requirement of characteristic theory to specify one quantity. However, this approach results in pressure-wave reflections, which can seriously delay the convergence of the numerical scheme.

An alternative boundary-point treatment is to extrapolate all dependent variables, allowing the outer and surface boundaries to determine a unique solution. Numerical experiments demonstrate that solutions obtained applying these two treatments are essentially the same near the airfoil. Furthermore, if the outer boundary is far enough away (i.e., 20 chords), there is generally no effect on global quantities such as lift and drag. The second approach shows noticeable improvement in the convergence behavior of the solution algorithm.

For internal flows where the inlet Mach number is subsonic, the specified flow quantities of equations (5.2) are replaced with the total pressure, total enthalpy, and flow inclination angle. These conditions are usually known for internal flow problems. The Riemann variable R^- is extrapolated from the interior of the domain. At a subcritical exit boundary the pressure is specified, while the Riemann variable R^+, the total enthalpy, and the velocity component parallel to the boundary are extrapolated from the interior. If supersonic flow occurs at the

inlet or exit boundary, the variables at that particular boundary are determined in the same manner described in this section for supersonic external flow problems.

6. Basic Time-Stepping Schemes

In section 6.1, the class of Runge-Kutta (R-K) schemes used for time integration is defined. The parameters associated with these R-K schemes and the requirements for determining the parameters are discussed. Then, stability analysis for the four-stage and five-stage schemes that are applied is conducted by considering a linear-wave equation. In section 6.2, stability properties of R-K schemes for systems of fluid dynamic equations are presented. This requires writing the Navier-Stokes equations in general curvilinear coordinates and defining associated Jacobian matrices. With this framework in place, an estimate for the time step is given in section 6.3.

6.1. Runge-Kutta Schemes

For problems where the area of a mesh cell is independent of time, the semidiscrete system of equation (3.2) becomes

$$\frac{d}{dt}\,\mathbf{W}_{i,j} + \mathbf{R}(\mathbf{W}_{i,j}) = 0 \tag{6.1.1}$$

where $\mathbf{R}(\mathbf{W}_{i,j})$ is the residual function defined by

$$\mathbf{R}(\mathbf{W}_{i,j}) = \frac{1}{\Omega_{i,j}}\left(\mathcal{L}_C + \mathcal{L}_D + \mathcal{L}_{AD}\right)\mathbf{W}_{i,j} \tag{6.1.2}$$

A variety of methods for the integration of ordinary differential equations (ODE's) can be used to advance the solution of equation (6.1.1) in time. Single-step, multistage schemes (such as R-K schemes) are usually preferred, rather than linear multistep schemes (such as the Adams-Bashforth scheme), because multistep schemes require more storage and introduce implementation difficulties when combined with a multigrid method. A four-stage R-K scheme (ref. 1) that belongs to the class of standard R-K schemes and is fourth-order accurate in time is used to solve a system of ODE's corresponding to the Euler equations. The four-stage R-K scheme can be written as

$$\left.\begin{aligned}
\mathbf{W}^{(0)} &= \mathbf{W}^{(n)} \\
\mathbf{W}^{(1)} &= \mathbf{W}^{(0)} - \frac{\Delta t}{2}\mathbf{R}^{(0)} \\
\mathbf{W}^{(2)} &= \mathbf{W}^{(0)} - \frac{\Delta t}{2}\mathbf{R}^{(1)} \\
\mathbf{W}^{(3)} &= \mathbf{W}^{(0)} - \Delta t\,\mathbf{R}^{(2)} \\
\mathbf{W}^{(4)} &= \mathbf{W}^{(0)} - \frac{\Delta t}{6}\left(\mathbf{R}^{(0)} + 2\mathbf{R}^{(1)} + 2\mathbf{R}^{(2)} + \mathbf{R}^{(3)}\right) \\
\mathbf{W}^{(n+1)} &= \mathbf{W}^{(4)}
\end{aligned}\right\} \tag{6.1.3}$$

where $\mathbf{R}^{(q)} = \mathbf{R}(\mathbf{W}^{(q)})$, the superscript n denotes the time level $n\,\Delta t$, and the mesh indices (i,j) associated with the solution vector $\mathbf{W}$ are suppressed for convenience. If interest is only in steady-flow problems, then the higher order accuracy in time is not important, and other classes of multistage schemes can be considered. Schemes can be constructed with certain desirable

stability and damping characteristics that lead to efficient steady-state solvers. For example, the solution at the $(q+1)$th stage (ref. 3) can be expressed as

$$\mathbf{W}^{(q+1)} = \mathbf{W}^{(0)} - \alpha_{q+1}\,\Delta t \mathbf{R}^{(q)} \tag{6.1.4}$$

where the residual function

$$\mathbf{R}^{(q)} = \frac{1}{\Omega}\left(\sum_{r=0}^{q} \beta_{qr}\,\mathcal{L}_C \mathbf{W}^{(r)} + \sum_{r=0}^{q} \delta_{qr}\,\mathcal{L}_D \mathbf{W}^{(r)} + \sum_{r=0}^{q} \gamma_{qr}\,\mathcal{L}_{AD} \mathbf{W}^{(r)}\right) \tag{6.1.5}$$

and the consistency conditions $\sum \beta_{qr} = 1$, $\sum \delta_{qr} = 1$, and $\sum \gamma_{qr} = 1$ must be satisfied. The basic parameters α_p (where $p = q+1$ $(q = 0, \ldots, m-1)$) and the weighting factors β_{qr}, δ_{qr}, and γ_{qr} must be prescribed to define the m-stage, time-stepping scheme. The desired stability and damping properties of the scheme provide the requirements for determining the basic parameters and weighting factors. Both hyperbolic and parabolic stability limits must be considered. The hyperbolic and parabolic limits are intervals along the imaginary and negative real axes, respectively, in the complex plane. The coefficients α_p can be chosen to have the best possible hyperbolic or parabolic stability limit without special regard to the high-frequency damping characteristics of the scheme. However, if the scheme is used as a driver of a multigrid method, the scheme must effectively damp the highest frequency error components.

Van der Houwen (ref. 39) gives the parameters α_p that correspond to the maximum (or nearly so) attainable Courant-Friedrichs-Lewy (CFL) number. For schemes with an odd number of stages, Van der Houwen proved that the largest possible stability interval along the imaginary axis of the complex domain is $(m-1)$. Vichnevetsky (ref. 40) conjectured that $(m-1)$ is also the optimal CFL number when m is even, and demonstrated this concept for $m = 2$ and 4. Sonneveld and Van Leer (ref. 41) proved that the $(m-1)$ CFL number limit is valid when m is even. Jameson (refs. 3 and 42) considers schemes with the α_p's of Van der Houwen, and defines appropriate weighting factors for the artificial dissipation evaluations to yield a good parabolic limit. Although the α_p's are obtained using only a hyperbolic stability limitation, they are still a good choice for a viscous flow solver, especially at high Reynolds numbers. That is, the convection (hyperbolic) limit on the time step remains the controlling stability factor for practical aerodynamic flows.

Several members of the class of schemes defined by equations (6.1.4) and (6.1.5) have been analyzed in reference 42 by considering the model problem

$$\frac{\partial w}{\partial t} + a\frac{\partial w}{\partial x} + \epsilon_4\,\Delta x^3 \frac{\partial^4 w}{\partial x^4} = 0 \tag{6.1.6}$$

Equation (6.1.6) is the 1-D, linear-wave equation with a constant-coefficient, third-order dissipation term. If the spatial derivatives in equation (6.1.6) are approximated with central differencing, then

$$\Delta t\frac{dw}{dt} = -\frac{N}{2}(w^n_{j+1} - w^n_{j-1}) - \epsilon_4\frac{N}{a}(w^n_{j+2} - 4w^n_{j+1} + 6w^n_j - 4w^n_{j-1} + w^n_{j-2}) \tag{6.1.7}$$

where $N = a\,\Delta t/\Delta x$ is the Courant number. Taking the Fourier transform of equation (6.1.7), obtain

$$\Delta t\frac{dw}{dt} = z\,w^n \tag{6.1.8}$$

where the Fourier symbol

$$z = -iN\sin\theta - 4\epsilon_4\frac{N}{a}(1-\cos\theta)^2 \tag{6.1.9}$$

Here, $i = \sqrt{-1}$, and θ is the Fourier angle. If the residual function for any stage q is given by

$$R^{(q)} = (\mathcal{L}_C + \mathcal{L}_{AD})\, w^{(q)} \tag{6.1.10}$$

then the amplification factor for an m-stage scheme is

$$g(z) = 1 + f(\theta) z(\theta) \tag{6.1.11}$$

where

$$f(\theta) = \kappa_1 + \kappa_2 z^2 + \cdots + \kappa_m z^m \tag{6.1.12}$$

Here, $\kappa_1 = \alpha_m$ with $\alpha_m = 1$ for consistency, and $\kappa_l = \kappa_{l-1}\alpha_{m-l+1}$ with $l = 2, 3, \ldots, m$. Since $g(z)$ is analytic, the maximum modulus theorem guarantees that all contours $|g(z)| < 1$ lie inside the absolute stability curve $|g(z)| = 1$. For this subclass of schemes, which are schemes satisfying the requirement that $|z| \leq (m-1)$ (refs. 3 and 41), the optimal polynomials are defined as

$$g(z) = P_k(z) = i^{k-1} T_{k-1}\left(\frac{-iz}{k-1}\right) + \frac{i^k}{2}\left[T_k\left(\frac{-iz}{k-1}\right) - T_{k-2}\left(\frac{-iz}{k-1}\right)\right] \tag{6.1.13}$$

where T_k is a Chebyshev polynomial, and $k \geq 2$. The coefficients κ_l for the four-stage and five-stage schemes given in reference 39 are

$$\kappa_1 = 1$$

$$\kappa_2 = \frac{1}{2}$$

$$\kappa_3 = \frac{1}{6}$$

$$\kappa_4 = \frac{1}{24}$$

and

$$\kappa_1 = 1$$

$$\kappa_2 = \frac{1}{2}$$

$$\kappa_3 = \frac{3}{16}$$

$$\kappa_4 = \frac{1}{32}$$

$$\kappa_5 = \frac{1}{128}$$

respectively.

In the more general situation, the amplification factor is not a polynomial in z. For example, consider the subclass of schemes defined by equation (6.1.5) that are called (m, n) schemes. The m refers to the number of stages, and n designates the number of evaluations of the dissipative contribution. For example, assume a $(m, 2)$ scheme, where the numerical dissipation terms are evaluated on the first and second stages and frozen for the remaining stages (similar to the (4.2) scheme used). Let $z_r = \Re(z)$ and $z_i = i\Im(z)$. Then, if $m \geq 3$, the f of equation (6.1.12) is replaced by

$$f = \kappa_1 - (\kappa_1\alpha_1 z_r + \kappa_2 z_i)z_i^0 + (\kappa_2\alpha_1 z_r + \kappa_3 z_i)z_i^1 - \cdots$$
$$+ (-1)^m(\kappa_{m-2}\alpha_1 z_r + \kappa_{m-1} z_i)z_i^{m-3} - (-1)^m\kappa_m z z_i^{m-2} \qquad (6.1.14)$$

Consider the (5,3) scheme generally used, where the dissipation terms are evaluated on the first, third, and fifth stages, and frozen on the second and fourth stages. For this scheme, the weighting factors for the dissipation terms (γ_{qr} in eq. (6.1.5)) are as follows:

$$\left.\begin{aligned}
\gamma_{00} &= 1 \\
\gamma_{10} &= 1 \\
\gamma_{11} &= 0 \\
\gamma_{20} &= \Gamma_3 \\
\gamma_{21} &= 0 \\
\gamma_{22} &= \overline{\gamma}_3 \\
\gamma_{30} &= \Gamma_3 \\
\gamma_{31} &= 0 \\
\gamma_{32} &= \overline{\gamma}_3 \\
\gamma_{33} &= 0 \\
\gamma_{40} &= \Gamma_3\Gamma_5 \\
\gamma_{41} &= 0 \\
\gamma_{42} &= \overline{\gamma}_3\Gamma_5 \\
\gamma_{43} &= 0 \\
\gamma_{44} &= \overline{\gamma}_5
\end{aligned}\right\} \qquad (6.1.15)$$

where $\Gamma_3 = (1 - \overline{\gamma}_3)$, $\Gamma_5 = (1 - \overline{\gamma}_5)$, $\overline{\gamma}_3 = 0.56$, and $\overline{\gamma}_5 = 0.44$. The symbol of the time-stepping operator f for this scheme is given by

$$f = \alpha_5\left[1 - \alpha_4 z_1(1 - \alpha_3 z_i) - \alpha_4 z_3 z_1(\alpha_3 z_2 z_i - \overline{\gamma}_3 z_r) - \Gamma_5\overline{\gamma}_3 z_3 z_r\right] \qquad (6.1.16)$$

where

$$z_1 = z_i + \overline{\gamma}_5 z_r$$

$$z_2 = z_i + \overline{\gamma}_3 z_r$$

$$z_3 = \alpha_2(1 - \alpha_1 z_i)$$

In a number of flow computations, four-stage and five-stage schemes are applied (refs. 19, 24, 43, and 44). For these schemes, the residual function is

$$\mathbf{R}^{(q)} = \frac{1}{\Omega}\left(\mathcal{L}_C\mathbf{W}^{(q)} + \mathcal{L}_D\mathbf{W}^{(0)} + \sum_{r=0}^{q}\gamma_{qr}\,\mathcal{L}_{AD}\mathbf{W}^{(r)}\right) \tag{6.1.17}$$

By evaluating the physical diffusion terms on the first stage only, the computational effort of the scheme is reduced. This incompatibility with the computation of the numerical dissipation terms does not cause any deterioration in the performance of the schemes. The evaluation of the numerical dissipation terms on certain stages (and the weighting of these evaluations) provides two advantages. First, the parabolic stability limit can be extended, and the high-frequency damping can be improved. Second, the expense of calculating the dissipation terms can be reduced. Reference 3 provides additional discussion on the weighting of dissipation.

The time-stepping parameters for the four-stage scheme are

$$\left.\begin{aligned}\alpha_1 &= \frac{1}{4}\\ \alpha_2 &= \frac{1}{3}\\ \alpha_3 &= \frac{1}{2}\\ \alpha_4 &= 1\end{aligned}\right\} \tag{6.1.18}$$

Since $\alpha_{m-1} = 1/2$, the scheme is second-order accurate in time. The numerical dissipation terms are evaluated the same as for equation (6.1.14). For the model problem of equation (6.1.6), the absolute stability curve for this scheme is presented in figure 6(a). The hyperbolic stability limit (as determined by the extent of the stability interval on the imaginary axis) is $2\sqrt{2}$. The parabolic stability limit (as determined by the extent of the stability interval on the negative real axis) is 4. The dashed line (fig. 6(a)) represents the locus of the Fourier symbol as defined in equation (6.1.9), and must lie inside the $|g| = 1$ curve for stability. Figure 6(b) shows the variation of the amplification factor g with the Fourier angle θ. The scheme exhibits good high-frequency damping, which is crucial for a rapidly convergent multigrid method. When analyzing the stability and damping properties, it is important to include all components of the scheme. For example, if the stability limit of the algorithm is extended through the introduction of an implicit residual smoothing procedure (discussed in section 7.2), some deterioration in the high-frequency damping occurs (figs. 6(c) and 6(d)).

In the case of the five-stage scheme, the basic parameters are

$$\left.\begin{aligned}\alpha_1 &= \frac{1}{4}\\ \alpha_2 &= \frac{1}{6}\\ \alpha_3 &= \frac{3}{8}\\ \alpha_4 &= \frac{1}{2}\\ \alpha_5 &= 1\end{aligned}\right\} \tag{6.1.19}$$

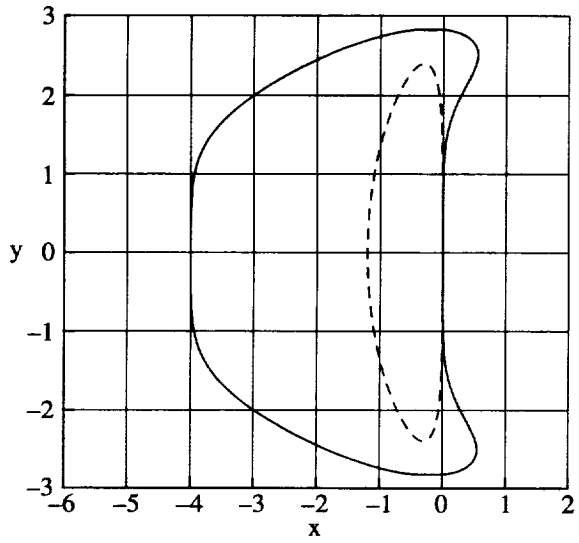

(a) Stability curves with two evaluations of dissipation; CFL = 2.4; $\kappa^{(2)} = 0$; $\kappa^{(4)} = 1/32$.

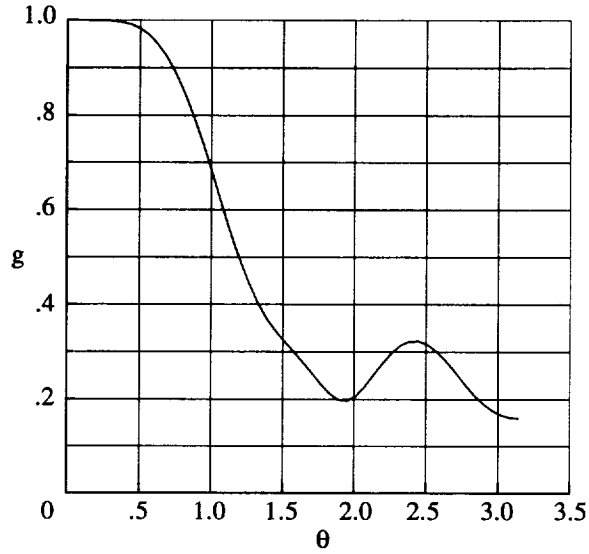

(b) Amplication factor with two evaluations of dissipation; CFL = 2.4; $\kappa^{(2)} = 0$; $\kappa^{(4)} = 1/32$.

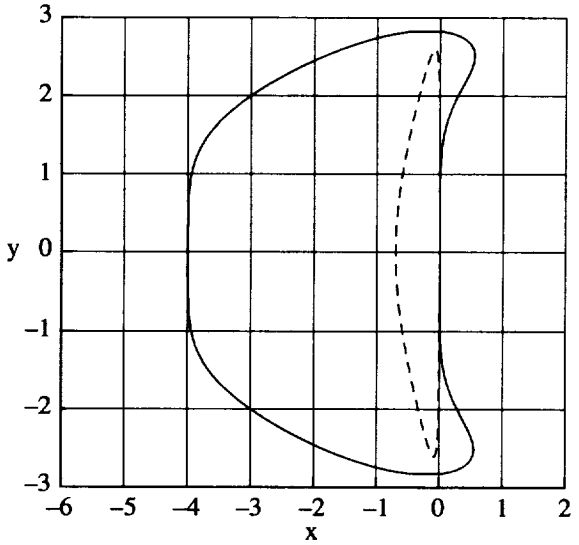

(c) Stability curves with implicit residual smoothing; CFL = 4.8; $\beta = 0.6$; $\kappa^{(2)} = 0$; $\kappa^{(4)} = 1/32$.

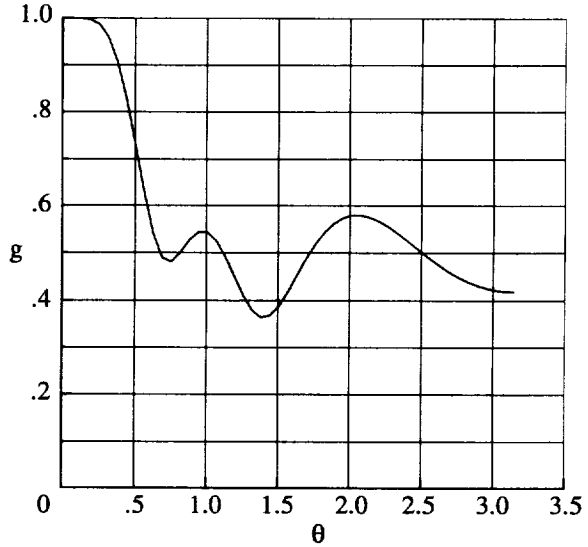

(d) Amplification factor with implicit residual smoothing; CFL = 4.8; $\beta = 0.6$.

Figure 6. Plots of four-stage R-K scheme; $\kappa^{(2)} = 0$; $\kappa^{(4)} = 1/32$; coefficients are 1/4, 1/3, 1/2, and 1.

A very large parabolic stability limit is established by evaluating the artificial dissipation terms on the first, third, and fifth stages with the weightings of equations (6.1.15). Figure 7(a) shows that for this scheme, the hyperbolic stability limit is 4 and the parabolic stability limit is about 9. Figure 7(b) shows that this five-stage scheme also has good high-frequency damping. Figures 7(c) and 7(d) show the stability curves for this scheme when implicit residual smoothing is applied. In practice, with the implicit residual smoothing, a CFL number of 7.5 is used for this scheme. For the four-stage scheme, a CFL number of 5.0 is used. So, with one additional evaluation of the implicitly smoothed residual function, the CFL number increases by a factor of 1.5.

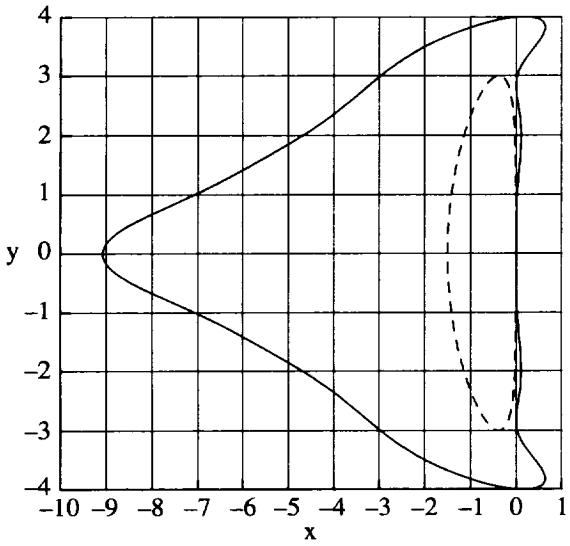

(a) Stability curves with three evaluations of dissipation; CFL = 3.0.

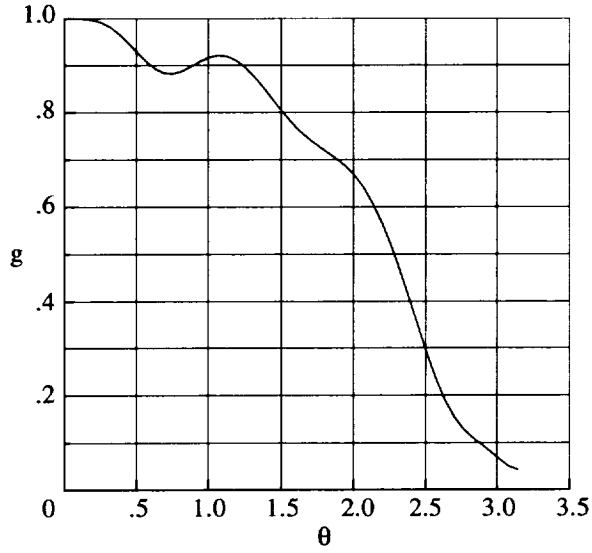

(b) Amplification factor with three evaluations of dissipation; CFL = 3.0.

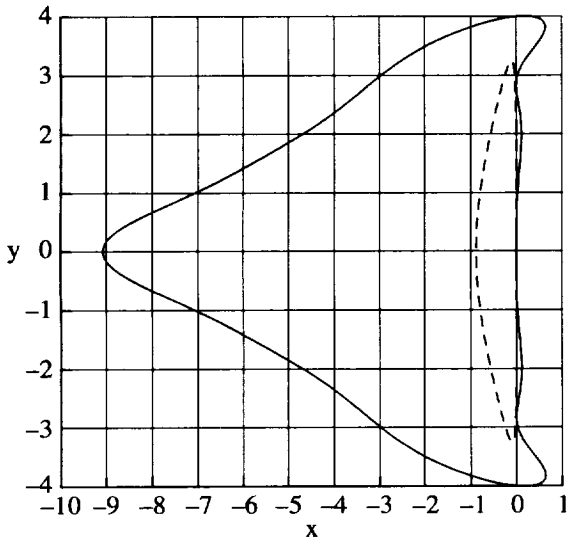

(c) Stability curves with implicit residual smoothing; CFL = 6.0; $\beta = 0.6$.

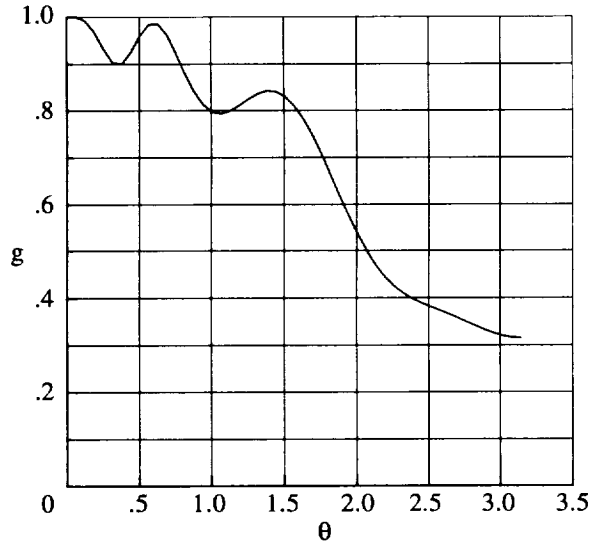

(d) Amplification factor with implicit residual smoothing; CFL = 6.0; $\beta = 0.6$.

Figure 7. Plots of five-stage R-K scheme; $\kappa^{(2)} = 0$; $\kappa^{(4)} = 1/32$; coefficients are 1/4, 1/6, 3/8, 1/2, and 1.

6.2. Stability of Runge-Kutta Schemes for Systems

The compressible Navier-Stokes equations can be classified as either hyperbolic-parabolic or incomplete-parabolic type (refs. 45–47). As discussed in section 6.1, these equations are solved numerically with a member of a class of multistage time-stepping schemes. By considering the hyperbolic (inviscid) and parabolic (viscous and numerical dissipation) operators separately, sufficient conditions for stability can be obtained. These conditions can be used as a starting point for estimating a time step for solving the full Navier-Stokes equations.

To estimate the restriction on the time step due to convection and diffusion, we consider the two-dimensional, Navier-Stokes equations expressed in generalized coordinates (ξ, η). These equations can be written as

$$\frac{\partial \widetilde{\mathbf{W}}}{\partial t} + \frac{\partial \widetilde{\mathbf{F}}^{(\xi)}}{\partial \xi} + \frac{\partial \widetilde{\mathbf{F}}^{(\eta)}}{\partial \eta} = \frac{\partial \widetilde{\mathbf{F}}_v^{(\xi)}}{\partial \xi} + \frac{\partial \widetilde{\mathbf{F}}_v^{(\eta)}}{\partial \eta} \tag{6.2.1}$$

where $\widetilde{\mathbf{W}} = J^{-1}\mathbf{W}$, with J^{-1} and $\mathbf{W}$ representing the inverse of the transformation Jacobian and the vector of conserved flow variables, respectively. The derivatives associated with the transformation from Cartesian coordinates (x, y) to (ξ, η) and the corresponding inverse transformation are related as

$$\begin{bmatrix} \xi_x & \eta_x \\ \xi_y & \eta_y \end{bmatrix} = \frac{1}{J^{-1}} \begin{bmatrix} y_\eta & -y_\xi \\ -x_\eta & x_\xi \end{bmatrix}$$

and the inverse of the transformation Jacobian is given by

$$J^{-1} = \frac{\partial(x, y)}{\partial(\xi, \eta)} = x_\xi y_\eta - x_\eta y_\xi = \Omega$$

The transformed inviscid flux vectors $\tilde{\mathbf{F}}^{(\xi)}$ and $\tilde{\mathbf{F}}^{(\eta)}$ are given by

$$\widetilde{\mathbf{F}}^{(\xi)} = J^{-1}(\xi_x \mathbf{F}^{(\xi)} - \xi_y \mathbf{F}^{(\eta)}) \tag{6.2.2}$$

$$\widetilde{\mathbf{F}}^{(\eta)} = J^{-1}(\eta_x \mathbf{F}^{(\xi)} - \eta_y \mathbf{F}^{(\eta)}) \tag{6.2.3}$$

Using the notation of reference 48, the viscous flux vectors $\widetilde{\mathbf{F}}_v^{(\xi)}$ and $\widetilde{\mathbf{F}}_v^{(\eta)}$ can be expressed as

$$\widetilde{\mathbf{F}}_v^{(\xi)} = \widetilde{B}^{(\xi,\xi)} \frac{\partial \widetilde{\mathbf{W}}}{\partial \xi} + \widetilde{B}^{(\xi,\eta)} \frac{\partial \widetilde{\mathbf{W}}}{\partial \eta} \tag{6.2.4}$$

$$\widetilde{\mathbf{F}}_v^{(\eta)} = \widetilde{B}^{(\eta,\eta)} \frac{\partial \widetilde{\mathbf{W}}}{\partial \eta} + \widetilde{B}^{(\eta,\xi)} \frac{\partial \widetilde{\mathbf{W}}}{\partial \xi} \tag{6.2.5}$$

where

$$\widetilde{B}^{(\alpha,\beta)} = B_1^{(\alpha,\beta)} M, \qquad \alpha, \beta \in \{\xi, \eta\} \tag{6.2.6}$$

and $B_1^{(\alpha,\beta)}$ is a viscous matrix obtained by rewriting the $\widetilde{\mathbf{F}}_v$ vectors in terms of primitive variables. The matrix M, which transforms nonconservative (primitive) variables to conservative variables, and the inverse of matrix M are given by

$$M = \begin{bmatrix} 1 & 0 & 0 & 0 \\ -u\rho^{-1} & \rho^{-1} & 0 & 0 \\ -v\rho^{-1} & 0 & \rho^{-1} & 0 \\ \phi^2 & -(\gamma-1)u & -(\gamma-1)v & (\gamma-1) \end{bmatrix} \tag{6.2.7}$$

and

$$M^{-1} = \begin{bmatrix} 1 & 0 & 0 & 0 \\ u & \rho & 0 & 0 \\ v & 0 & \rho & 0 \\ (\gamma-1)^{-1}\phi^2 & \rho u & \rho v & (\gamma-1)^{-1} \end{bmatrix} \tag{6.2.8}$$

respectively, with $\phi^2 = (\gamma-1)(u^2+v^2)/2$. The viscous matrices $\widetilde{B}^{(\xi,\xi)}$, $\widetilde{B}^{(\eta,\eta)}$, $\widetilde{B}^{(\xi,\eta)}$, and $\widetilde{B}^{(\eta,\xi)}$ are defined according to

$$\widetilde{B}^{(\alpha,\beta)} = \begin{bmatrix} 0 & 0 & 0 & 0 \\ 0 & \mathcal{B}_{x,x}^{\alpha,\beta} & \mathcal{B}_{x,y}^{\alpha,\beta} & 0 \\ 0 & \mathcal{B}_{y,x}^{\alpha,\beta} & \mathcal{B}_{y,y}^{\alpha,\beta} & 0 \\ -\mathcal{B}^{\alpha,\beta}p\rho^{-2} & \mathcal{B}_{x,x}^{\alpha,\beta}u + \mathcal{B}_{y,x}^{\alpha,\beta}v & \mathcal{B}_{y,y}^{\alpha,\beta}v + \mathcal{B}_{x,y}^{\alpha,\beta}u & \mathcal{B}^{\alpha,\beta}\rho^{-1} \end{bmatrix} \tag{6.2.9}$$

with

$$\mathcal{B}_{a,b}^{\alpha,\beta} = \frac{\sqrt{\gamma}M}{Re}\left(\lambda\frac{\partial\alpha}{\partial a}\frac{\partial\beta}{\partial b} + \mu\frac{\partial\alpha}{\partial b}\frac{\partial\beta}{\partial a} + \mu\nabla\alpha\cdot\nabla\beta\,\delta_{a,b}\right) \tag{6.2.10}$$

$$\mathcal{B}^{\alpha,\beta} = \frac{\sqrt{\gamma}M}{Re}\left(\frac{\gamma}{\gamma-1}\right)\frac{\mu}{Pr}\nabla\alpha\cdot\nabla\beta \tag{6.2.11}$$

where the nondimensionalization of section 3.1 is employed, ∇ is the gradient operator, and $\delta_{a,b}$ is the Kronecker delta. Using the Jacobian matrices $\widetilde{A}^{(\alpha)} = \partial\widetilde{\mathbf{F}}^{(\alpha)}/\partial\widetilde{\mathbf{W}}$, where $\alpha \in \{\alpha, \beta\}$, equation (6.2.1) can be rewritten as

$$\frac{\partial\widetilde{\mathbf{W}}}{\partial t} + \widetilde{A}^{(\xi)}\frac{\partial\widetilde{\mathbf{W}}}{\partial\xi} + \widetilde{A}^{(\eta)}\frac{\partial\widetilde{\mathbf{W}}}{\partial\eta} = \frac{\partial}{\partial\xi}\left(\widetilde{B}^{(\xi,\xi)}\frac{\partial\widetilde{\mathbf{W}}}{\partial\xi} + \widetilde{B}^{(\xi,\eta)}\frac{\partial\widetilde{\mathbf{W}}}{\partial\eta}\right) + \frac{\partial}{\partial\eta}\left(\widetilde{B}^{(\eta,\xi)}\frac{\partial\widetilde{\mathbf{W}}}{\partial\xi} + \widetilde{B}^{(\eta,\eta)}\frac{\partial\widetilde{\mathbf{W}}}{\partial\eta}\right) \tag{6.2.12}$$

where

$$\widetilde{A}^{(\alpha)} = \begin{bmatrix} 0 & \alpha_x & \alpha_y & 0 \\ -uU^{(\alpha)} + \alpha_x\phi^2 & U^{(\alpha)} - (\gamma-2)\alpha_x u & \alpha_y u - (\gamma-1)\alpha_x v & (\gamma-1)\alpha_x \\ -vU^{(\alpha)} + \alpha_y\phi^2 & \alpha_x v - (\gamma-1)\alpha_y u & U^{(\alpha)} - (\gamma-2)\alpha_y v & (\gamma-1)\alpha_y \\ U^{(\alpha)}(\phi^2-\omega) & \alpha_x\omega - (\gamma-1)uU^{(\alpha)} & \alpha_y\omega - (\gamma-1)vU^{(\alpha)} & \gamma U^{(\alpha)} \end{bmatrix} \tag{6.2.13}$$

with $U^{(\alpha)} = \alpha_x u + \alpha_y v$, and $\omega = \gamma E - \phi^2$. Assume the coefficient matrices of equation (6.2.12) are locally constant in space and time, and transform to primitive variables. Then, obtain

$$\frac{\partial \mathbf{W}_P}{\partial t} + \overline{A}^{(\xi)} \frac{\partial \mathbf{W}_P}{\partial \xi} + \overline{A}^{(\eta)} \frac{\partial \mathbf{W}_P}{\partial \eta} = \overline{B}^{(\xi,\xi)} \frac{\partial^2 \mathbf{W}_P}{\partial \xi^2} + \overline{B}^{(\eta,\eta)} \frac{\partial^2 \mathbf{W}_P}{\partial \eta^2} + \left(\overline{B}^{(\xi,\eta)} + \overline{B}^{(\eta,\xi)} \right) \frac{\partial^2 \mathbf{W}_P}{\partial \xi \partial \eta} \tag{6.2.14}$$

where

$$\mathbf{W}_P = [\rho \quad u \quad v \quad p]^T \tag{6.2.15}$$

$$\overline{A}^{(\alpha)} = M \tilde{A}^{(\alpha)} M^{-1} = \begin{bmatrix} U^{(\alpha)} & \rho\alpha_x & \rho\alpha_y & 0 \\ 0 & U^{(\alpha)} & 0 & \rho^{-1}\alpha_x \\ 0 & 0 & U^{(\alpha)} & \rho^{-1}\alpha_y \\ 0 & \gamma p \alpha_x & \gamma p \alpha_y & U^{(\alpha)} \end{bmatrix} \tag{6.2.16}$$

$$\overline{B}^{(\alpha,\beta)} = M B_1^{(\alpha,\beta)} = \rho^{-1} \begin{bmatrix} 0 & 0 & 0 & 0 \\ 0 & \mathcal{B}_{x,x}^{\alpha,\beta} & \mathcal{B}_{x,y}^{\alpha,\beta} & 0 \\ 0 & \mathcal{B}_{y,x}^{\alpha,\beta} & \mathcal{B}_{y,y}^{\alpha,\beta} & 0 \\ -(\gamma-1)\mathcal{B}^{\alpha,\beta} p \rho^{-1} & 0 & 0 & (\gamma-1)\mathcal{B}^{\alpha,\beta} \end{bmatrix} \tag{6.2.17}$$

The eigenvalues of the matrices $\overline{A}^{(\alpha)}$ are

$$\left.\begin{array}{l} U^{(\alpha)} \\ U^{(\alpha)} \\ U^{(\alpha)} + c\sqrt{\alpha_x^2 + \alpha_y^2} \\ U^{(\alpha)} - c\sqrt{\alpha_x^2 + \alpha_y^2} \end{array}\right\} \tag{6.2.18}$$

The eigenvalues of the matrices $\overline{B}^{(\alpha,\alpha)}$ are

$$\left.\begin{array}{l} 0 \\ \gamma \dfrac{\mu}{Pr} \Gamma_1 \\ \mu \Gamma_1 \\ (2\mu + \lambda)\Gamma_1 \end{array}\right\} \tag{6.2.19}$$

where

$$\Gamma_1 = \frac{\sqrt{\gamma} M}{Re} \frac{1}{\rho} (\alpha_x^2 + \alpha_y^2)$$

For the matrices $\overline{B}^{(\alpha,\beta)}$, the eigenvalues are

$$\left.\begin{array}{l} 0 \\ \dfrac{\sqrt{\gamma}M}{Re}\left[2\dfrac{\gamma}{Pr}\dfrac{\mu}{\rho}(\nabla\alpha\cdot\nabla\beta)\right] \\ \dfrac{\sqrt{\gamma}M}{Re}\left[\dfrac{(\lambda+3\mu)}{\rho}(\nabla\alpha\cdot\nabla\beta)+\dfrac{(\lambda+\mu)}{\rho}|\nabla\alpha|\,|\nabla\beta|\right] \\ \dfrac{\sqrt{\gamma}M}{Re}\left[\dfrac{(\lambda+3\mu)}{\rho}(\nabla\alpha\cdot\nabla\beta)-\dfrac{(\lambda+\mu)}{\rho}|\nabla\alpha|\,|\nabla\beta|\right] \end{array}\right\} \tag{6.2.20}$$

Abarbanel and Gottlieb (ref. 49) showed that the matrices of equation (6.2.14) can be simultaneously symmetrized with the similarity transformation determined by

$$S=\begin{bmatrix} \sqrt{\gamma}\rho c^{-1} & 0 & 0 & 0 \\ 0 & 1 & 0 & 0 \\ 0 & 0 & 1 & 0 \\ \frac{1}{\sqrt{\gamma}}\rho c & 0 & 0 & \frac{\sqrt{\gamma-1}}{\sqrt{\gamma}}\rho c \end{bmatrix} \tag{6.2.21}$$

$$S^{-1}=\begin{bmatrix} \frac{1}{\sqrt{\gamma}}\rho^{-1}c^{-1} & 0 & 0 & 0 \\ 0 & 1 & 0 & 0 \\ 0 & 0 & 1 & 0 \\ -\frac{1}{\sqrt{\gamma(\gamma-1)}}\rho c & 0 & 0 & \frac{\sqrt{\gamma}}{\sqrt{\gamma-1}}\rho^{-1}c^{-1} \end{bmatrix} \tag{6.2.22}$$

Using this similarity transformation, rewrite equation (6.2.14) as

$$\frac{\partial\mathbf{V}}{\partial t}+A^{(\xi)}\frac{\partial\mathbf{V}}{\partial\xi}+A^{(\eta)}\frac{\partial\mathbf{V}}{\partial\eta}=B^{(\xi,\xi)}\frac{\partial^2\mathbf{V}}{\partial\xi^2}+B^{(\eta,\eta)}\frac{\partial^2\mathbf{V}}{\partial\eta^2}+\left(B^{(\xi,\eta)}+B^{(\eta,\xi)}\right)\frac{\partial^2\mathbf{V}}{\partial\xi\partial\eta} \tag{6.2.23}$$

where

$$\left.\begin{array}{l} A^{(\alpha)}=S^{-1}\overline{A}^{(\alpha)}S \\ B^{(\alpha,\beta)}=S^{-1}\overline{B}^{(\alpha,\beta)}S \end{array}\right\} \tag{6.2.24}$$

with $\alpha,\beta\in\{\xi,\eta\}$.

Define as a discrete computational domain $\{(\xi,\eta):1\le\xi\le \mathrm{L},\,1\le\eta\le \mathrm{L},\text{ and }\Delta\xi=\Delta\eta=1\}$, where L = N, the number of mesh intervals in either coordinate direction. Let a discrete, vector function, such as $\mathbf{V}(i\,\Delta\xi, j\,\Delta\eta)=\mathbf{V}(i,j)$, be denoted by $\mathbf{V}_{i,j}$. If the spatial derivatives of equation (6.2.23) are approximated with second-order central differences, the semidiscrete representation

$$\frac{d}{dt}\mathbf{V}_{i,j}+\mathcal{L}\mathbf{V}_{i,j}=0 \tag{6.2.25}$$

is obtained, where

$$\mathcal{L}\mathbf{V}_{i,j} = (A^{(\xi)})_{i,j}\mu_\xi\delta_\xi\mathbf{V}_{i,j} + (A^{(\eta)})_{i,j}\mu_\eta\delta_\eta\mathbf{V}_{i,j} - (B^{(\xi,\xi)})_{i,j}\delta_\xi^2\mathbf{V}_{i,j}$$
$$- \left[(B^{(\xi,\eta)})_{i,j} + (B^{(\eta,\xi)})_{i,j}\right]\mu_\xi\delta_\xi\mu_\eta\delta_\eta\mathbf{V}_{i,j} - (B^{(\eta,\eta)})_{i,j}\delta_\eta^2\mathbf{V}_{i,j} \qquad (6.2.26)$$

Then, taking the Fourier transform of equation (6.2.25) yields

$$\Delta t\frac{d}{dt}\hat{\mathbf{V}}_{i,j} = -\Delta t\hat{\mathcal{L}}\hat{\mathbf{V}}_{i,j} = Z\hat{\mathbf{V}}_{i,j}$$

where the caret indicates a transformed quantity, and

$$Z = Z_C + Z_D \qquad (6.2.27)$$

with

$$Z_C = -i\,\Delta t\left(A^{(\xi)}\sin\theta_\xi + A^{(\eta)}\sin\theta_\eta\right)$$
$$Z_D = -\Delta t\left[4B^{(\xi,\xi)}\sin^2\frac{\theta_\xi}{2} + (B^{(\xi,\eta)} + B^{(\eta,\xi)})\sin\theta_\xi\sin\theta_\eta + 4B^{(\eta,\eta)}\sin^2\frac{\theta_\eta}{2}\right]$$

and $i = \sqrt{-1}$.

If all terms in the flow equations and the numerical dissipation are evaluated at each step of the R-K scheme, then the amplification matrix G for an m-stage scheme is a function of one variable. In particular

$$G(Z) = I + \kappa_1 Z + \kappa_2 Z^2 + \cdots + \kappa_m Z^m \qquad (6.2.28)$$

where κ_1 is a function of the coefficients of the R-K scheme. (See eq. (6.1.12) for definition.) Let $\lambda_q(G)$ be any eigenvalue of $G(Z)$, and let $\lambda_q(\mathcal{L})$ be any eigenvalue of $\mathcal{L}$. Also, let $z = -\Delta t\lambda_q(\mathcal{L})$. The eigenvalue $\lambda_q(G)$ is related to z as

$$\lambda_q(G) = 1 + \kappa_1 z + \kappa_2 z^2 + \cdots + \kappa_m z^m \qquad (6.2.29)$$

The stability of a scheme requires that the amplification matrix satisfies the condition $\| G^n \| \leq C$ for all n. The spectral radius σ of a matrix is defined as equal to the largest eigenvalue in absolute value. If the matrix G is normal (i.e., $GG^* = G^*G$), then its norm is equivalent to the spectral radius $\sigma(G)$. Thus, a normal matrix requires that $\sigma(G^n) = \sigma^n(G) \leq C$. This condition is equivalent to the Von Neumann condition for stability that requires

$$\sigma(G) \leq 1 \qquad (6.2.30)$$

Hence, if Z and G are normal matrices, the condition for stability is

$$|g(z)| = |g\left(-\Delta t\lambda_q(\mathcal{L})\right)| \leq 1 \qquad (6.2.31)$$

for all q.

To determine sufficient conditions for stability, consider separately the hyperbolic and parabolic operators associated with equation (6.2.1). First examine the stability for the Euler equations (i.e., $Re \to \infty$ in eq. (6.2.1)). The following theorem gives a sufficient condition for stability:

Theorem 6.1 *Suppose the R-K scheme satisfies the property that*

$$[-i\,N_{CFL}, i\,N_{CFL}] \subset \{z \in \mathcal{C} : |g(z)| \leq 1\} \tag{6.2.32}$$

where N_{CFL} is the CFL number for the R-K scheme. Assume smooth initial data, such that the Cauchy problem for the Euler equations is well-posed. If the Euler equations are solved with this R-K scheme and second-order centered difference approximations for the spatial derivatives, the condition

$$\Delta t\,[\sigma(\alpha A^{(\xi)} + \beta A^{(\eta)})] \leq N_{CFL} \tag{6.2.33}$$

where $|\alpha| \leq 1$, and $|\beta| \leq 1$ is sufficient for stability of the linearized problem.

The proof follows directly. Since the matrices $A^{(\xi)}$ and $A^{(\eta)}$ are symmetric, the amplification matrix $G(Z)$ is normal. Furthermore, for a central difference scheme, the Fourier transform of the first derivative is a pure imaginary number. Hence, $Z = -i\,\Delta t\left(A^{(\xi)}\sin\theta_\xi + A^{(\eta)}\sin\theta_\eta\right)$, and so the result follows (remember that $\Delta\xi = \Delta\eta = 1$).

Now consider the parabolic equation derived from equation (6.2.23) by eliminating the first-order spatial derivatives. The Fourier symbol of the difference operator is given by equation (6.2.27) when $A^{(\alpha)} \equiv 0$. Let N_D denote the diffusion number of the R-K scheme (i.e., N_D defines the stability interval along the negative real axis). Then, the maximum allowable time step is $N_D\,\Delta t_D$, where $\Delta t_D = \Delta x^2/(4\mu)$ for the 1-D scalar diffusion equation with central differencing, with μ being the diffusion coefficient. A sufficient condition for stability is defined as follows:

Theorem 6.2 *Suppose the R-K scheme satisfies the property that*

$$[-N_D, 0] \subset \{z \in \mathcal{C} : |g(z)| \leq 1\} \tag{6.2.34}$$

where N_D is the diffusion number for the R-K scheme. Assume smooth initial data, such that the Cauchy problem for the viscous equations is well-posed. If the viscous equations are solved with this R-K scheme and second-order centered spatial differencing, the condition

$$\max(\Delta t\,\sigma_D) \leq N_D \tag{6.2.35}$$

with

$$\sigma_D = 4\,\sigma\left[B^{(\xi,\xi)}\sin^2\frac{\theta_\xi}{2} + B^{(\eta,\eta)}\sin^2\frac{\theta_\eta}{2} + \frac{1}{4}(B^{(\xi,\eta)} + B^{(\eta,\xi)})\sin\theta_\xi\sin\theta_\eta\right]$$

is sufficient for stability of the linearized equation.

Since

$$Z = -\Delta t\left[4\left(B^{(\xi,\xi)}\sin^2\frac{\theta_\xi}{2} + B^{(\eta,\eta)}\sin^2\frac{\theta_\eta}{2}\right) + (B^{(\xi,\eta)} + B^{(\eta,\xi)})\sin\theta_\xi\sin\theta_\eta\right] \tag{6.2.36}$$

is a negative real symmetric matrix, $G(Z)$ is again normal. Therefore, the proof is similar to the proof of theorem 6.1. Note that if the cross-derivative terms are neglected, the inequality of equation (6.2.35) reduces to

$$\Delta t\left[4\,\sigma\left(B^{(\xi,\xi)} + B^{(\eta,\eta)}\right)\right] \leq N_D \tag{6.2.37}$$

Next, suppose numerical dissipation in the form of fourth-difference terms is added to the discrete viscous equations. Then

$$\begin{aligned}\mathcal{L}\mathbf{V}_{i,j} = &-(B^{(\xi,\xi)})_{i,j}\delta_\xi^2\mathbf{V}_{i,j} - (B^{(\eta,\eta)})_{i,j}\delta_\eta^2\mathbf{V}_{i,j} \\ &- \left[(B^{(\xi,\eta)})_{i,j} + (B^{(\eta,\xi)})_{i,j}\right]\mu_\xi\delta_\xi\mu_\eta\delta_\eta\mathbf{V}_{i,j} \\ &+ \varepsilon^{(4)}\sigma(\tilde{A}^{(\xi)})\delta_\xi^4\mathbf{V}_{i,j} + \varepsilon^{(4)}\sigma(\tilde{A}^{(\eta)})\delta_\eta^4\mathbf{V}_{i,j} \qquad (6.2.38)\end{aligned}$$

and the Fourier symbol of equation (6.2.27) is replaced by $Z = Z_D + Z_{AD}$, where Z_D is defined the same as in equation (6.2.27), and

$$Z_{AD} = -16\,\Delta t\,\varepsilon^{(4)}\sigma\left(\tilde{A}^{(\xi)}\sin^4\frac{\theta_\xi}{2} + \tilde{A}^{(\eta)}\sin^4\frac{\theta_\eta}{2}\right) I$$

with I being the identity matrix.

Lemma 6.3 *If only the viscous terms and the fourth-difference dissipation terms are considered, then the condition*

$$\max\left[\Delta t\,(\sigma_D + \sigma_{AD})\right] \le N_D \qquad (6.2.39)$$

with σ_D the same as given in equation (6.2.35) and

$$\sigma_{AD} = 16\,\varepsilon^{(4)}\sigma\left(\tilde{A}^{(\xi)}\sin^4\frac{\theta_\xi}{2} + \tilde{A}^{(\eta)}\sin^4\frac{\theta_\eta}{2}\right)$$

is sufficient for the linearized stability of the multistage scheme.

The proof is the same as the proof for theorem 6.2. If cross-derivative terms are neglected, the inequality of equation (6.2.39) becomes

$$\Delta t\left[4\,\sigma\left(B^{(\xi,\xi)} + B^{(\eta,\eta)}\right) + 16\,\varepsilon^{(4)}\sigma\left(\tilde{A}^{(\xi)} + \tilde{A}^{(\eta)}\right)\right] \le N_D \qquad (6.2.40)$$

6.3. Time Step Estimate

Now consider the situation where the R-K scheme simultaneously satisfies the properties of equations (6.2.32) and (6.2.34). Also consider the 1-D case in the ξ direction. The R-K scheme then depends on the matrix Z, where $Z = -\Delta t\left(iA^{(\xi)}\sin\theta + 4B^{(\xi,\xi)}\sin^2\theta_\xi/2\right)$. Since $A^{(\xi)}$ and $B^{(\xi,\xi)}$ do not commute, the matrix Z, and thus the amplification matrix G, are no longer normal matrices. Hence, the Von Neumann condition on the largest eigenvalue of matrix G is now a necessary, but not a sufficient, condition for stability. Thus, there is no simple way to go from properties of matrix Z to properties of matrix G. The spectral mapping theorem relates the eigenvalues of matrix Z to the eigenvalues of matrix G. Since the eigenvalues do not tell the entire stability story, energy estimates based on norms must be used. However, no simple relationship exists between the norm of matrix Z and the norm of matrix G.

In practice, a simplified stability condition is used to estimate the time step. There is no strict mathematical proof of stability with this condition; nevertheless, it seems to work well. Consider

$$\Delta t_C = \frac{N_{CFL}}{\sigma_C}$$

$$\Delta t_D = \frac{N_D}{\sigma_D}$$

where

$$\sigma_C = \sigma(\widetilde{A}^{(\xi)}) + \sigma(\widetilde{A}^{(\eta)})$$
$$\sigma_D = \sigma(\widetilde{B}^{(\xi,\xi)}) + \sigma(\widetilde{B}^{(\eta,\eta)}) + \sigma(\widetilde{B}^{(\xi,\eta)})$$

Let

$$\frac{1}{\Delta t} = \frac{1}{\Delta t_C} + \frac{1}{\Delta t_D}$$

so that

$$\Delta t = \frac{N_{CFL}}{\sigma_C + (N_{CFL}/N_D)\sigma_D} \tag{6.3.1}$$

Schemes in which $N_{CFL} \approx N_D$ have been considered. The time step for each cell in the computational domain is then computed as

$$\Delta t = \frac{N_{CFL}\,\Omega}{\lambda_C + \lambda_D} \tag{6.3.2}$$

where Ω is the cell area and

$$\lambda_C = \lambda_\xi + \lambda_\eta$$
$$\lambda_D = (\lambda_D)_\xi + (\lambda_D)_\eta + (\lambda_D)_{\xi\eta}$$

with λ_ξ and λ_η defined by equation (4.2.5), and

$$\left.\begin{aligned}
(\lambda_D)_\xi &= \frac{\sqrt{\gamma}M}{Re}\frac{\gamma\mu}{\rho Pr}\Omega^{-1}(x_\eta^2 + y_\eta^2) \\
(\lambda_D)_\eta &= \frac{\sqrt{\gamma}M}{Re}\frac{\gamma\mu}{\rho Pr}\Omega^{-1}(x_\xi^2 + y_\xi^2) \\
(\lambda_D)_{\xi\eta} &= \frac{\sqrt{\gamma}M}{Re}\frac{1}{\rho\Omega}\left[-(\lambda+3\mu)(y_\eta y_\xi + x_\xi x_\eta) + (\lambda+\mu)\sqrt{(y_\eta^2 + x_\eta^2)(y_\xi^2 + x_\xi^2)}\,\right]
\end{aligned}\right\} \tag{6.3.3}$$

For the thin-layer, Navier-Stokes equations, take $\lambda_D = (\lambda_D)_\eta$, where η is the direction normal to the boundary layer.

Remark 6.4 *So far, only central differencing is considered for the spatial approximations in estimating a time step for an explicit R-K scheme. Since a numerical-flux function for an upwind scheme can generally be expressed as the sum of a centered (physical) contribution and a numerical dissipation contribution, then equation (6.3.1) is also a reasonable estimate for the time step when an upwind scheme is used.*

7. Convergence Acceleration Techniques

7.1. Local Time Stepping

The first technique employed to accelerate convergence of the basic explicit time-stepping scheme to a steady-state solution is local time stepping, where each cell is updated using an individual time step. For simplicity, the one-dimensional Euler equations are used to understand the meaning of local time stepping from the discrete point of view. Suppose the Euler equations are written in the form

$$\frac{\partial \mathbf{W}}{\partial t} + A\frac{\partial \mathbf{W}}{\partial x} = 0$$

If the equations are discretized in an explicit sense, then

$$\Delta\widetilde{\mathbf{W}} = \widetilde{A}\widetilde{\mathbf{W}}^n$$

where the tilde indicates that the vector or matrix is for the complete discrete system. The block matrix $\tilde{A}$ is a function of $\Delta t_{\min}/\Delta x$, with $\Delta t_{\min}$ being the minimum time step permitted in the domain, and each element of $\tilde{A}$ being a 3 by 3 matrix. Let the explicit matrix $\tilde{A}$ for the system of difference equations be preconditioned by the diagonal matrix Λ, given by

$$\Lambda = \text{Diag}\left[\begin{array}{cccc} \overline{\Delta t}_2 I & \overline{\Delta t}_3 I & \cdots & \overline{\Delta t}_{N-2} I \quad \overline{\Delta t}_{N-1} I \end{array}\right]$$

where

$$\overline{\Delta t}_i = \frac{\Delta t_i}{\Delta t_{\min}} \qquad i = 2 \qquad N-1$$

Here, Δt_i is the largest local time step allowed by stability, and I is a 3 by 3 identity matrix. This process results in a significant speedup in the transport of information, and an increase by roughly a factor of two in the convergence rate of explicit schemes.

7.2. Residual Smoothing

The local stability range of the basic time-stepping scheme can be extended by applying a procedure called implicit residual smoothing. This technique was first introduced by Lerat (ref. 50) for the Lax-Wendroff scheme, and later devised by Jameson (ref. 51) for R-K schemes. The constant-coefficient approach of Jameson is discussed in section 7.2.1. Some basic properties of residual smoothing are also presented. Then, variable coefficients for implicit smoothing are discussed. The coefficients introduced in this paper, and those of Martinelli (ref. 27), are derived and compared. In section 7.2.3, coefficients are developed for implicit residual smoothing that allow a time-step estimate independent of a physical diffusion limit.

7.2.1. Constant coefficients. The constant-coefficient, implicit residual averaging of Jameson (ref. 51) can be applied in two dimensions using the factored form

$$(1 - \beta_\xi \nabla_\xi \Delta_\xi)(1 - \beta_\eta \nabla_\eta \Delta_\eta)\overline{\mathcal{R}}_{i,j}^{(m)} = \mathcal{R}_{i,j}^{(m)} \qquad (7.2.1)$$

where the quantity $\nabla\Delta$ is a standard second-difference operator, and thus

$$\nabla_\xi \Delta_\xi \overline{\mathcal{R}}_{i,j}^{(m)} = \overline{\mathcal{R}}_{i-1,j}^{(m)} - 2\overline{\mathcal{R}}_{i,j}^{(m)} + \overline{\mathcal{R}}_{i+1,j}^{(m)}$$

The quantity β is a smoothing coefficient, and (ξ, η) are the coordinates of a uniformly spaced, computational domain. The residual of the unsmoothed scheme $\mathcal{R}_{i,j}^{(m)}$ is defined by

$$\mathcal{R}_{i,j}^{(m)} = \alpha_m \frac{\Delta t_{i,j}}{\Omega_{i,j}}[\mathcal{L}_C \mathbf{W}_{i,j}^{(m-1)} + \mathcal{L}_D \mathbf{W}_{i,j}^{(0)} + \text{AD}^{(m)}] \qquad (m = 1,5) \qquad (7.2.2)$$

and computed in the Runge-Kutta stage m, $\text{AD}^{(m)}$ is the total artificial dissipation at stage m, and $\overline{\mathcal{R}}_{i,j}^{(m)}$ is the final residual at stage m after the sequence of smoothings in the ξ and η directions. A tridiagonal system of equations is solved for each coordinate direction to obtain the unknown residuals $\overline{\mathcal{R}}_{i,j}^{(m)}$. To determine β_ξ and β_η, Jameson (ref. 51) considers the model problem of equation (6.1.6) without numerical dissipation (i.e., the convection equation). Then, the semidiscrete equation (6.1.7) becomes

$$\Delta t \frac{dw}{dt} = -\Delta t \mathcal{L} w_j$$

with

$$\Delta t \mathcal{L} w_j = \frac{N}{2}(w^n_{j+1} - w^n_{j-1})$$

and the Fourier symbol of the difference operator $-\Delta t \mathcal{L}$ is given by

$$z = -\Delta t \mathcal{L} = -iN \sin\theta \tag{7.2.3}$$

Let $\Delta\overline{w}_j$ define the correction, or residual, obtained from the implicit smoothing procedure, so that

$$(1 - \beta\nabla\Delta)\,\Delta\overline{w}_j = \Delta w_j \tag{7.2.4}$$

and the Fourier symbol of equation (7.2.3) is replaced by

$$z = -i\frac{N\sin\theta}{1 + 4\beta\sin^2\frac{\theta}{2}} \tag{7.2.5}$$

A sufficient condition for stability is as follows:

$$\max\ |z| \le N^* \tag{7.2.6}$$

for all θ, and N^* is the Courant number of the unsmoothed scheme. Solving for $\sin\theta$ and $\cos\theta$ corresponding to the maximum of $|z|$ yields

$$\left.\begin{aligned} \sin\theta &= \frac{\sqrt{1+4\beta}}{1+2\beta} \\ \cos\theta &= \frac{2\beta}{1+2\beta} \end{aligned}\right\} \tag{7.2.7}$$

Using equations (7.2.7) and the sufficient condition of equation (7.2.6), the smoothing coefficient is determined by

$$\beta \ge \frac{1}{4}\left[\left(\frac{N}{N^*}\right)^2 - 1\right] \tag{7.2.8a}$$

or

$$\beta \ge \frac{1}{4}\left[\left(\frac{\Delta t}{\Delta t^*}\right)^2 - 1\right] \tag{7.2.8b}$$

where Δt^* is the time step of the unsmoothed scheme. In subsequent discussion, this β will be referred to as the 1-D smoothing coefficient and will be designated by β_{1-D}.

Instead, consider the diffusion equation

$$\frac{\partial w}{\partial t} = \mu\frac{\partial^2 w}{\partial x^2}$$

If the spatial derivative is again approximated with a central difference, and a Fourier transform is taken of the resulting semidiscrete equation, the Fourier symbol of the product of Δt and the difference operator are given by

$$z = -N_D \sin^2\frac{\theta}{2}$$

where the diffusion number $N_D = 4\Delta t\mu/\Delta x^2$. If the residual smoothing operator of equation (7.2.4) is applied, then

$$z = \frac{-N_D \sin^2\theta/2}{1 + 4\beta_D \sin^2\theta/2} \tag{7.2.9}$$

A sufficient stability condition for an R-K scheme is

$$\max |z| \leq N_D^*$$

for all θ, where N_D^* is the diffusion number of the unsmoothed scheme. With the same procedure employed for the convection equation, the smoothing coefficient is determined as

$$\beta_D \geq \frac{1}{4}\left(\frac{N_D}{N_D^*} - 1\right) = \frac{1}{4}\left(\frac{\Delta t_D}{\Delta t_D^*} - 1\right) \tag{7.2.10}$$

Thus, for the scalar diffusion equation, the smoothing coefficient β_D is proportional to $\mu\,\Delta t/(\Delta x)^2$. As will be shown in section 7.2.3, this type of β can be combined with the type of β given by equations (7.2.8) to yield a formulation suitable for a convection-diffusion equation.

Some properties of implicit residual smoothing are now examined. If residual smoothing is applied on each stage of an R-K scheme, the stability function given in equation (6.1.11) still applies, with the z of the original (basic) scheme modified as in equation (7.2.5) or (7.2.9). This stability behavior leads to the following theorem:

Theorem 7.1 *Let $\mathcal{L}$ be the Fourier symbol of any discrete spatial operator for the convection-diffusion equation. Let equation (6.1.11) be the stability polynomial for an explicit m-stage R-K scheme. Apply implicit residual smoothing, as in equation (7.2.4), after every stage of the R-K scheme.*

If the original scheme is unconditionally unstable, then the smoothed scheme is also unconditionally unstable. If the original scheme is conditionally stable, then the smoothed scheme can be made unconditionally stable by choosing $\beta\,\Delta t$ sufficiently large.

Proof. Let z and z_s be the symbols of the original and smoothed schemes, respectively. Then,

$$z_s = \frac{z}{1 + 4\beta \sin^2 \theta/2} \tag{7.2.11}$$

Define $\mathbf{r}$ as the position vector corresponding to z. Thus, $\mathbf{r}$ emanates from the origin of the complex domain and has magnitude $|z|$. Let $\mathbf{r}_s$ be the position vector associated with z_s. If the original R-K scheme is stable, then $\mathbf{r}$ does not terminate outside the stability region S, determined by the Von Neumann condition $|g(z)| \leq 1$, where $g(z)$ is the stability polynomial. If the original scheme is unstable, then there is no $\Delta t > 0$ small enough to allow $\mathbf{r}$ to be in S. Since the denominator of equation (7.2.11) merely acts as a scaling factor of $\mathbf{r}$, the residual smoothing cannot stabilize the unstable original scheme.

Suppose β is proportional to Δt, as in equations (7.2.8) or (7.2.10). Then, $\mathbf{r}_s$ does not terminate outside the boundary of S for any value of Δt, since β can always be made sufficiently large. Moreover, the scheme is unconditionally stable.

Remark 7.2 *Even though the explicit R-K scheme can be made unconditionally stable with the implicit residual smoothing, there is a practical limit on the time step when solving the hyperbolic problem and taking $\beta \propto \Delta t^2$, as in equations (7.2.8). That is, if Δt is too large, convergence slows down.*

Lemma 7.3 *Apply an explicit m-stage R-K scheme with implicit residual smoothing to the scalar equation*

$$\frac{\partial w}{\partial t} + \varepsilon^{(4)} \Delta x^3 \frac{\partial^4 w}{\partial x^4} = 0 \tag{7.2.12}$$

where $\varepsilon^{(4)}$ is a constant coefficient. Assume that the residual smoothing coefficient β is proportional to N^2. Then, the symbol of the smoothed scheme vanishes as $\Delta t \to \infty$ and the stability polynomial $g(z) \to 1$.

Proof. The symbol for the difference operator of equation (7.2.12) when implicit residual smoothing is applied is given by

$$z_s = \frac{-16\varepsilon^{(4)} N \sin^4 \theta/2}{1 + 4\beta \sin^2 \theta/2}$$

Using $\beta \sim N^2$ and taking Δt to be large, then

$$z_s \sim -\frac{4}{N}\varepsilon^{(4)} \sin^2 \frac{\theta}{2}$$

Therefore, $z_s \to 0$ as $\Delta t \to \infty$. From equation (6.1.11), it follows immediately that $g(z) \to 1$ as $z_s \to 0$.

Remark *As evident from Lemma 7.3, the limit on the extension of stability with the implicit smoothing and equations (7.2.8) is caused by the requirement to have a certain background dissipation (i.e., high-frequency damping). If $\beta \sim N$, as in the parabolic problem, then the symbol z_s does not vanish.*

The use of constant coefficients in the implicit treatment (eqs. (7.2.8)) proves satisfactory (extending the Courant number by a factor of two to three) even for highly stretched meshes of viscous-flow computations (ref. 16), provided additional support such as enthalpy damping (ref. 1) is introduced. However, the use of enthalpy damping, which assumes constant total enthalpy throughout the flow field, precludes the solution of problems with heat-transfer effects. By using variable coefficients β_ξ and β_η, which account for the variation in mesh-cell-aspect ratio, residual smoothing can be applied without the support of enthalpy damping.

*7.2.2. **Variable coefficients.*** The alternating direction implicit (ADI) scheme and the implicit scheme of Lerat (ref. 52) exhibit a functional dependence of variable smoothing coefficients on the characteristic speeds λ_ξ and λ_η, as defined in section 4.2 of this report. Appendix B shows this functional dependence. Then, with a 2-D stability analysis similar to the 1-D analysis of the previous section, variable smoothing coefficients can be obtained as

$$\left.\begin{aligned} \beta_\xi &= \max\left\{\frac{1}{4}\left[\left(\frac{N}{N^*}\frac{1}{1+r_{\eta\xi}}\right)^2 - 1\right], 0\right\} \\ \beta_\eta &= \max\left\{\frac{1}{4}\left[\left(\frac{N}{N^*}\frac{1}{1+r_{\eta\xi}^{-1}}\right)^2 - 1\right], 0\right\} \end{aligned}\right\} \tag{7.2.13}$$

where again $r_{\eta\xi} = \lambda_\eta/\lambda_\xi i$. The limiting cases are $\beta_\xi \to \beta_{1-D}, \beta_\eta \to 0$ as $r_{\eta\xi} \to 0$ and $\beta_\xi \to 0, \beta_\eta \to \beta_{1-D}$, as $r_{\eta\xi} \to \infty$.

A problem exists with the smoothing coefficients of equations (7.2.13). In the typical case of $N/N^* = 2$, the smoothing coefficients vanish when $r_{\eta\xi} = 1$, making the scheme unstable.

Martinelli (ref. 27) eliminates this difficulty by modifying the residual smoothing coefficients of equations (7.2.13) as follows:

$$\left.\begin{aligned}\beta_\xi &= \max\left\{\frac{1}{4}\left[\left(\frac{N}{N^*}\frac{\phi(r_{\eta\xi})}{1+r_{\eta\xi}}\right)^2 - 1\right], 0\right\} \\ \beta_\eta &= \max\left\{\frac{1}{4}\left[\left(\frac{N}{N^*}\frac{\phi(r_{\eta\xi}^{-1})}{1+r_{\eta\xi}^{-1}}\right)^2 - 1\right], 0\right\}\end{aligned}\right\} \tag{7.2.14}$$

where

$$\phi(r) = 1 + r^\zeta \tag{7.2.15}$$

and the exponent ζ is taken to be 2/3. The function ϕ is the same function used for scaling the artificial dissipation coefficients. The introduction of this function seems appropriate because of the direct relationship between residual smoothing and artificial dissipation. For example, a desired high-frequency, damping behavior of the scheme can be maintained when the dissipation is increased by increasing the residual smoothing.

The variable smoothing coefficients β_ξ and β_η of equations (7.2.14) cannot be uniquely determined from a sufficient condition for stability, as the constant coefficient β was in equations (7.2.8). Wigton and Swanson (ref. 53) use an additional constraint to derive the parameters of equations (7.2.14). For completeness the short derivation of reference 53 is presented.

Consider the following sufficient condition for stability:

$$\frac{N}{N^*}\frac{1}{1+r_{\eta\xi}}\frac{1}{\sqrt{1+4\beta_\xi}} + \frac{N}{N^*}\frac{1}{1+r_{\eta\xi}^{-1}}\frac{1}{\sqrt{1+4\beta_\eta}} \le 1 \tag{7.2.16}$$

as derived in appendix B. Let the Courant numbers for the two coordinate directions ξ and η be given by

$$\left.\begin{aligned}N_\xi &= \frac{\Delta t_{\text{act}}}{\Delta t_\xi} = N\frac{\lambda_\xi}{\lambda_\xi+\lambda_\eta} = \frac{N}{1+r_{\eta\xi}} \\ N_\eta &= \frac{\Delta t_{\text{act}}}{\Delta t_\eta} = N\frac{\lambda_\eta}{\lambda_\xi+\lambda_\eta} = \frac{N}{1+r_{\eta\xi}^{-1}}\end{aligned}\right\} \tag{7.2.17}$$

where Δt_{act} is the 2-D allowable time step for convection, and Δt_ξ and Δt_η are the corresponding 1-D time steps. If the Courant number N in equation (7.2.16) is replaced according to equations (7.2.17), the result is

$$\frac{N_\xi}{N^*}\frac{1}{\sqrt{1+4\beta_\xi}} + \frac{N_\eta}{N^*}\frac{1}{\sqrt{1+4\beta_\eta}} \le 1 \tag{7.2.18}$$

As suggested by lemma 7.3, β_ξ and β_η should be as small as possible and still maintain stability. With this objective in mind, $\beta_\xi + \beta_\eta$ is minimized subject to equality in equation (7.2.18). Apply the method of Lagrange multipliers and consider the function

$$F(\beta_\xi, \beta_\eta) = \beta_\xi + \beta_\eta + \omega\left(\frac{N_\xi}{N^*}\frac{1}{\sqrt{1+4\beta_\xi}} + \frac{N_\eta}{N^*}\frac{1}{\sqrt{1+4\beta_\eta}}\right)$$

After equating the partial derivatives of $F(\beta_\xi, \beta_\eta)$, with respect to β_ξ and β_η, to zero, obtain

$$N_\xi \frac{1}{(1+4\beta_\xi)^{3/2}} = N_\eta \frac{1}{(1+4\beta_\eta)^{3/2}} \tag{7.2.19}$$

Now, solving for $\sqrt{1+4\beta_\eta}$ and substituting the resulting expression into equation (7.2.16) yields

$$\frac{N}{N^*} \frac{1}{1+r_{\eta\xi}} \frac{1}{\sqrt{1+4\beta_\xi}} \left[1 + \frac{1+r_{\eta\xi}}{1+r_{\eta\xi}^{-1}} \left(\frac{N_\eta}{N_\xi}\right)^{-1/3}\right] \leq 1 \tag{7.2.20}$$

With the equality of equation (7.2.20) holding, and using equations (7.2.17), obtain the smoothing coefficients of equations (7.2.14). As shown in reference 53, the function ϕ arises without any consideration of numerical dissipation terms. The role of the ϕ function is to connect the values of β corresponding to low-aspect-ratio and high-aspect-ratio cells.

The variation of β_ξ from equations (7.2.14) with $r_{\eta\xi}$ is shown as a solid line in figure 8(a). For this curve, the ratio of Courant numbers N/N^* is assumed to be 2. Observe that $\beta_\xi \to \beta_{1-D}$ for $r_{\eta\xi} \to 0$, and $\beta_\xi \to 0$ for $r_{\eta\xi} \to \infty$. In the case of $r_{\eta\xi} = 1$, $\beta_\xi = \beta_\eta = \beta_{1-D}$ (a value of 0.75 when $N/N^* = 2$). Based upon numerical calculations for inviscid flows using typical inviscid meshes, smoothing coefficients β_ξ and β_η that are constant with a value of about 0.4 result in rapid convergence. Values for $\beta_\xi \geq 0.75$ and/or $\beta_\eta \geq 0.75$ can cause a significant slowdown in convergence. To provide improved smoothing coefficients, when $r_{\eta\xi} \approx 1$ the formulas of equations (7.2.14) can be replaced with

$$\left.\begin{aligned} \beta_\xi &= \max\left\{\frac{1}{4}\left[\left(\frac{N}{N^*}\frac{1}{1+\psi\, r_{\eta\xi}}\right)^2 - 1\right], 0\right\} \\ \beta_\eta &= \max\left\{\frac{1}{4}\left[\left(\frac{N}{N^*}\frac{1}{1+\psi\, r_{\eta\xi}^{-1}}\right)^2 - 1\right], 0\right\} \end{aligned}\right\} \tag{7.2.21}$$

where ψ is a parameter to be specified. Here, the connection function ϕ is removed by introducing ψ. Figure 8(a) shows the curve representing β_ξ when $N/N^* = 2$ and $\psi = 0.25$. For the case of $r_{\eta\xi} = 1$, β_ξ is 0.39.

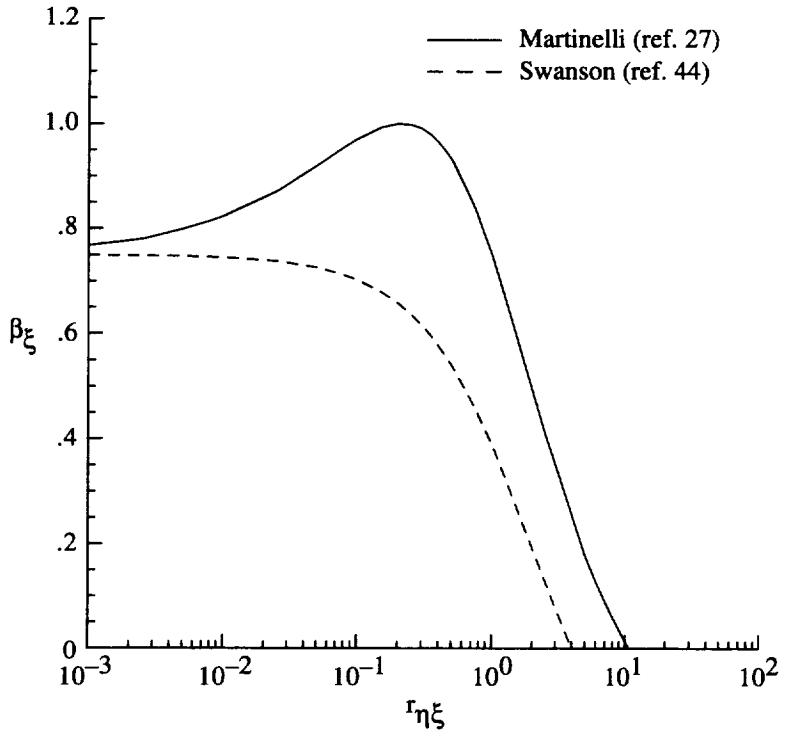

(a) Variation of coefficient β_ξ with mesh cell aspect ratio $r_{\eta\xi}$.

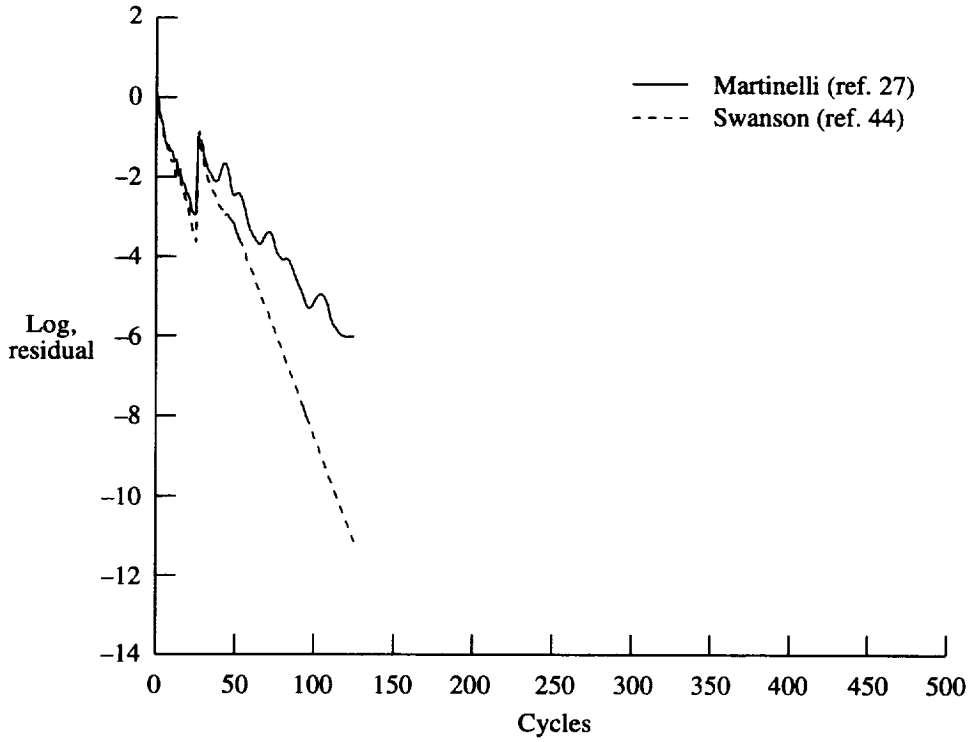

(b) Residual histories. RAE 2822 airfoil, $M_\infty = 0.75$, $\alpha = 3°$, 224 by 32 grid.

Figure 8. Implicit residual smoothing coefficient for two forms of variable coefficients.

To investigate stability using the smoothing coefficients of equations (7.2.21), consider the sufficient stability condition

$$\frac{N}{N^*}\,\frac{1}{1+r_{\eta\xi}}\,\frac{\sin\theta_\xi}{\lambda_\xi\lambda_\eta}+\frac{N}{N^*}\,\frac{1}{1+r_{\eta\xi}^{-1}}\,\frac{\sin\theta_\eta}{\lambda_\xi\lambda_\eta}\le 1 \tag{7.2.22}$$

for all θ_ξ and θ_η. In equation (7.2.22)

$$\left.\begin{aligned}\lambda_\xi &= 1+2\beta_\xi\left(1-\cos\theta_\xi\right)\\ \lambda_\eta &= 1+2\beta_\eta\left(1-\cos\theta_\eta\right)\end{aligned}\right\} \tag{7.2.23}$$

and $r_{\eta\xi}=\lambda_\eta/\lambda_\xi$. This condition comes from the 2-D stability analysis given in appendix B. (See eq. (B18).) If $r_{\eta\xi}\ll 1$, the condition of equation (7.2.22) reduces to approximately

$$\frac{N}{N^*}\,\frac{\sin\theta_\xi}{\lambda_\xi}\le 1 \tag{7.2.24}$$

for all θ_ξ. Using equations (7.2.7), obtain

$$\frac{N}{N^*}\,\frac{1}{\sqrt{1+4\beta_\xi}}\le 1 \tag{7.2.25}$$

Substituting for β_ξ according to equations (7.2.21), the inequality equation (7.2.25) is satisfied. Now, if $r_{\eta\xi}\gg 1$, the condition of equation (7.2.22) reduces to approximately

$$\frac{N}{N^*}\,\frac{\sin\theta_\eta}{\lambda_\eta}\le 1 \tag{7.2.26}$$

for all θ_η. From equations (7.2.7) and the definition of β_η in equations (7.2.21), the inequality of equation (7.2.26) is satisfied. Consider the case of $r_{\eta\xi}=1$. Assume $\theta_\xi=\theta_\eta$ and $\beta_\xi=\beta_\eta$. Then equation (7.2.22) becomes

$$\tilde{F}\le 1 \tag{7.2.27}$$

for all θ_ξ, where

$$\tilde{F}=\frac{N}{N^*}\,\frac{\sin\theta_\xi}{{\lambda_\xi}^2}$$

It can be shown that

$$\tilde{F}_{\max}\le\frac{N}{N^*}\left[\frac{\left(1+8\beta_\xi\right)^5}{\left(1+4\beta_\xi\right)\left(1+10\beta_\xi\right)^4}\right]^{\frac{1}{2}}\frac{1}{\sqrt{1+4\beta_\xi}}$$

Then

$$\tilde{F}_{\max}\le 0.9\,\frac{N}{N^*}\,\frac{1}{\sqrt{1+4\beta_\xi}} \tag{7.2.28}$$

By substituting for β_ξ and taking $\psi\approx 0.11$, the condition of equation (7.2.27) is satisfied. From numerical experiments, this estimate for ψ seems to be conservative. A value for ψ of 0.125

worked well for both central and upwind schemes. Moreover, for central schemes $\psi = 0.25$ also works without causing stability problems.

Calculations were performed for a case of inviscid, transonic flow over an RAE 2822 airfoil to evaluate the variable smoothing coefficients of equations (7.2.14) and (7.2.21). A typical inviscid mesh with 224 by 32 cells was used. Figure 8(b) shows the convergence histories corresponding to the formulations of Martinelli (eqs. (7.2.14)) and Swanson (eqs. (7.2.21)). Convergence is measured by the logarithm of the root-mean-square of the residual of the continuity equation. For each computation, the basic explicit scheme of equation (6.1.4) and a multigrid method (described in section 7.3) were employed. The average rate of reduction of the residual was defined by $R_f = (\text{rate})^N R_i$, where R is the residual for the continuity equation, the subscripts f and i mean final and initial values, respectively, and N denotes the number of multigrid cycles. With the coefficients of equations (7.2.14), the average rate of residual reduction is 0.889, while with the coefficients of equations (7.2.21), the average rate of residual reduction is 0.789. As expected, the two formulations exhibit only small differences in convergence behavior in the case of turbulent flow calculations, since the high-aspect-ratio cells of the mesh, usually defined to resolve the boundary layer, determine the convergence rate.

7.2.3. Removal of diffusion limit. The diffusion restriction on the time step (eq. (6.3.1)) can be a significant factor in viscous regions of a flow field, causing excessive restrictions on the allowable time step Δt. In this section the diffusion-based, smoothing coefficient of equation (7.2.10) is utilized to construct a new smoothing parameter that allows the removal of this diffusion restriction.

Considering the thin-layer form of the 2-D Navier-Stokes equations allows use of the smoothing coefficient of equations (7.2.21) in the streamwise-like (ξ) direction. A possible formulation for the normal η direction depends on a diffusion-type β near the surface, and a convection-type β when the viscous effects are no longer important. Consider the dependency in equation (7.2.10) on the ratio of the actual Δt to the Δt of the basic explicit scheme. To remove the diffusion limit on the time step, the actual time step must be independent of diffusion effects. Thus, set $N_D = 0$ in equation (6.3.2), giving

$$\Delta t = \Delta t_{\text{act}} = \frac{N\,\Omega}{\lambda_\xi + \lambda_\eta} \tag{7.2.29}$$

where Ω is the area of the mesh cell being considered. In the part of the boundary layer where diffusion effects dominate, define the time step of the unsmoothed scheme (Δt^*) by

$$\Delta t^* = (\Delta t_D)_\eta = \frac{N_D\,\Omega}{(\lambda_D)_\eta} \tag{7.2.30}$$

where

$$(\lambda_D)_\eta = \frac{\sqrt{\gamma} M}{Re} \frac{\gamma \mu}{\rho Pr} \Omega^{-1} (x_\xi^2 + y_\xi^2)$$

Then define

$$(\beta_D)_\eta = \frac{1}{4} \left[\frac{\Delta t_{\text{act}}}{(\Delta t_D)_\eta} - 1 \right] \tag{7.2.31}$$

If $(\Delta t_D)_\eta = \Delta t_{\text{act}}$, $\beta_D = 0$. This means that the full parabolic stability limit is being used for the physical diffusion terms. Since the numerical dissipation of the scheme is not included in the analysis, replace equation (7.2.31) with

$$(\beta_D)_\eta = \frac{1}{4}\left[C_1 \frac{\Delta t_{\text{act}}}{(\Delta t_D)_\eta} - 1\right] \tag{7.2.32}$$

where C_1 is a constant. Equation (7.2.32) accounts for any possible influence on the stability caused by a single evaluation of the physical viscous terms in the multistage time-stepping scheme. By using equations (7.2.29) and (7.2.30) to replace Δt_{act} and $(\Delta t_D)_\eta$, respectively, equation (7.2.32) can be rewritten as

$$(\beta_D)_\eta = \frac{1}{4}\left[C_1 \frac{N}{N_D} \frac{(\lambda_D)_\eta}{\lambda_\xi + \lambda_\eta} - 1\right] \tag{7.2.33}$$

which can be approximated by

$$(\beta_D)_\eta = \frac{1}{4}\overline{C}_1 \frac{(\lambda_D)_\eta}{\lambda_\xi + \lambda_\eta} \tag{7.2.34}$$

Either equation (7.2.33) or equation (7.2.34) can be used, provided the constant is defined properly. Both equations successfully remove the diffusion restriction on the time step. In this paper, the simpler form of equation (7.2.34) is used, and has also been considered by Radespiel and Kroll (ref. 54). Numerical experiments have shown that a satisfactory value for $\overline{C}_1$ is 5.

For the full Navier-Stokes equations (including all viscous terms), a coefficient β_D for the streamwise-like direction (ξ) should also be defined. Using the form of $(\beta_D)_\eta$ in equation (7.2.34), $(\beta_D)_\xi$ is defined as

$$(\beta_D)_\xi = \frac{1}{4}\overline{C}_1 \frac{(\lambda_D)_\xi}{\lambda_\xi + \lambda_\eta} \tag{7.2.35}$$

where

$$(\lambda_D)_\xi = \frac{\sqrt{\gamma} M}{R\epsilon} \frac{\gamma \mu}{\rho Pr} \Omega^{-1} (x_\eta^2 + y_\eta^2)$$

The variable coefficient of equation (7.2.34) generally cannot be used alone. For example, in an airfoil flow, $(\beta_D)_\eta$ goes to 0 too fast at the leading edge, resulting in a 0-value in the inviscid region. This difficulty is overcome by calculating β_η as

$$\beta_\eta = \max[(\beta_D)_\eta, (\beta_C)_\eta]$$

where $(\beta_C)_\eta$ is defined by equations (7.2.21). In a similar manner, $(\beta_D)_\xi$ in equation (7.2.35) is redefined.

According to the theory presented in reference 55, the residual smoothing is evaluated only on the even steps of an R-K time scheme. In practice, the residual smoothing is evaluated during every stage, which is more expensive but produces a more robust algorithm.

7.3. Multigrid Method

The concept of multigrid acceleration of an iterative scheme was first suggested by Fedorenko (ref. 56). The fundamental ideas of this approach currently used in many applications are principally due to reference 57. Although most of the theory developed for the multigrid method is for elliptic problems, a number of effective multigrid solvers (refs. 3, 58, 59, and 60) have been constructed for the Euler equations of gas dynamics, which are hyperbolic. Transonic and

subsonic flows have been computed with these solvers. Some multigrid methods (refs. 19, 20, 22, and 23) have also been devised for the numerical solution of the compressible Navier-Stokes equations. In section 7.3.1, the basic theory of the multigrid process is briefly reviewed. Then, the operators used in the present method are defined. Section 7.3 concludes with a discussion of the various elements of the multigrid technique of this work.

7.3.1. Basic concepts of multigrid methods. In the simplest sense, the multigrid method involves applying a sequence of grids to solve a discrete problem. More specifically, a faster rate of development of the solution on a fine grid is achieved by approximating the fine-grid problem on successively coarser grids in the sequence. With suitable coarse-grid approximations of the fine-grid problem, the low-frequency error components on the fine grid appear as high-frequency error components on the coarser grids. The low-frequency components on the fine grid where the discrete solution is desired are precisely the error components that dramatically slow the convergence of single-grid schemes. Thus, with a good high-frequency damping scheme, an effective multigrid process (i.e., much more rapid removal of low-frequency errors than a single-grid scheme) can be constructed. As will become evident, the driving scheme for the multigrid process is not only important for providing smoothing on each grid, but also for removing high-frequency errors resulting from interpolation of corrections for the fine-grid approximation.

Two additional advantages are derived from displacing part of the effort in solving a set of discrete equations to coarse grids. One advantage is that the larger mesh spacing permits larger time steps, meaning that information is propagated rapidly in the domain of interest. Moreover, for explicit time-stepping schemes such as the multistage schemes described previously in this report, the increased time step is particularly important because the allowable time step depends on the speed of sound. This acoustic dependence is even more critical for viscous flows. A second benefit of the coarse grids is that they require less computational work. For example, in two dimensions, the computational effort needed is decreased roughly by a factor of four on successively coarser meshes. Thus, the objective of the multigrid process is to spend much more time on the coarse grids than on the fine grid.

The basic ideas of the multigrid process are revealed by considering the continuum problem

$$\mathcal{L}W(x,y) = S(x,y)$$

$$\Lambda W(x,y) = \Phi(x,y)$$

where the first equation is associated with the domain Ω, and the second equation is associated with its boundary $\partial\Omega$. The symbols $\mathcal{L}$ and Λ are general nonlinear, differential operators, and both S and Φ are source terms. Let $G_0, G_1, ..., G_N$ be a set of grids, where G_N is the finest grid, and each successively coarser grid $G_k (k \leq N-1)$ is generated by eliminating every other mesh line in each coordinate direction of the next-finer mesh. The discrete problem on G_N is as follows:

$$\left.\begin{aligned} \mathcal{L}_N W_N(x,y) &= S_N(x,y) && (x,y \in G_N) \\ \Lambda_N W_N(x,y) &= \Phi_N && (x,y \in \partial G_N) \end{aligned}\right\} \tag{7.3.1}$$

and W_N is the exact discrete solution. If $w_N(x,y)$ is an approximate discrete solution, equations (7.3.1) can be written as

$$\left.\begin{aligned} \mathcal{L}_N w_N &= S_N + R_N \\ \Lambda_N w_N &= \Phi_N + (R_B)_N \end{aligned}\right\} \tag{7.3.2}$$

where R_N and $(R_B)_N$ are residual functions. Subtracting equations (7.3.2) from equations (7.3.1) gives the residual equations for the G_N problem. That is,

$$\mathcal{L}_N W_N - \mathcal{L}_N w_N = -R_N$$

$$\Lambda_N W_N - \Lambda_N w_N = -(R_B)_N$$

These equations can be adequately approximated on G_{N-1} if the residual functions and corrections $(W_N - w_N)$ are smooth. Smoothing is accomplished by performing an iteration with an effective high-frequency damping scheme. The approximations of the residual equations on the coarser grid G_{N-1} are

$$\left.\begin{aligned} \mathcal{L}_{N-1} W_{N-1} - \mathcal{L}(I_N^{N-1} w_N) &= -I_N^{N-1} R_N \\ \Lambda_{N-1} W_{N-1} - \Lambda(I_N^{N-1} w_N) &= -I_N^{N-1} (R_B)_N \end{aligned}\right\} \tag{7.3.3}$$

where I_N^{N-1} is a restriction operator. Note that if $R_N = 0$, then $W_{N-1} = I_N^{N-1} w_N$, and once a steady state is reached on the fine grid, all corrections on the coarse grid are 0. Furthermore, for a linear problem, the two terms on the left-hand side of equations (7.3.3) can be combined and the error equation $\mathcal{L}(\text{error}) = -I_N^{N-1} R_N$ is obtained. In general, the operator I_l^m is used to indicate restriction when $l > m$ and prolongation when $l < m$. Thus, a restriction operator transfers information from a fine grid to a coarse grid, and a prolongation operator (i.e., interpolating polynomial) transfers information from a coarse grid to a fine grid. Equations (7.3.3) can be rewritten as

$$\mathcal{L}_{N-1} w_{N-1} = \overline{S}_{N-1}$$

$$\Lambda_{N-1} w_{N-1} = (\overline{S}_B)_{N-1}$$

where

$$\overline{S}_{N-1} = R_{N-1} + F_{N-1}$$

$$(\overline{S}_B)_{N-1} = (R_B)_{N-1} + (F_B)_{N-1}$$

and

$$\left.\begin{aligned} F_{N-1} &= I_N^{N-1}(-R_N) + \mathcal{L}_{N-1}(I_N^{N-1} w_N) \\ (F_B)_{N-1} &= I_N^{N-1}(-R_B)_N + \Lambda_{N-1}(I_N^{N-1} w_N) \end{aligned}\right\} \tag{7.3.4}$$

Thus, the discrete problem on G_{N-1} has the same form as that on G_N, except the forcing functions of equations (7.3.4) are added to the residual functions. An improvement to the approximate solution w_N can be obtained by adding a coarse-grid correction. The fine-grid solution is then given by

$$w_N \leftarrow w_N + I_{N-1}^N (w_{N-1} - I_N^{N-1} w_N)$$

where the correction $(w_{N-1} - I_N^{N-1} w_N)$ is an approximation to the smoothed function $W_N - w_N$.

In this work, the smoother chosen to solve equations (7.3.3) is a multistage R-K scheme of the type discussed in section 6. Thus, a time derivative is added to the steady-state equations, and the resulting equations are advanced in pseudotime with several iterations of the multistage method. Usually, one complete R-K time step is performed on the finest mesh, and two or three time steps are performed on coarser meshes.

Instead of immediately passing a correction from G_{N-1} to G_N, the solution w_{N-1} and residual R_{N-1} can be restricted to the grid G_{N-2}. Iteration sweeps can then be performed to

obtain a smooth approximation of the correction function $W_{N-2} - w_{N-2}$. If this correction is passed to G_{N-1}, iterations are performed, and the correction of G_{N-1} is transferred to G_N, a multigrid cycle of three grids is completed. This cycle is called a V cycle.

There are other fixed-cycle strategies (i.e., W cycle), and variable-cycle strategies that depend on a prescribed residual level, or a certain slowdown, in smoothing rate before changing to a coarser grid problem (ref. 57). For each coarse grid G_k in a cycle, the full current approximation w_k and the initial (basic) approximation w_{k+1} (the approximation on grid G_{k+1} that is transferred to grid G_k) are stored. The approximation w_k is the sum of the G_k correction and the basic approximation. Brandt (ref. 57) refers to a scheme that stores the full, current approximation rather than only the correction as the full approximation storage (FAS) scheme.

7.3.2. Transfer operators. The intergrid transfer operators employed in the present multigrid method were introduced by Jameson (ref. 3) and assume that the unknowns are stored at the center of a mesh cell. The restriction operator for the residual is defined by

$$I_{k+1}^{k} R_{k+1} = \frac{1}{\Omega_k} \sum_{l=1}^{4} (\Omega_{k+1} R_{k+1})_l \tag{7.3.5}$$

where the residual function R_{k+1} is expressed in the usual way as

$$R_{k+1} = \frac{1}{\Omega_{k+1}} \mathcal{L}_{k+1} w_{k+1}$$

with $\mathcal{L}_{k+1}$ and Ω_{k+1} denoting the spatial-discretization operator and the cell area, respectively, on grid G_{k+1}. Thus, the modified residuals $\mathcal{L}_{k+1} w_{k+1}$ of the four fine-grid cells corresponding to a coarse-grid cell are summed. In this manner, the residual transfer operation is conservative. To transfer the solution from G_{k+1} to G_k, the following volume-weighted operator is used:

$$I_{k+1}^{k} w_{k+1} = \frac{\sum_{l=1}^{4} (\Omega_{k+1} w_{k+1})_l}{\sum_{l=1}^{4} (\Omega_{k+1})_l}$$

Again, the summations are over the four fine-grid cells, and the operator conserves mass, momentum, and energy. The prolongation of corrections from G_k to G_{k+1} is accomplished with bilinear interpolation.

In elliptic multigrid methods, the residual-restriction operator is frequently defined as the adjoint of the correction-prolongation operator, meaning that one operator is the transpose of the other. (See appendix C for discussion of the adjoint property.) Such a relationship is convenient for analyzing multigrid schemes (ref. 61). In typical multigrid methods using a cell-vertex, finite-volume formulation for spatial discretization (refs. 3 and 24), the restriction operator is defined with full weighting (ref. 61), and bilinear interpolation is used for the prolongation operator. For full weighting, the restriction operator I_{k+1}^{k} is defined by

$$I_{k+1}^{k} (R_{i,j})_{k+1} = 4 \mu_x^2 \mu_y^2 (R_{i,j})_{k+1}$$

where μ is a standard averaging operator, and thus

$$\mu_x R_{i,j} = \frac{1}{2} (R_{i+1/2,j} + R_{i-1/2,j})$$

and

$$\mu_x^2 R_{i,j} = \frac{1}{4}(R_{i+1,j} + 2R_{i,j} + R_{i-1,j})$$

These operators are adjoint on a uniformly spaced mesh. The operators used in this paper do not have the adjoint property.

Suppose the bilinear-interpolation operator is replaced with a piecewise, constant-prolongation operator. This new prolongation operator transfers the same correction to all fine-grid cells that comprise a coarse-grid cell. Using the inner product definition of functions, this prolongation operator can be shown to be the adjoint of the restriction operator of equation (7.3.5). (See appendix C.) However, this type of prolongation is not considered an appropriate choice. That is, if the Navier-Stokes equations are solved, prolongation does not satisfy the requirement for the intergrid transfer operators, which states that the sum of the order m_p of the prolongation operator, and the order m_r of the restriction operator must exceed the order $2m$ of the differential operator being considered (ref. 61). With the piecewise, constant prolongation, $m_p + m_r = 2$. In the case of the bilinear interpolation, $m_p + m_r = 3 > 2m = 2$, and the requirement is satisfied. Note that frequently a restriction operator is chosen that is not the adjoint of the prolongation operator.

7.3.3. Elements of present method. Section 7.3.2 states that a forcing function is required to properly define a coarse-grid problem for the multigrid method. After initialization of the coarse-grid solution, the forcing term P_k is constructed as

$$P_k = I_{k+1}^k \overline{R}_{k+1} - R_k(I_{k+1}^k w_{k+1})$$

where $\overline{R}_{k+1}$ is the sum of the residual R_{k+1} and forcing function P_{k+1}, and $0 < k < N$. If $k = N - 1$, then $\overline{R}_N = R_N$. In the case of the multistage time-stepping scheme, the $(q+1)$st stage becomes

$$w_k^{(q+1)} = w_k^{(0)} - \alpha_{q+1} \Delta t_k \overline{R}_k$$

where

$$\overline{R}_k = R_k(w_k^{(q)}) + P_k^{(0)}$$

$$R_k(w_k^{(q)}) = \frac{1}{\Omega_k}\left(\mathcal{L}_k^C w_k^{(q)} + \mathcal{L}_k^D w_k^{(0)} - AD^{(q)}\right)$$

and the superscripts C and D mean that the discrete operators are associated with the convection and physical, viscous terms, respectively. The quantity AD represents the appropriate artificial dissipation terms for a given stage. The residuals on G_k are smoothed with an R-K scheme. Information is transferred from one grid to another with a fixed cycle strategy.

Both V-type and W-type cycles have been considered. Figures 9(a) and 9(b) show the structure of these W-type cycles with four and five levels, respectively. The comparable V-type cycles consist of the first and last legs of these W-type cycles. Although the W-type cycle becomes complex as the number of grids increases, it has a recursive definition. Thus, the W-type cycle is essentially as easy to program as the V-type cycle. The work of these cycles is as follows for V-type cycle

$$\text{Work}_{\text{MG}} < \frac{4}{3} \text{Work}_{\text{FINE}}$$

and for W-type cycle

$$\text{Work}_{\text{MG}} < 2 \text{Work}_{\text{FINE}}$$

The subscript MG indicates multigrid cycle, and the subscript FINE refers to one time step on the finest mesh. The work associated with grid transfer operations has been neglected. At

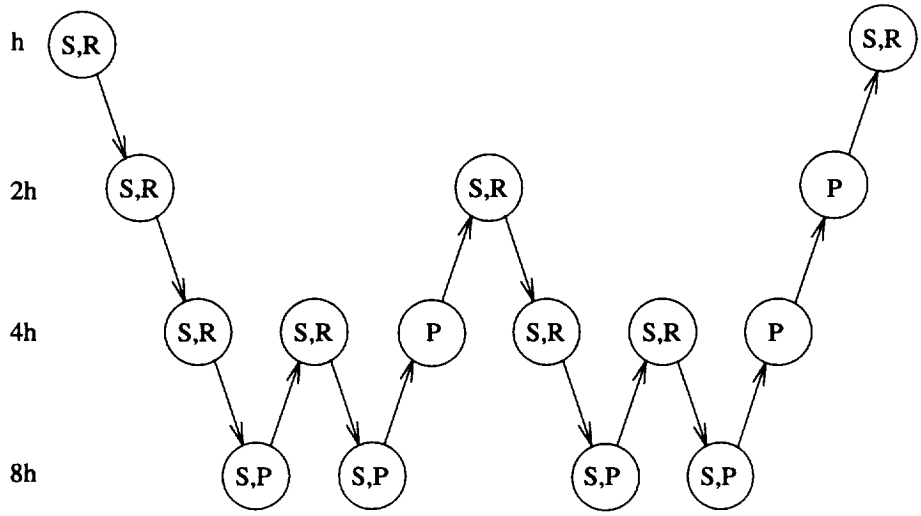

(a) Four-level cycle.

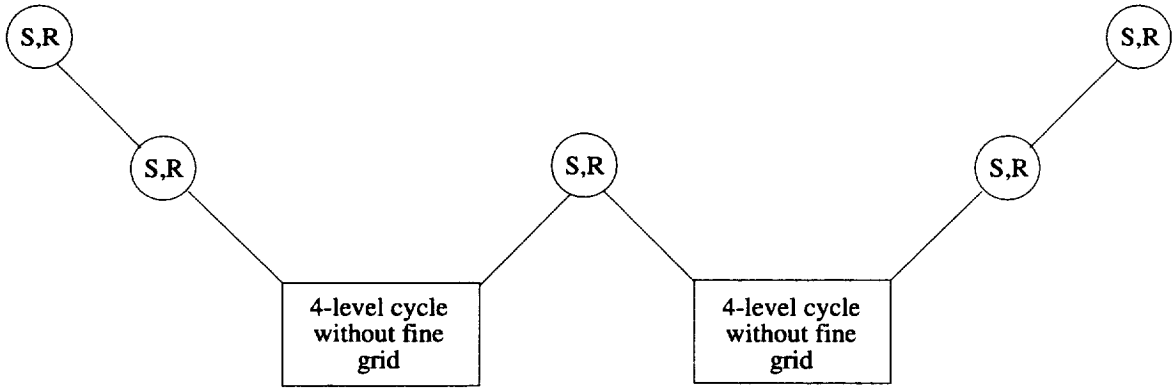

(b) Five-level cycle.

Figure 9. Structure of multigrid W-type cycle; letter designations are defined as S: solve equations, R: restrict solution and residuals, and P: prolongate corrections.

a given grid level, additional R-K steps can be performed in both cycles. In particular, the application of two R-K steps on G_{N-1} and three R-K steps on all successively coarser grids is an effective strategy. Multiple coarse-grid time steps reduce the number of cycles necessary to reach a prescribed level of convergence (i.e., engineering accuracy, meaning three to four orders of magnitude of reduction in the residual). However, the computational time required to realize this level is about the same with or without the additional steps. The principal advantage of these multiple iterations is the improved smoothing of residuals, which is important for difficult, nonlinear-flow problems.

Without additional coarse grid sweeps, the W-type cycle generally requires about the same amount of computer time for convergence (engineering accuracy) as the V-type cycle. The advantage of the W-type cycle is that it provides improved robustness. Therefore, a W-type cycle is used in the applications of this paper.

When solving the Navier-Stokes equations, the viscous terms are computed on each mesh in the multigrid process rather than only on the finest mesh (i.e., as in the convective coarse-grid correction scheme of Johnson (ref. 62). Computing on each mesh provides improved convergence

behavior for low Reynolds number (i.e., $O(1000)$) flow cases. For turbulent flows, the viscosity associated with Reynolds stresses is evaluated only on the finest grid, and then determined on each successively coarser grid by a simple averaging of surrounding finer grid values. Averaging is done to obtain a consistent estimate of the eddy viscosity on coarse meshes when an algebraic turbulence model is being applied. The artificial dissipation model for the finest grid is replaced on coarser grids with a simple, constant-coefficient, second-difference dissipation model. On each grid, the boundary conditions are updated at every R-K stage.

In describing the multigrid method, section 7.3.1 states that on coarse grids approximations are constructed for the residual equations at the boundary points (eqs. (7.3.3)). In constructing coarse grid approximations, the solution at the boundary points on a coarse grid is driven by the residuals for the boundary points on the next finer grid. However, for the present cell-centered, finite-volume scheme, such a treatment for the boundary points is not computationally convenient (i.e., the boundary points do not lie on the boundaries themselves, but are located in auxiliary cells outside of the domain). Instead, the fine-grid boundary conditions discussed in section 5 are applied on the coarse grids, and fine-grid accuracy is not maintained at coarse-grid boundary points. When transferring coarse-grid corrections to a finer grid, only the changes in the solution at the boundary points caused by R-K time stepping are used. Although this method of treating boundary points can possibly affect the asymptotic convergence rate of the multigrid method, it does not change the fine-grid boundary values if the method converges.

The robustness of the multigrid method is enhanced significantly by smoothing the corrections for the fine grid solution. That is,

$$W^{(n+1)} = W^{(n)} + \Delta W_{\text{tot}}$$

where

$$\Delta W_{\text{tot}} = \Delta W_f + \Delta W_c$$

The quantity ΔW_f is the solution correction from the finest grid, and ΔW_c is the resultant solution correction from the coarse grids. This smoothing of the corrections reduces the high-frequency oscillations introduced by the bilinear interpolation of the coarse-mesh corrections and allows convergence of the scheme for a broader range of artificial dissipation coefficients. The factored scheme described for implicit residual averaging with constant coefficients ($\epsilon_\xi = \epsilon_\eta = 0.1$) is used for the smoothing.

The full multigrid (FMG) method is employed to provide an improved initial solution on the finest grid in the multigrid procedure. The FMG method initializes the solution on a coarser grid of the basic sequence of grids, and iterates the solution for a prescribed number of cycles using the FAS scheme. The solution is then interpolated to the next finer grid. The process is repeated until the finest grid is reached. In this paper, three refinement levels are used for a standard mesh density (e.g., 320 by 64 cells). The first and second levels include three and four grids, respectively, and 50 cycles are performed on each. There are five grids in the final level.

8. Turbulence Modeling

The numerical solution of the instantaneous Navier-Stokes equations for turbulent flows requires computing power well beyond what is currently available (ref. 63). To make turbulent flow problems tractable using existing computers, a time-averaged form of the Navier-Stokes equations must be solved. If the appropriate expansions of Favre variables (ref. 64) are substituted for the flow variables in equation (3.1), and the resulting equations are time averaged, the mass-averaged form of the Navier-Stokes equations is obtained. These equations have the same form as their laminar flow counterparts, except that the stress tensor is augmented by the Reynolds stress tensor, the heat flux vector is augmented by the heat flux terms associated with

turbulence, and additional mean-energy dissipation terms appear (in many cases, these terms can be neglected). Closure for this system of time-averaged equations is realized by using the eddy-viscosity hypothesis, which states that the Reynolds stress and heat flux terms are related to mean flow-field gradients. Moreover, the effective viscosity is obtained by simply adding the turbulent viscosity to the molecular viscosity. The Reynolds heat flux terms are approximated using the constant, Prandtl-number assumption. Thus, the effective nondimensional transport coefficients for diffusion and heat conduction are

$$\mu = \mu_l + \mu_t \tag{8.1a}$$

and

$$k = k_l + k_t = \left(\frac{\mu}{\mathrm{Pr}}\right)_l + \left(\frac{\mu}{\mathrm{Pr}}\right)_t \tag{8.1b}$$

respectively. The subscript l refers to laminar values, and the subscript t refers to turbulent values. The laminar and turbulent Prandtl numbers are 0.72 and 0.9, respectively.

For aerodynamic computations, the primary requirement for an eddy-viscosity model is to provide a good representation of turbulence to allow accurate predictions of mean flow-field characteristics. The desire to utilize such capability on a routine basis creates the need for turbulence models with a high degree of numerical compatibility. That is, these models must demonstrate a favorable interaction with numerical schemes, and must not prevent reliable and efficient calculations. This section presents the two turbulent viscosity models applied in this paper. Specific modifications of the originally published forms of the models used to improve physical modeling and/or numerical compatibility are discussed.

The basic turbulence model considered is the widely used algebraic model of Baldwin and Lomax (ref. 65). This two-layer model defines the nondimensional turbulent viscosity as

$$\mu_t = \min\left[(\mu_t)_i,\ (\mu_t)_o\right] \tag{8.2}$$

where the subscripts i and o denote inner and outer values, respectively. The viscosity in each layer is proportional to the product of a length scale and a velocity scale. In the inner part of the boundary layer,

$$(\mu_t)_i = \overline{\mathrm{Re}}\ \rho\ L^2\ \Omega \tag{8.3}$$

where $\overline{\mathrm{Re}} = \mathrm{Re}/(\sqrt{\gamma}M)$, Ω is the magnitude of the vorticity vector, L is the length scale given by $L = KDd$, $K = 0.4$ (Von Kármán's constant), D represents the Van Driest damping factor, and d denotes the distance from the wall. The damping factor D is defined as

$$\left.\begin{aligned} D &= 1 - \exp\left(\frac{-d^+}{A^+}\right) \\ d^+ &= d\,\frac{\sqrt{\overline{\mathrm{Re}}\ \rho_w\,(\tau_l)_{\max}}}{\mu_w} \end{aligned}\right\} \tag{8.4}$$

where $A^+ = 26$. In this definition of the law-of-the-wall coordinate d^+, the original shear stress at the wall is replaced with the maximum laminar value. Substituting the maximum laminar value prevents the eddy viscosity from vanishing when the shear stress goes to 0 at a separation point. The laminar value eliminates a nonphysical behavior of the turbulence and generally

removes numerical difficulties. In the outer part of the boundary layer, the turbulent viscosity becomes

$$(\mu_t)_o = \overline{\mathrm{Re}}\, C_{\mathrm{Clau}}\, C_{cp}\, \rho\, F_{\mathrm{wake}}\, F_{\mathrm{Kleb}}(d) \tag{8.5}$$

where $C_{\mathrm{Clau}} = 0.0168$ (Clauser's constant), the additional constant $C_{cp} = 1.6$, and

$$F_{\mathrm{wake}} = \min\left(d_{\max}\, F_{\max},\ C_{\mathrm{wake}}\, d_{\max}\, \frac{U_{\mathrm{dif}}^2}{F_{\max}} \right) \tag{8.6}$$

with $F_{\max}$ being the maximum value of the function

$$F(d) = d\, \Omega\, D \tag{8.7}$$

across the layer, and $d_{\max}$ is the value of d at which $F_{\max}$ occurs. The quantity U_{dif} is the difference between the magnitudes of the maximum and minimum velocity vectors that occurs across the layer. The function $F_{\mathrm{Kleb}}(d)$ represents the Klebanoff intermittency factor, and is defined by

$$F_{\mathrm{Kleb}}(d) = \left[1 + 5.5 \left(C_{\mathrm{Kleb}} \frac{d}{d_{\max}} \right)^6 \right]^{-1} \tag{8.8}$$

Baldwin and Lomax (ref. 65) defined the constant C_{wake} to be 0.25. This value is generally unsatisfactory in transonic airfoil flows because it produces oscillatory movement of a shock wave. A remedy for this problem is to set $C_{\mathrm{wake}} = 1.0$.

The Baldwin-Lomax (B-L) model just described is also used for wake regions. For wake flows, the Van Driest damping factor is set to unity. The B-L model can also be used to represent transition to turbulence. However, the specification of a transition location according to experiment is generally preferred.

When implementing the B-L model, care must be exercised when determining the maximum of the function $F(d)$, especially for complex flows. Multiple peaks can occur in this function in the vicinity of separation. The second peak is chosen in this case. Due to the rapid evolution of the numerical solution with the multigrid method, the turbulent viscosity is updated every multigrid cycle. Less frequent evaluation can cause either a slowdown or a stall in convergence.

The B-L turbulence model represents a balance of production and dissipation of turbulence. When the boundary layer on a solid surface is subjected to an adverse pressure gradient strong enough to cause flow separation, the production and dissipation of turbulence balance break down. The inner part of the boundary layer responds immediately to the adverse pressure gradient, but the outer boundary layer experiences a delayed reaction. This delayed behavior creates a disequilibrium of the two regions. If the size of the separated flow region is large enough to alter the surface-pressure distribution, then the history effects cannot be neglected in the turbulence model. In general, both the convection and diffusion of turbulence should be modeled to accurately predict the turbulent stresses.

Johnson and King (ref. 66) proposed a model to account for nonequilibrium effects and used the two-layer, algebraic model of Cebeci and Smith (ref. 67) as a foundation for their model. In principle, any equilibrium model, such as the B-L model (ref. 65), could be chosen. The basic idea of the Johnson-King (J-K) model is to find an appropriate nonequilibrium factor to modify the variation of the equilibrium outer-eddy viscosity. The nonequilibrium factor is determined so that a transport equation for the maximum shear stress in the boundary layer is satisfied. In reference 68, the implementation of a modified version of the J-K nonequilibrium model is presented. Reference 69 gives a similar modified form. The elements of these forms of the J-K model are described in the remainder of this section.

In reference 68, a turbulence reference quantity is defined as

$$G_m = \left(\Omega \frac{\mu_t}{\rho}\right)_m \tag{8.9}$$

where the index m denotes the maximum of G across the shear layer. This quantity is then used to replace the maximum turbulent shear stress divided by density (i.e., the correlation of fluctuating velocity components given by $(-\overline{u'v'})_m$ appearing in the original J-K model (ref. 66)). The advantage of using G_m is that it is invariant with respect to coordinate systems. In the formulation of reference 66, the turbulent viscosity is constructed as an exponential blending of the inner and outer viscosities. That is,

$$\mu_t = (\mu_t)_o \left\{1 - \exp\left[\frac{(\mu_t)_i}{(\mu_t)_o}\right]\right\} \tag{8.10}$$

The inner viscosity is given by

$$(\mu_t)_i = \mathrm{Re}\ \rho D^2 K\ d\ \sqrt{\mathrm{Re}\ g_m} \tag{8.11}$$

with

$$D = 1 - \exp\left[\frac{-d}{A^+ \mu_w}\sqrt{\rho_w\ \max(\rho_w g_m, \tau_w)}\right] \tag{8.12}$$

An appropriate value of A^+ is 17 (rather than the equilibrium value of 26) (ref. 70). The original J-K model requires determining the edge of the boundary layer, since the foundation model was the Cebeci and Smith model. This requirement is removed in references 68 and 69 by using the B-L model. Moreover, the outer turbulent viscosity is expressed as

$$(\mu_t)_o = \sigma\ \overline{Re}\ C_{\mathrm{Clau}} C_{cp} \rho F_{\mathrm{wake}} F_{\mathrm{Kleb}}(d) \tag{8.13}$$

where σ is the nonequilibrium factor previously mentioned and the other quantities are defined the same as for the B-L model.

Assuming that G is proportional to the turbulent kinetic energy, and introducing a time derivative, the ordinary differential equation in reference 66 governing the trajectory of the maximum shear stress is replaced with

$$\frac{\partial G_m}{\partial t} + u_m \frac{\partial G_m}{\partial x} + v_m \frac{\partial G_m}{\partial y} + a_1 \frac{G_m}{L_m}\left[{G_m}^{1/2} - (G_{\mathrm{eq}})_m^{1/2}\right] + G_m^{3/2}\mathcal{D}_m = 0 \tag{8.14}$$

where u_m and v_m are the Cartesian velocity components at the location of G_m. The quantity $(G_{\mathrm{eq}})_m$ is the equilibrium value of G at the location of G_m, and the length scale L_m is defined as

$$L_m = 0.4 d_m \quad \left(\frac{d_m}{\delta} \le 0.225\right) \tag{8.15}$$

$$L_m = 0.09\delta \quad \left(\frac{d_m}{\delta} > 0.225\right) \tag{8.16}$$

with δ being the boundary-layer thickness. An estimate of δ given in reference 71 is $1.9 d_{\max}$. In the original J-K model, the diffusion term $\mathcal{D}_m$ is defined as

$$\mathcal{D}_m = \frac{a_2 F(\sigma)}{\delta\left[0.7 - (d_m/\delta)\right]} \tag{8.17}$$

where

$$F(\sigma) = |\sigma^{1/2} - 1| \tag{8.18}$$

The constants a_1 and a_2 are taken to be 0.25 and 0.5, respectively. With the $F(\sigma)$ given by equation (8.18), there is a singular-like (nonphysical) behavior of the diffusion term at $\sigma = 1$. In reference 68, $F(\sigma)$ is expressed as

$$F(\sigma) = \max\left(0\,,\ \sigma^{1/2} - 1\right) \tag{8.19}$$

and thus has a smooth behavior at $\sigma = 1$. This $F(\sigma)$ makes the diffusion term 0 in regions of reverse flow (where $\sigma < 1$). The use of equation (8.19) produces greater differences between the predicted shock position and the shock position indicated by experiment for a transonic, shock-induced, separated airfoil flow with strong nonequilibrium effects.

If g_m^{-2} is substituted for G_m in equation (8.14), the resulting linear equation is given by

$$\frac{\partial g_m}{\partial t} + u_m \frac{\partial g_m}{\partial x} + v_m \frac{\partial g_m}{\partial y} + \mathcal{S}_m - \frac{1}{2}\left(\mathcal{D}_m + \frac{a_1}{L_m}\right) = 0 \tag{8.20}$$

where the source term is

$$\mathcal{S}_m = \frac{a_1}{2L_m}\left(g_{\text{eq}}\right)_m^{-1} g_m$$

Equation (8.14) is strictly valid along the curve determined by the maximum shear stress. However, equation (8.14) is solved along the solid surface of interest to facilitate the numerical solution method. The misalignment between these surfaces creates errors in the convection terms (ref. 68). To reduce these errors, the velocity components u_m and v_m are replaced with their projections onto the wall boundary. The spatial discretization of the modified equation is accomplished by applying the finite-volume technique to the layer of mesh cells adjacent to the solid surface. A fourth-difference dissipation term is appended to this semidiscrete equation. The same five-stage R-K scheme described in section 6 in conjunction with local time stepping is used to numerically integrate the equations in time. With implicit treatment of the linear source term in equation (8.20), a Courant number of about 3 can be used. The computation of g_m, and thus the turbulent viscosity, must be adequately converged to allow convergence of the fluid dynamic system of equations. The turbulence model is applied once every time step in the solution of the Navier-Stokes equations, and R-K time steps are performed for each update of the turbulence field.

Once the distribution of g_m is known, a new variation for the nonequilibrium factor σ is calculated with the following equation:

$$\sigma^{n+1} = \sigma^n \left[\frac{g_m}{(\Omega\mu_t/\rho)_m}\right] \tag{8.21}$$

where σ^n is σ at time level n (ref. 70).

An alternative technique used to solve for g_m that is equal to $(-\overline{u'v'})_m^{-1/2}$ is a space marching procedure (ref. 66). When applying this procedure, eliminate the time derivative of equation (8.20), transform to arbitrary curvilinear coordinates (ξ, η), and assume g_m is independent of the normal coordinate η (i.e., a ξ curve coincides with the transport path of g_m). Then, obtain

$$U_m \frac{\partial g_m}{\partial \xi} + \mathcal{S}_m = \frac{1}{2}\left(\mathcal{D}_m + \frac{a_1}{L_m}\right) \tag{8.22}$$

with $U_m = \xi_x u_m + \xi_y v_m$. A discrete equation for $(g_m)_{i+1}$ can be written as

$$\{(g_{\mathrm{eq}})_m^{-1}\left[A_1 + (g_{\mathrm{eq}})_m\right]\}_i\,(g_m)_{i+1} = (A_1 + g_m)_i + \left(A_1 \frac{L_m}{a_1} \mathcal{D}_m\right)_i \tag{8.23}$$

where the index i means evaluated at the previous ξ location,

$$A_1 = \frac{a_1 \Delta s_\xi}{2 L_m U_m}$$

with Δs_ξ representing distance along the integration path, and U_m denoting the magnitude of the velocity vector at the actual location where g_m occurs. Again, for convenience, the integration path is taken to be coincident with the geometry being considered. This particular approach generally seems more robust, and thus is used for all J-K computations. The original argument in favor of the time-dependent technique concerned simplicity in extending to three dimensions. However, reference 72 indicates that the steady equation for g_m can be solved easily with first-order, upwind differencing and point-Gauss-Seidel relaxation. Reference 73 provides additional discussion on implementation and various forms of the J-K model.

9. Concluding Remarks

The elements of a class of explicit multistage time-stepping schemes with centered spatial differencing and multigrid are defined and discussed in this report. Additional understanding is gained from analysis of a number of components of these schemes. Through this approach, the benefit of a local mode analysis in evaluating boundary-point difference stencils for the numerical dissipation is demonstrated. The stability of the multistage Runge-Kutta schemes is examined. Hyperbolic and parabolic operator splitting is applied to determine sufficient conditions of stability for the Euler and Navier-Stokes (in the absence of convection) equations, respectively. The difficulty in rigorously deriving a sufficient condition for the full Navier-Stokes equations is discussed. A simple time-step estimate that works well in practice is given. The basic properties of the implicit process of residual smoothing for extending stability are given. Two forms of variable coefficients for the residual smoothing procedure are considered. The formulas introduced in this report are shown to perform much better than the formulas of reference 20 for typical meshes used to compute inviscid, airfoil-flow solutions. With these formulas, a new set of variable coefficients is constructed that eliminates the general requirement of including a diffusion limit in the time-step estimate. The implicit residual smoothing is also used as the basis for one of several techniques that are included to enhance the robustness of the basic multigrid method.

Both the equilibrium model of Baldwin and Lomax and the nonequilibrium model of Johnson and King are considered for turbulence closure. The implementation of these models, including two alternatives for the Johnson-King model, is described in detail. Some modifications to the original formulations of the models are made to improve numerical compatibility of the models (i.e., make it easier to converge numerical algorithm with the model), and in the case of the Johnson-King model, to simplify implementation and improve prediction capability.

NASA Langley Research Center
Hampton, VA 23681-2199
January 3, 1997

Appendix A
Equations for Boundary Points

Consider the elements of the solution vector

$$\mathbf{W}' = [\, c \quad u \quad v \quad s \,]^T$$

as dependent variables, where c is the speed of sound and s is the entropy. The Euler equations relative to the rotated Cartesian coordinate system (x_t, x_n) can be written as

$$\frac{\partial \mathbf{W}'}{\partial t} + A'' \frac{\partial \mathbf{W}'}{\partial x_t} + B'' \frac{\partial \mathbf{W}'}{\partial x_n} = 0 \tag{A1}$$

where

$$A'' = A' \cos\theta + B' \sin\theta$$

$$B'' = -A' \sin\theta + B' \cos\theta$$

and

$$\mathbf{A}' = \begin{bmatrix} u & c(\gamma-1)/2 & 0 & 0 \\ 2c(\gamma-1)^{-1} & u & 0 & -c^2(\gamma-1)^{-1} \\ 0 & 0 & u & 0 \\ 0 & 0 & 0 & u \end{bmatrix}$$

$$\mathbf{B}' = \begin{bmatrix} v & 0 & c(\gamma-1)/2 & 0 \\ 0 & v & 0 & 0 \\ 2c(\gamma-1)^{-1} & 0 & v & -c^2(\gamma-1)^{-1} \\ 0 & 0 & 0 & v \end{bmatrix}$$

In equation (A1), θ is the angle that the rotated coordinate system makes with the unrotated system. Suppose the Riemann invariants of 1-D gas dynamics are changed to dependent variables. This is done by first assuming that the flow is locally homentropic, and by redefining the matrices $\mathbf{A}'$ and $\mathbf{B}'$ as the reduced matrices

$$\left.\begin{aligned} \mathbf{A}' &= \begin{bmatrix} u & c(\gamma-1)/2 & 0 \\ 2c(\gamma-1)^{-1} & u & 0 \\ 0 & 0 & u \end{bmatrix} \\ \mathbf{B}' &= \begin{bmatrix} v & 0 & c(\gamma-1)/2 \\ 0 & v & 0 \\ 2c(\gamma-1)^{-1} & 0 & v \end{bmatrix} \end{aligned}\right\} \tag{A2}$$

Then, with the matrix

$$\mathbf{Q}^{-1} = \begin{bmatrix} 0 & \cos\theta & -\sin\theta \\ 1/\sqrt{2} & -(\gamma-1)\sin\theta/(2\sqrt{2}) & (\gamma-1)\cos\theta/(2\sqrt{2}) \\ 1/\sqrt{2} & (\gamma-1)\sin\theta/(2\sqrt{2}) & -(\gamma-1)\cos\theta/(2\sqrt{2}) \end{bmatrix}$$

the reduced form of the solution vector $\mathbf{W}'$ can be transformed to a new vector that is a function of the Riemann invariants. In addition, the similarity transformation with Q^{-1} and

$$\mathbf{Q} = \begin{bmatrix} 0 & 1/\sqrt{2} & -1/\sqrt{2} \\ \cos\theta & -\sqrt{2}\sin\theta/(\gamma-1) & -\sqrt{2}\sin\theta/(\gamma-1) \\ \sin\theta & -\sqrt{2}\cos\theta/(\gamma-1) & -\sqrt{2}\cos\theta/(\gamma-1) \end{bmatrix}$$

can be used to diagonalize the reduced form of the matrix B''. Thus, if equation (A1), with A' and B' defined by equations (A2), is premultiplied by Q^{-1}, the result is

$$Q^{-1}\frac{\partial \mathbf{W}'}{\partial t} + \left(Q^{-1}A''Q\right)Q^{-1}\frac{\partial \mathbf{W}'}{\partial x_t} + \left(Q^{-1}B''Q\right)Q^{-1}\frac{\partial \mathbf{W}'}{\partial x_n} = 0 \tag{A3}$$

If Q^{-1} is considered locally constant, and the variation of $\mathbf{W}'$ in the tangential direction is taken to be negligible, equation (A3) becomes

$$\frac{\partial \widetilde{\mathbf{W}}}{\partial t} + \Lambda_{B''}\frac{\partial \widetilde{\mathbf{W}}}{\partial x_n} = 0 \tag{A4}$$

where $\Lambda_{B''}$ is a diagonal matrix of the eigenvalues $(q_n, q_n + c, q_n - c)$ of B'', and $\widetilde{\mathbf{W}}$ is the vector of characteristic variables defined by

$$\widetilde{\mathbf{W}} = \begin{bmatrix} q_t & \frac{1}{\sqrt{2}}\frac{\gamma-1}{2}R^+ & \frac{1}{\sqrt{2}}\frac{\gamma-1}{2}R^- \end{bmatrix}^T$$

with

$$R^+ = q_n + \frac{2c}{\gamma-1}$$

$$R^- = q_n - \frac{2c}{\gamma-1}$$

$$q_t = u\,\cos\theta + v\,\sin\theta$$

$$q_n = -u\,\sin\theta + v\,\cos\theta$$

Appendix B
Development of Residual Smoothing Coefficients

To obtain insight into an appropriate form for variable smoothing coefficients, consider first the approximate factorization scheme

$$\left(I + \frac{\Delta t}{\Omega}\mu_\xi\,\delta_\xi\widetilde{A}\right)\left(I + \frac{\Delta t}{\Omega}\mu_\eta\,\delta_\eta\widetilde{B}\right)\Delta\widetilde{\mathbf{W}}_{i,j} = -\mathcal{R}_{i,j} \tag{B1}$$

where $\Delta\widetilde{\mathbf{W}}_{i,j}$ is the product of the solution vector for the Euler equations and the volume Ω (as determined by a transformation Jacobian), $\mathcal{R}_{i,j}$ is the residual vector for the system, and (ξ, η) are arbitrary curvilinear coordinates. The operators μ and δ are standard averaging and central difference operators, respectively. Thus,

$$\mu_\xi\widetilde{\mathbf{W}}_{i,j} = \frac{1}{2}\left(\widetilde{\mathbf{W}}_{i+1/2,j} + \widetilde{\mathbf{W}}_{i-1/2,j}\right)$$

$$\delta_\xi\widetilde{\mathbf{W}}_{i,j} = \left(\widetilde{\mathbf{W}}_{i+1/2,j} - \widetilde{\mathbf{W}}_{i-1/2,j}\right)$$

The transformed, flux-Jacobian matrices are defined as

$$\left.\begin{aligned}\widetilde{A} &= \xi_x A + \xi_y B\\ \widetilde{B} &= \eta_x A + \eta_y B\end{aligned}\right\} \tag{B2}$$

The spectral radii of these matrices are as follows:

$$\left.\begin{aligned}\sigma_{\widetilde{A}} &= \sigma(\widetilde{A}) = \frac{\lambda_\xi}{\Omega}\\ \sigma_{\widetilde{B}} &= \sigma(\widetilde{B}) = \frac{\lambda_\eta}{\Omega}\end{aligned}\right\} \tag{B3}$$

where λ_ξ and λ_η are the characteristic speeds defined in equations (4.2.5). If the matrices $\widetilde{A}$ and $\widetilde{B}$ are approximated as

$$\widetilde{A} = \sigma_{\widetilde{A}} I$$

$$\widetilde{B} = \sigma_{\widetilde{B}} I$$

respectively, then equation (B1) can be replaced with

$$\left(I + \frac{\Delta t}{\Omega}\sigma_{\widetilde{A}}\mu_\xi\,\delta_\xi\right)\left(I + \frac{\Delta t}{\Omega}\sigma_{\widetilde{B}}\mu_\eta\,\delta_\eta\right)\Delta\widetilde{\mathbf{W}}_{i,j} = -\mathcal{R}_{i,j} \tag{B4}$$

when the scalings are taken to be locally constant. Define

$$\left.\begin{aligned}\beta_\xi &= \frac{\Delta t}{\Omega}\sigma_{\widetilde{A}}\\ \beta_\eta &= \frac{\Delta t}{\Omega}\sigma_{\widetilde{B}}\end{aligned}\right\} \tag{B5}$$

as the implicit smoothing coefficients for the ξ and η directions, respectively. Using equations (B3), and taking

$$\Delta t = \frac{\Omega}{\lambda_\xi + \lambda_\eta} \tag{B6}$$

the smoothing coefficients of equations (B5) become

$$\left.\begin{aligned}\beta_\xi &= \frac{\lambda_\xi}{\lambda_\xi + \lambda_\eta} \\ \beta_\eta &= \frac{\lambda_\eta}{\lambda_\xi + \lambda_\eta}\end{aligned}\right\} \tag{B7}$$

Now, consider the case where parabolic implicit smoothing operators are used instead of hyperbolic implicit smoothing operators. In particular, consider the implicit finite-volume method of Lerat (ref. 52). This scheme includes two stages. The first stage is a physical stage in which the change of the solution vector of the Euler equations is evaluated using a Lax-Wendroff scheme. To remove the time step limit of the explicit scheme, a mathematical stage is applied in the following integral form:

$$\iint_{\Omega_{i,j}} (\Delta\mathbf{W})^* d\Omega + \omega\frac{\Delta t^2}{2}\int_{\Gamma_{i+\frac{1}{2},j}\cup\Gamma_{i-\frac{1}{2},j}} \tilde{\sigma}_A^2 \left[\mathbf{n}\cdot\nabla(\Delta\mathbf{W})^*\right] d\Gamma = \iint_{\Omega_{i,j}} \Delta\overline{\mathbf{W}} d\Omega \tag{B8}$$

$$\iint_{\Omega_{i,j}} \Delta\mathbf{W}\, d\Omega + \omega\frac{\Delta t^2}{2}\int_{\Gamma_{i,j+\frac{1}{2}}\cup\Gamma_{i,j-\frac{1}{2}}} \tilde{\sigma}_B^2 \left[\mathbf{n}\cdot\nabla(\Delta\mathbf{W}\right] d\Gamma = \iint_{\Omega_{i,j}} (\Delta\mathbf{W})^* d\Omega \tag{B9}$$

where $\Delta\mathbf{W}$ is the change in the solution vector, the superscript $(*)$ indicates a provisional value, the overbar refers to a value from the explicit physical stage, the quantity $\Omega_{i,j}$ is a mesh cell volume, the vector $\mathbf{n}$ is a unit normal to the boundary curve Γ, and ω is a constant taken to be $-1/2$. In equations (B8) and (B9), the eigenvalues $\tilde{\sigma_A}$ and $\tilde{\sigma_B}$, respectively, are related to the spectral radii of equations (B3) as

$$\tilde{\sigma_A} = \frac{\tilde{\sigma_A}\,\Omega}{\sqrt{x_\eta^2 + y_\eta^2}}$$

$$\tilde{\sigma_B} = \frac{\tilde{\sigma_B}\,\Omega}{\sqrt{x_\xi^2 + y_\xi^2}}$$

Assuming that the quantities inside the integral signs associated with the boundary curves are locally constant, and that the curvilinear coordinates ξ and η are orthogonal, the integral equations (B8) and (B9) can be approximated by

$$\Delta\mathbf{W}_{i,j}^* - \frac{1}{4}\frac{\Delta t^2}{\Omega_{i,j}}\left\{\left(\frac{\tilde{\sigma}_A^2\Gamma^2}{\Omega}\right)_{i+\frac{1}{2}j}\left[(\Delta\mathbf{W})_{i+1,j}^* - (\Delta\mathbf{W})_{i,j}^*\right]\right\}$$

$$+\frac{1}{4}\frac{\Delta t^2}{\Omega_{i,j}}\left\{\left(\frac{\tilde{\sigma}_A^2\Gamma^2}{\Omega}\right)_{i-\frac{1}{2}j}\left[(\Delta\mathbf{W})_{i,j}^* - (\Delta\mathbf{W})_{i-1,j}^*\right]\right\} = \overline{(\Delta\mathbf{W})}_{i,j} \tag{B10}$$

$$\Delta\mathbf{W}_{i,j} - \frac{1}{4}\frac{\Delta t^2}{\Omega_{i,j}}\left\{\left(\frac{\hat{\sigma}^2_{\tilde{B}}\Gamma^2}{\Omega}\right)_{i,j+\frac{1}{2}}\left[(\Delta\mathbf{W})_{i,j+1} - (\Delta\mathbf{W})_{i,j}\right]\right\}$$

$$+\frac{1}{4}\frac{\Delta t^2}{\Omega_{i,j}}\left\{\left(\frac{\hat{\sigma}^2_{\tilde{B}}\Gamma^2}{\Omega}\right)_{i,j-\frac{1}{2}}\left[(\Delta\mathbf{W})_{i,j} - (\Delta\mathbf{W})_{i,j-1}\right]\right\} = (\Delta\mathbf{W})^*_{i,j} \qquad \text{(B11)}$$

where the unknowns are located at the cell centers. If the coefficients

$$\frac{\hat{\sigma}^2_{\tilde{A}}\Gamma^2}{\Omega}$$

and

$$\frac{\hat{\sigma}^2_{\tilde{B}}\Gamma^2}{\Omega}$$

(which are evaluated at the cell faces) are taken to be locally constant, and the time step is defined as equation (B6), then the smoothing parameters β_ξ and β_η depend upon

$$\left.\begin{array}{c}\left[\dfrac{\lambda_\xi}{(\lambda_\xi+\lambda_\eta)}\right]^2 \\ \left[\dfrac{\lambda_\eta}{(\lambda_\xi+\lambda_\eta)}\right]^2\end{array}\right\} \qquad \text{(B12)}$$

respectively, which are the squares of the smoothing coefficients obtained for the ADI scheme.

The results from the 1-D stability analysis of section 7.2.1, and the understanding of the functional dependence of the smoothing coefficients on λ_ξ and λ_η, provide a foundation for developing β_ξ and β_η, respectively. To determine formulas for β_ξ and β_η, the 2-D stability of a multistage, time-stepping scheme with implicit residual smoothing is examined. Consider the 2-D, scalar, hyperbolic wave equation

$$\frac{\partial w}{\partial t} + a\frac{\partial w}{\partial x} + b\frac{\partial w}{\partial y} = 0 \qquad \text{(B13)}$$

Using central difference approximations for the spatial derivatives, a semidiscrete form for equation (B13) is written as

$$\Delta t\frac{dw}{dt} = -\frac{N_\xi}{2}\left(w^n_{i+1,j} - w^n_{i-1,j}\right) - \frac{N_\eta}{2}\left(w^n_{i,j+1} - w^n_{i,j-1}\right) \qquad \text{(B14)}$$

where the Courant numbers

$$\left.\begin{array}{l}N_\xi = \lambda_\xi\dfrac{\Delta t}{\Omega} = (a\,\Delta y)\dfrac{\Delta t}{\Omega} \\ N_\eta = \lambda_\eta\dfrac{\Delta t}{\Omega} = (b\,\Delta x)\dfrac{\Delta t}{\Omega}\end{array}\right\} \qquad \text{(B15)}$$

By taking the Fourier transform of equation (B14), the following is obtained:

$$\Delta t \frac{d\hat{w}}{dt} = z\hat{w}^n$$

where the Fourier symbol z is given by

$$z = -i\left(N_\xi \sin\theta_\xi + N_\eta \sin\theta_\eta\right) \tag{B16}$$

The caret indicates a transformed quantity, and θ_ξ and θ_η are the Fourier angles for the two coordinate directions. If implicit residual smoothing is applied, the Fourier symbol of equation (B16) is replaced by

$$z = -i\frac{N_\xi \sin\theta_\xi + N_\eta \sin\theta_\eta}{\chi_\xi \chi_\eta}$$

where

$$\left.\begin{aligned} \chi_\xi &= 1 + 2\beta_\xi\left(1 - \cos\theta_\xi\right) \\ \chi_\eta &= 1 + 2\beta_\eta\left(1 - \cos\theta_\eta\right) \end{aligned}\right\} \tag{B17}$$

A sufficient condition for stability can be written as

$$\max\ |z| \leq N^* \tag{B18}$$

for all θ_ξ and θ_η, where N^* is the Courant number of the unsmoothed scheme. Let

$$\tilde{F} = |z| = N_\xi \frac{\sin\theta_\xi}{\chi_\xi \chi_\eta} + N_\eta \frac{\sin\theta_\eta}{\chi_\xi \chi_\eta}$$

Then,

$$\tilde{F} \leq N_\xi \frac{\sin\theta_\xi}{\chi_\xi} + N_\eta \frac{\sin\theta_\eta}{\chi_\eta}$$

or

$$\tilde{F} \leq N_\xi f(\theta_\xi) + N_\eta g(\theta_\eta)$$

and

$$\tilde{F}_{\max} \leq N_\xi f_{\max} + N_\eta g_{\max}$$

Then, a sufficient condition for stability is given by

$$N_\xi f_{\max} + N_\eta g_{\max} \leq N^* \tag{B19}$$

From equation (7.2.7) of section 7.2.1, it follows that

$$\left.\begin{aligned} f_{\max} &= \frac{1}{\sqrt{1 + 4\beta_\xi}} \\ g_{\max} &= \frac{1}{\sqrt{1 + 4\beta_\eta}} \end{aligned}\right\} \tag{B20}$$

Substituting equation (B19) into equations (B20) yields

$$N_\xi \frac{1}{\sqrt{1 + 4\beta_\xi}} + N_\eta \frac{1}{\sqrt{1 + 4\beta_\eta}} \leq N^* \tag{B21}$$

But

$$\left.\begin{aligned} N_\xi &= \frac{\Delta t_{\text{act}}}{\Delta t_\xi} = N\frac{\lambda_\xi}{\lambda_\xi + \lambda_\eta} = \frac{N}{1 + r_{\eta\xi}} \\ N_\eta &= \frac{\Delta t_{\text{act}}}{\Delta t_\eta} = N\frac{\lambda_\eta}{\lambda_\xi + \lambda_\eta} = \frac{N}{1 + r_{\eta\xi}^{-1}} \end{aligned}\right\} \tag{B22}$$

where $r_{\eta\xi}$ is the ratio of the modified characteristic speeds $(\lambda_\eta/\lambda_\xi)$ and is also proportional to mesh-cell-aspect ratio. Thus, equation (B21) becomes

$$\frac{N}{N^*}\frac{1}{1 + r_{\eta\xi}}\frac{1}{\sqrt{1 + 4\beta_\xi}} + \frac{N}{N^*}\frac{1}{1 + r_{\eta\xi}^{-1}}\frac{1}{\sqrt{1 + 4\beta_\eta}} \le 1 \tag{B23}$$

In the cases of low-aspect-ratio cells $(r_{\eta\xi} \ll 1)$ and high-aspect-ratio cells $(r_{\eta\xi} \gg 1)$, equation (B23) can be replaced by

$$\frac{N_\xi}{N^*}\frac{1}{\sqrt{1 + 4\beta_\xi}} \le 1$$

and

$$\frac{N_\eta}{N^*}\frac{1}{\sqrt{1 + 4\beta_\eta}} \le 1$$

respectively. Thus, write

$$\left.\begin{aligned} \beta_\xi &= \max\left\{\frac{1}{4}\left[\left(\frac{N}{N^*}\frac{1}{1 + r_{\eta\xi}}\right)^2 - 1\right], 0\right\} \\ \beta_\eta &= \max\left\{\frac{1}{4}\left[\left(\frac{N}{N^*}\frac{1}{1 + r_{\eta\xi}^{-1}}\right)^2 - 1\right], 0\right\} \end{aligned}\right\} \tag{B24}$$

Note that these expressions are related to the smoothing coefficients of equations (B12) for the implicit method of Lerat.

The formulas of equations (B24) can also be obtained by substituting the appropriate time step estimates into the 1-D smoothing coefficient of equations (7.2.8) in section 7.2.1. That is, the time step of the smoothed scheme is defined as in equation (B6), and the time step of the unsmoothed scheme is a 1-D time step.

Appendix C
Multigrid Transfer Operators

When constructing a multigrid method, appropriate intergrid transfer (i.e., restriction and prolongation) operators must be chosen. Often, these operators are selected so that they are adjoint operators. Such a choice provides convenience in the analysis of the multigrid scheme (i.e., two-level multigrid analysis). In this section, the natural choice for the restriction operator of the residual function when a cell-centered, finite-volume scheme is used for discretization is considered. Moreover, the restriction process involves simply summing the fine-grid residuals for the fine-grid cells that comprise the coarse-grid cell. A piecewise constant prolongation operator is shown to be an adjoint operator.

Consider a 1-D domain $\Omega = \{x \in \Re : 0 \leq x \leq L\}$. Define a fine grid G_f and a coarse grid G_c that cover the domain Ω, such that $G_c \subset G_f$. Generate G_c by eliminating every other mesh point of G_f (delineated by crossed lines in fig. C1). Let the mesh interval $(\Delta x_j)_f = \left(x_{j+1/2} - x_{j-1/2}\right)_f$ of G_f be constant. Define $h = h_f = (\Delta x_j)_f$. Then, the coarse-grid mesh interval is $h_c = 2h$. Let R be the residual function, and let $(v)_h$ be a correction to the fine-grid solution. Assume that the unknowns are stored at the center of a mesh cell. The restriction operator for the residual is defined by

$$I_h^{2h} R_h = \frac{1}{h_c} \sum_{l=1}^{2} (h_f R_f)_l$$

Suppose that the prolongation operator I_{2h}^h for the coarse-grid correction simply transfers the same correction to the fine-grid cells that determine the coarse-grid cell. The operators I_h^{2h} and I_{2h}^h are adjoint operators if

$$(R_h \, , \, I_{2h}^h v_{2h}) = [(I_{2h}^h)^* R_h \, , \, v_{2h}] = (I_h^{2h} R_h \, , \, v_{2h}) \tag{C1}$$

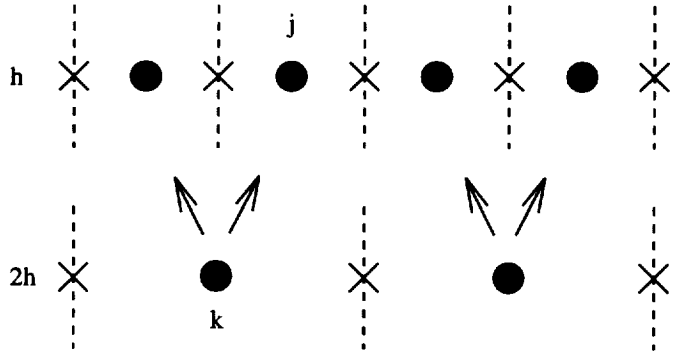

Figure C1. Cells of two grid levels.

where $(\cdot\,,\,\cdot)$ denotes an inner product, and the asterisk indicates transpose. To show that these operators satisfy equation (C1), consider the inner product definition for functions. Let the index k denote a coarse-grid cell, and let the indices j and $j-1$ represent the corresponding fine-grid cells. Then

$$(I_h^{2h} R_h\,,\; v_{2h})_{2h} = \sum_k \left[\frac{h_j}{h_k}(R_j)_h + \frac{h_{j-1}}{h_k}(R_{j-1})_h\right](v_k)_{2h}\, h_k$$

and

$$\begin{aligned}(R_h\,,\; I_{2h}^h v_{2h})_h &= \sum_{j\,\text{even}} (R_j)_h\,(v_k)_{2h}\, h_j + \sum_{j\,\text{even}} (R_{j-1})_h (v_k)_{2h}\, h_{j-1} \\ &= \sum_{j\,\text{even}} \left[(R_j)_h\, h_j + (R_{j-1})_h\, h_{j-1}\right](v_k)_{2h}\end{aligned}$$

Thus, these operators are shown to be adjoint operators. Note that if the piecewise constant prolongation operator is replaced by a linear interpolation operator, the operators are not adjoint.

10. References

1. Jameson, A.; Schmidt, Wolfgang; and Turkel, Eli: Numerical Solution of the Euler Equations by Finite Volume Methods Using Runge Kutta Time Stepping Schemes. AIAA-81-1259, June 1981.

2. Beam, R. M.; and Warming, R. F.: An Implicit Finite-Difference Algorithm for Hyperbolic Systems in Conservation-Law Form—Application to Eulerian Gasdynamic Equations. *J. Comput. Phys.*, vol. 22, Sept. 1976, pp. 87–110.

3. Jameson, Antony: Multigrid Algorithms for Compressible Flow Calculations. *Multigrid Methods II—Proceedings of the Second European Conference*, Springer-Verlag, 1986, pp. 166–201.

4. Pulliam, T. H.; and Chaussee, D. S.: A Diagonal Form of an Implicit Approximate-Factorization Algorithm. *J. Comput. Phys.*, vol. 39, Feb. 1981, pp. 347–363.

5. Ni, R. H.: A Multiple Grid Scheme for Solving the Euler Equations. *AIAA J.*, vol. 20, no. 11, Nov. 1982, pp. 1565–1571.

6. Davis, R. L.; Ni, R. H.; and Carter, J. E.: Cascade Viscous Flow Analysis Using the Navier-Stokes Equations. AIAA-86-0033, Jan. 1986.

7. Kallinderis, John G.; and Baron, Judson R.: Adaptation Methods for a New Navier-Stokes Algorithm. AIAA-87-1167, June 1987.

8. Hall, M. G.: Cell Vertex Multigrid Schemes for Solution of the Euler Equations. *Numerical Methods for Fluid Dynamics II*, K. W. Morton and M. J. Baines, eds., Clarendon Press, 1986, pp. 303–345.

9. Arthur, M. T.; Blaylock, T.; and Anderson, J. M.: A Cell-Vertex Multigrid Euler Scheme for Use With Multiblock Grids. AIAA-89-0472, Jan. 1989.

10. Couaillier, V.: Solution of the Euler Equations—Explicit Schemes Acceleration by a Multigrid Method. *Proceedings of the Second European Conference on Multigrid Methods*, ONERA TP no. 1985-129, presented at the Second European Conference on Multigrid Methods (Cologne, West Germany), Oct. 1985.

11. Cambier, L.; Couaillier, V.; and Veuillot, J. P.: Numerical Solution of the Navier-Stokes Equations by a Multigrid Method. *La Rech. Aerosp.*, no. 2, 1988, pp. 23–42.

12. Van Leer, Bram: Flux-Vector Splitting for the Euler Equations. *Lecture Notes in Physics—Eighth International Conference on Numerical Methods in Fluid Dynamics*, Springer-Verlag, 1982, pp. 507–512.

13. Roe, P. L.: Approximate Riemann Solvers, Parameter Vectors, and Difference Schemes. *J. Comput. Phys.*, vol. 43, Oct. 1981, pp. 357–372.

14. Jameson, A.; and Baker, T. J.: Multigrid Solution of the Euler Equations for Aircraft Configurations. AIAA-84-0093, Jan. 1984.

15. Jameson, A.; Baker, T. J.; and Weatherill, N. P.: Calculation of Inviscid Transonic Flow Over a Complete Aircraft. AIAA-86-0103, Jan. 1986.

16. Swanson, R. C.; and Turkel, E.: A Multistage Time-Stepping Scheme for the Navier-Stokes Equations. AIAA-85-0035, Jan. 1985.

17. Vatsa, V. N.: Accurate Numerical Solutions for Transonic Viscous Flow Over Finite Wings. *J. Aircr.*, vol. 24, June 1987, pp. 377–385.

18. Martinelli, L.; Jameson, A.; and Grasso, F.: A Multigrid Method for the Navier Stokes Equations. AIAA-86-0208, Jan. 1986.

19. Swanson, R. C.; and Turkel, Eli: Artificial Dissipation and Central Difference Schemes for the Euler and Navier-Stokes Equations. AIAA-87-1107, June 1987.

20. Martinelli, Luigi; and Jameson, Antony: Validation of a Multigrid Method for the Reynolds Averaged Equations. AIAA-88-0414, Jan. 1988.

21. Jameson, Antony; and Jayaram, Mohan: Multigrid Solution of the Navier-Stokes Equations for Flow Over Wings. AIAA-88-0705, Jan. 1988.

22. Radespiel, R.; Rossow, C.; and Swanson, R. C.: An Efficient Cell-Vertex Multigrid Scheme for the Three-Dimensional Navier-Stokes Equations. AIAA-89-1953, June 1989.

23. Vatsa, Veer N.; and Wedan, Bruce W.: Development of an Efficient Multigrid Code for 3-D Navier-Stokes Equations. AIAA-89-1791, June 1989.

24. Swanson, R. C.; and Radespiel, R.: Cell Centered and Cell Vertex Multigrid Schemes for the Navier Stokes Equations. *AIAA J.*, vol. 29, May 1991, pp. 697–703.

25. Malone, J. B.; and Swanson, R. C.: Inverse Airfoil Design Procedure Using a Multigrid Navier-Stokes Method. *Proceedings of the Third International Conference on Inverse Design Concepts and Optimization in Engineering Sciences*, Pennsylvania State Univ., 1991, pp. 55–66.

26. Peyret, R.; and Taylor, T. D.: *Computational Methods for Fluid Flow.* Springer-Verlag, 1985.

27. Martinelli, Luigi: Calculations of Viscous Flows With a Multigrid Method. Ph.D. Diss., Princeton Univ., Oct. 1987.

28. Turkel, Eli: Accuracy of Schemes With Nonuniform Meshes for Compressible Fluid Flows. *Appl. Numer. Math.*, vol. 2, Dec. 1986, pp. 529–550.

29. Hirsch, Charles: *Numerical Computation of Internal and External Flows. Volume 2: Computational Methods for Inviscid and Viscous Flows.* John Wiley & Sons, 1988.

30. Von Neumann, J.; and Richtmyer, R. D.: A Method for the Numerical Calculations of Hydrodynamical Shocks. *J. Math. Phys.*, vol. 21, 1950, pp. 232–237.

31. MacCormack, R. W.; and Baldwin, B. S.: A Numerical Method for Solving the Navier-Stokes Equations With Application to Shock-Boundary Layer Interactions. AIAA-75-1, Jan. 1975.

32. MacCormack, R. W.: The Effect of Viscosity in Hypervelocity Impact Cratering. AIAA-69-354, Apr. 1969.

33. Caughey, David A.; and Turkel, Eli: Effects of Numerical Dissipation on Finite-Volume Solutions of Compressible Flow Problems. AIAA-88-0621, Jan. 1988.

34. Eriksson, L. E.; and Rizzi, A.: Analysis by Computer of the Convergence to Steady State of Discrete Approximations to the Euler Equations. AIAA-83-1951, July 1983.

35. Pulliam, T. H.: Artificial Dissipation Models for the Euler Equations. AIAA-85-0438, Jan. 1985.

36. Yee, H. C.: *Upwind and Symmetric Shock-Capturing Schemes.* NASA TM-89464, 1987.

37. Swanson, R. C.; and Turkel, E.: Aspects of a High-Resolution Scheme for the Navier-Stokes Equations. AIAA-93-3372, July 1993.

38. Thomas, J. L.; and Salas, M. D.: Far-Field Boundary Conditions for Transonic Lifting Solutions to the Euler Equations. AIAA-85-0020, July 1986.

39. Van Der Houwen, Pieter Jacobus: *Construction of Integration Formulas for Initial Value Problems.* North-Holland Publ. Co., 1977.

40. Vichnevetsky, R.: New Stability Theorems Concerning One-Step Numerical Methods for Ordinary Differential Equations. *Math. & Comput. Simul.*, vol. 25, 1983, pp. 199–205.

41. Sonneveld, P.; and Van Leer, B.: A Minimax Problem Along the Imaginary Axis. *Nieuw Archief Voor Wiskunde*, vol. 3, 1985, pp. 19–22.

42. Jameson, A.: Transonic Flow Calculations for Aircraft. *Numerical Methods in Fluid Dynamics*, Springer-Verlag, 1985, pp. 156–242.

43. Arnone, A.; and Swanson, R. C.: A Navier-Stokes Solver for Turbomachinery Applications. *J. of Turbomach.*, vol. 115, no. 2, Apr. 1993, pp. 305–313.

44. Maksymiuk, C. M.; Swanson, R. C.; and Pulliam, T. H.: *A Comparison of Two Central Difference Schemes for Solving the Navier-Stokes Equations.* NASA TM-102815, 1990.

45. Strikwerda, J. C.: Initial Boundary Value Problems for Incompletely Parabolic Systems. Ph.D. Thesis. Stanford Univ., 1976.

46. Belov, Yu. Ya.; and Yanenko, N. N.: Influence of Viscosity on the Smoothness of Solutions of Incompletely Parabolic Systems. *Math. Notes.*, vol. 10, 1971, pp. 480–483.

47. Gustafsson, B.; and Sundstrom, A.: Incompletely Parabolic Problems in Fluid Dynamics. *SIAM J. Appl. Math.*, vol. 35, Sept. 1978, pp. 343–357.

48. Müller, Bernhard: Linear Stability Condition for Explicit Runge-Kutta Methods to Solve the Compressible Navier-Stokes Equations. *Math. Methods Appl. Sci.*, vol. 12, Feb. 1990, pp. 139–151.

49. Abarbanel, S.; and Gottlieb, D.: Optimal Time Splitting for Two- and Three-Dimensional Navier-Stokes Equations With Mixed Derivatives. *J. Comput. Phys.*, vol. 41, May 1981, pp. 1–33.

50. Lerat, A.: Une Classe De Schémas Aux Différences Implicites Pour Les Systèmes Hyperboliques De Lois De Conservation. *C. R. Acad. Sci.*, vol. 288A, 1979, pp. 1033–1036.

51. Jameson, A.: The Evolution of Computational Methods in Aerodynamics. *J. Appl. Mech.*, vol. 50, no. 4b, Dec. 1983, pp. 1052–1070.

52. Lerat, A.; Sides, J.; and Daru, V.: An Implicit Finite-Volume Method for Solving the Euler Equations. *Lect. Phys.*, vol. 170, 1982, pp. 343–349.

53. Wigton, L. B.; and Swanson, R. C.: Variable Coefficient Implicit Residual Smoothing. *12th International Conference on Numerical Methods in Fluid Dynamics*, Univ. of Oxford, July 1990, pp. 1–11.

54. Radespiel, R.; and Kroll, N.: *Multigrid Schemes With Semicoarsening for Accurate Computations of Hypersonic Viscous Flows.* IB 129-90/19, DLR, 1991.

55. Swanson, R. C.; and Turkel, E.: Pseudo-Time Algorithms for the Navier-Stokes Equations. *Advances in Numerical and Applied Mathematics*, Mar. 1986, pp. 331–359.

56. Fedorenko, R. P.: The Speed of Convergence of One Iterative Process. *USSR Comput. Math. & Math. Phys.*, vol. 4, 1964, pp. 227–235.

57. Brandt, A.: Multi-Level Adaptive Solutions to Boundary-Value Problems. *Math. Comput.*, vol. 31, Apr. 1977, pp. 333–390.

58. Jameson, A.; and Yoon, S.: Multigrid Solution of the Euler Equations Using Implicit Schemes. AIAA-85-0293, Jan. 1985.

59. Anderson, W. K.; Thomas, J. L.; and Whitfield, D. L.: Multigrid Acceleration of the Flux Split Euler Equations. AIAA-86-0274, Jan. 1986.

60. Mulder, Wim A.: A High-Resolution Euler Solver. AIAA-89-1949, June 1989.

61. Hackbusch, W.: *Multi-Grid Methods and Application.* Springer-Verlag, 1985.

62. Johnson, G. M.: *Convergence Acceleration of Viscous Flow Computations.* NASA TM-83039, 1982.

63. Rubesin, Morris W.: Turbulence Modeling for Aerodynamic Flows. AIAA-89-0606, Jan. 1989.

64. Rubesin, M. W.; and Rose, W. C.: *The Turbulent Mean-Flow, Reynolds-Stress, and Heat Flux Equations in Mass-Averaged Dependent Variables.* NASA TM-X-62248, 1973.

65. Baldwin, B.; and Lomax, H.: Thin-Layer Approximation and Algebraic Model for Separated Turbulent Flows. AIAA-78-257, Jan. 1978.

66. Johnson, D. A.; and King, L. S.: A Mathematically Simple Turbulence Closure Model for Attached and Separated Turbulent Boundary Layers. *AIAA J.*, vol. 23, Nov. 1985, pp. 1684–1692.

67. Cebeci, Tuncer; and Smith, A. M. O.: *Analysis of Turbulent Boundary Layers.* Academic Press, 1974.

68. Radespiel, R.: *A Cell-Vertex Multigrid Method for the Navier-Stokes Equations.* NASA TM-101557, 1989.

69. Abid, Ridha; Vatsa, Veer N.; Johnson, Dennis A.; and Wedan, Bruce W.: Prediction of Separated Transonic Wing Flows With a Non-Equilibrium Algebraic Model. AIAA-89-0558, Jan. 1989.

70. Abid, Ridha: Extension of the Johnson-King Turbulence Model to the 3-D Flows. AIAA-88-0223, Jan. 1988.

71. Stock, H. W.; and Haase, W.: The Determination of Turbulent Length Scales in Algebraic Turbulence Models for Attached and Slightly Separated Flows Using Navier-Stokes Methods. AIAA-87-1302, June 1987.

72. Marx, Yves P.: Numerical Simulation of Turbulent Flows Around Airfoil and Wing. *Proceedings of the Eighth GAMM-Conference on Numerical Methods in Fluid Mechanics.* Pieter Wesseling, ed., Vieweg, 1989, pp. 323–332.

73. Rumsey, Christopher L.; and Vatsa, Veer N.: A Comparison of the Predictive Capabilities of Several Turbulence Models Using Upwind and Central-Difference Computer Codes. AIAA-93-0192, Jan. 1993.

REPORT DOCUMENTATION PAGE

Form Approved
OMB No. 0704-0188

1. AGENCY USE ONLY *(Leave blank)*	2. REPORT DATE	3. REPORT TYPE AND DATES COVERED
	August 1997	Technical Paper

4. TITLE AND SUBTITLE
Multistage Schemes With Multigrid for Euler and Navier-Stokes Equations
Components and Analysis

5. FUNDING NUMBERS
WU-505-59-53-01

6. AUTHOR(S)
R. C. Swanson and Eli Turkel

7. PERFORMING ORGANIZATION NAME(S) AND ADDRESS(ES)
NASA Langley Research Center
Hampton, VA 23681-2199

8. PERFORMING ORGANIZATION REPORT NUMBER
L-17201

9. SPONSORING/MONITORING AGENCY NAME(S) AND ADDRESS(ES)
National Aeronautics and Space Administration
Washington, DC 20546-0001

10. SPONSORING/MONITORING AGENCY REPORT NUMBER
NASA TP-3631

11. SUPPLEMENTARY NOTES
Swanson: Langley Research Center, Hampton, VA; Turkel: Tel-Aviv University, Tel-Aviv, Israel.

12a. DISTRIBUTION/AVAILABILITY STATEMENT
Unclassified–Unlimited
Subject Category 02
Availability: NASA CASI (301) 621-0390

12b. DISTRIBUTION CODE

13. ABSTRACT *(Maximum 200 words)*

A class of explicit multistage time-stepping schemes with centered spatial differencing and multigrid are considered for the compressible Euler and Navier-Stokes equations. These schemes are the basis for a family of computer programs (flow codes with multigrid (FLOMG) series) currently used to solve a wide range of fluid dynamics problems, including internal and external flows. In this paper, the components of these multistage time-stepping schemes are defined, discussed, and in many cases analyzed to provide additional insight into their behavior. Special emphasis is given to numerical dissipation, stability of Runge-Kutta schemes, and the convergence-acceleration techniques of multigrid and implicit residual smoothing. Both the Baldwin and Lomax algebraic equilibrium model and the Johnson and King one-half equation nonequilibrium model are used to establish turbulence closure. Implementation of these models is described.

14. SUBJECT TERMS	15. NUMBER OF PAGES
Euler; Navier-Stokes; Runge-Kutta; Multigrid	81
	16. PRICE CODE: A05

17. SECURITY CLASSIFICATION OF REPORT	18. SECURITY CLASSIFICATION OF THIS PAGE	19. SECURITY CLASSIFICATION OF ABSTRACT	20. LIMITATION OF ABSTRACT
Unclassified	Unclassified	Unclassified	

NSN 7540-01-280-5500

Standard Form 298 (Rev. 2-89)
Prescribed by ANSI Std. Z39-18
298-102